Electrochemical Hydrogen Storage in Organic Molecules

Dissertation

zur Erlangung des akademischen Grades eines Doktors der Naturwissenschaften

-Dr. rer. nat.-

an der Universität Duisburg-Essen

vorgelegt von

Frederic Buttler

geboren in Mülheim an der Ruhr

Max Planck Institut für Chemische Energiekonversion
(CEC MPG Mülheim an der Ruhr)

2017

Die vorliegende Arbeit wurde im Zeitraum vom 1.11.2013 bis zum 31.1.2017 im Arbeitskreis von Herrn Prof. Dr. Schlögl am Institut für chemische Energiekonversion in Mülheim an der Ruhr durchgeführt.

Tag der Disputation: 26.6.2017

Gutachter: Prof. Dr. R. Schlögl

Prof. Dr. M. Albrecht

Vorsitzender: Prof. Dr. S. Schulz

"It is, it was and it will be"

Zoran Pavlovic (Mülheim 2014)

"I don't ask questions, i only give answers"

Frederic Buttler (Erice 2016)

"Only one more measurement then i am ready"

all scientists and engineers

"When you study natural science and the miracles of creation, if you don't turn into a mystic you are not a natural scientist"

Albert Hofmann (WIRED magazine, 16.1.2006)

Contents

1. Introduction

1.1 Renewable energy storage and the scope of this work 1

1.2 *N*-heterocycles as "Liquid Organic Hydrogen Carrier" (LOHC) 3

1.3 CO_2 capture on *N*-heterocycles and electrochemical reduction 5

2. Techniques and theorie

2.1 Kinetics of electrode reactions and Rotating disc electrode (RDE) theory 7

2.2 Nuclear Magnetic Resonance (NMR) 10

2.2.1 Magnetism and nuclear spin 10

2.2.2 Chemical shift and spin-spin coupling 11

2.2.3 Relaxation 13

2.3 NMR spectroscopy techniques 14

2.3.1 ^{13}C-BB (CPD) and ^{13}C-dept

2.3.2 HMQC and HMBC

2.4 Infrared spectroscopy (IR) 15

2.5 Ultraviolet-visible absorption (UV-Vis) 16

3. Experimental

3.1 Electrochemical setup for hydrogen oxidation on Pt and procedure 17

3.2 Electrochemical setup for LOHC measurements and procedure 18

3.3 CO_2 capture measurements with piperazine 20

3.4 Hydrogenation of guaiazulene on Pd(10%)/C 21

3.5 NMR 21

3.6 IR 21

3.7 UV-Vis 22

4. Results and discussion

4.1 Hydrogen oxidation kinetics on Pt in alkaline media 23

4.2 Electrochemical tests of possible LOHCs on Pt 28

4.2.1 Carbazoles 30

4.2.2 Simple *N*-heterocycles 40

4.3 Electrochemical tests of possible LOHCs on Intermetallic Phases 44

4.3.1 Octahydro-n-ethylcarbazole 45

4.3.2 2-Methylpiperidine in water 47

4.3.3 2-Methyldecahydroquinoline 50

4.3.4 Indoline 52

4.3.5 Diaza-heterocycles 54

4.3.6 Conclusion 57

4.4 Hydrogenation of Guaiazulene and electrochemical oxidation on Pt 60

4.4.1 Conclusion 68

4.5 CO_2 capture with saturated N-heterocycles and electrochemical reduction in acetonitrile 69

4.5.1 Piperazine 71

4.5.2 Conclusion 76

5. Summary and discussion / Zusammenfassung und Diskussion

References 79

Supporting information 86

Attachment 96

Erklärung

Danksagung

1 Introduction

1.1 Renewable energy storage and the scope of this work

The need for an efficient energy storage becomes clear when looking at the high consumption of fossil fuels in our time. Not only that these fuels are limited, the burning of these produce greenhouse gases like carbon dioxide (CO_2) or methane. Besides rising temperatures due to high concentrations of these gases recent research has shown that CO_2 has a direct influence on the stoma development of plants. Stoma are pores which regulate exchange of O_2 and CO_2 but also the transpiration in the leaves of the plants. With higher CO_2 concentration less stoma are found on the leaves which leads to lesser transpiration and finally less harvest [1]. As we see arguments of vital importance are speaking for the research of alternative fuels. Renewable energies like wind or solar power are a solution away from fossil fuels but suffer from power fluctuations. A storage over a long period of time is needed to compensate these fluctuations and provide a steady supply of energy [2]. Furthermore the transportation sector still is in need for fuels which are easy to handle and cheap. Alternatives like biodiesel or natural gases are already on the market but can only be considered as a compromise solution due to the creation of methane, CO_2 and a limited production/distribution infrastructure. Another promising alternative is hydrogen which has a gravimetric energy storage density of 33.3 kWh kg^{-1} [3, 4] which is the highest among the known energy storage compounds. On the other hand hydrogen is gaseous with a low volumetric capacity (0.003 kWh/l at 1 bar [4]) and thus a storage in its unbound form is a big problem. Hydrogen can be stored physically as a supercritical fluid, as an adsorbate or chemically as a liquid on a carrier which are mainly *N*-heterocycles (LOHC). Besides the direct storage of hydrogen, it can be used to reduce CO_2 to chemical species like formic acid (HCOOH), ethylene (C_2H_4), methane (CH_4) or methanol (CH_3OH). The scheme in figure 1 shows how a system for the production of fuels could look like. First energy is absorbed on solar panels, which produces electricity for the electrol-

ysis of water to hydrogen and oxygen. Hydrogen can be chemically bound to LOHCs and dehydrogenated when needed. Another possible way to use *N*-heterocycles is to catch CO_2, electrochemically reduce the formed carbamate and hydrogenate it to a valuable compound like methanol.

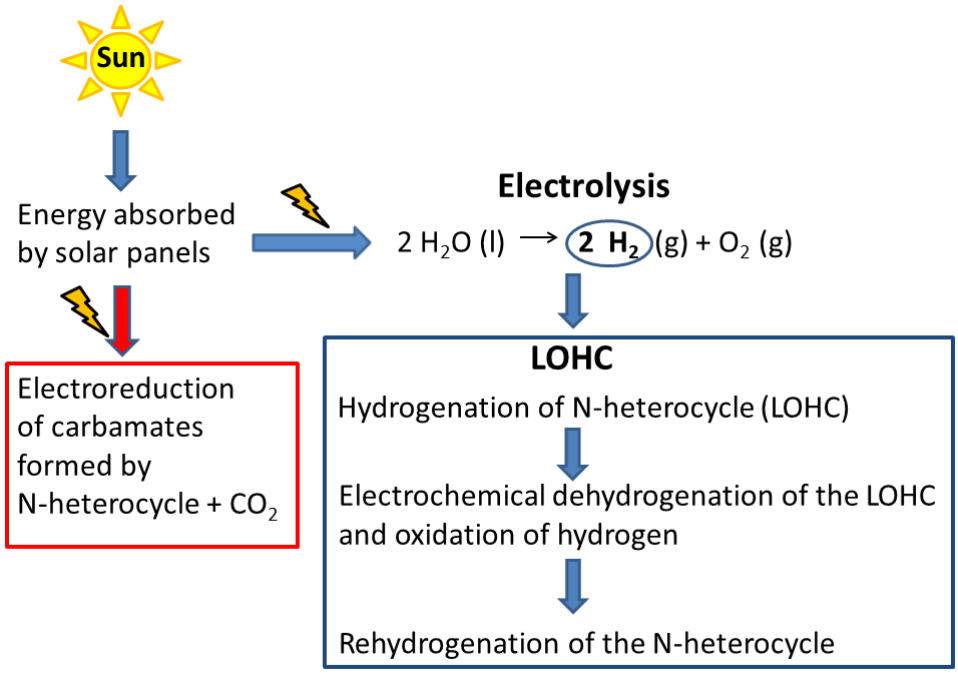

Figure 1: Scheme of renewable energy storage. Hydrogen is either used to hydrogenate the N-heterocycle or as reducing agent in the carbamate reduction process.

In this work both ideas were tried to be realized with the main focus on the hydrogen storage (LOHC) idea. Different systems were investigated including different catalysts, electrolytes, solvents and molecules regarding the electrocatalytic activity and the product distribution upon electrochemical oxidation. Two molecules were identified as CO_2 catchers and were reduced electrochemically. Electrochemical techniques including cyclic voltammetry (CV) and chronoamperometry (CA) were used to get a better understanding of the electrochemical reduction/oxidation behavior of these molecules. Reactants and products of the reaction were analyzed mainly by Nucleus Magnetic Resonance spectroscopy (NMR) but also Infra Red spectroscopy (IR), Ultraviolet-Visible absorption spectroscopy (UV/Vis) and Gas Chromatography (GC) were used.

1.2 *N*-heterocycles as "Liquid Organic Hydrogen Carrier" (LOHC)

A lot of effort has been spent to store gaseous hydrogen efficient. Storing methods like high pressure tanks, cryogenics or metal hydrides have some serious drawbacks like the need for high pressures or extremely low temperatures which makes them inapplicable for the mainstream energy distribution [5]. Another promising approach to store hydrogen are LOHCs on which hydrogen is bound chemically. The following scheme in figure 2 shows the idea of the LOHC system: First the molecule (here n-ethylcarbazole) gets hydrogenated over a heterogenous catalyst like PtRu. The hydrogenated molecule is distributed/stored in tanks and dehydrogenated in a direct LOHC fuel cell (DLFC) where the dehydrogenation process and the hydrogen oxidation process run simultaneously.

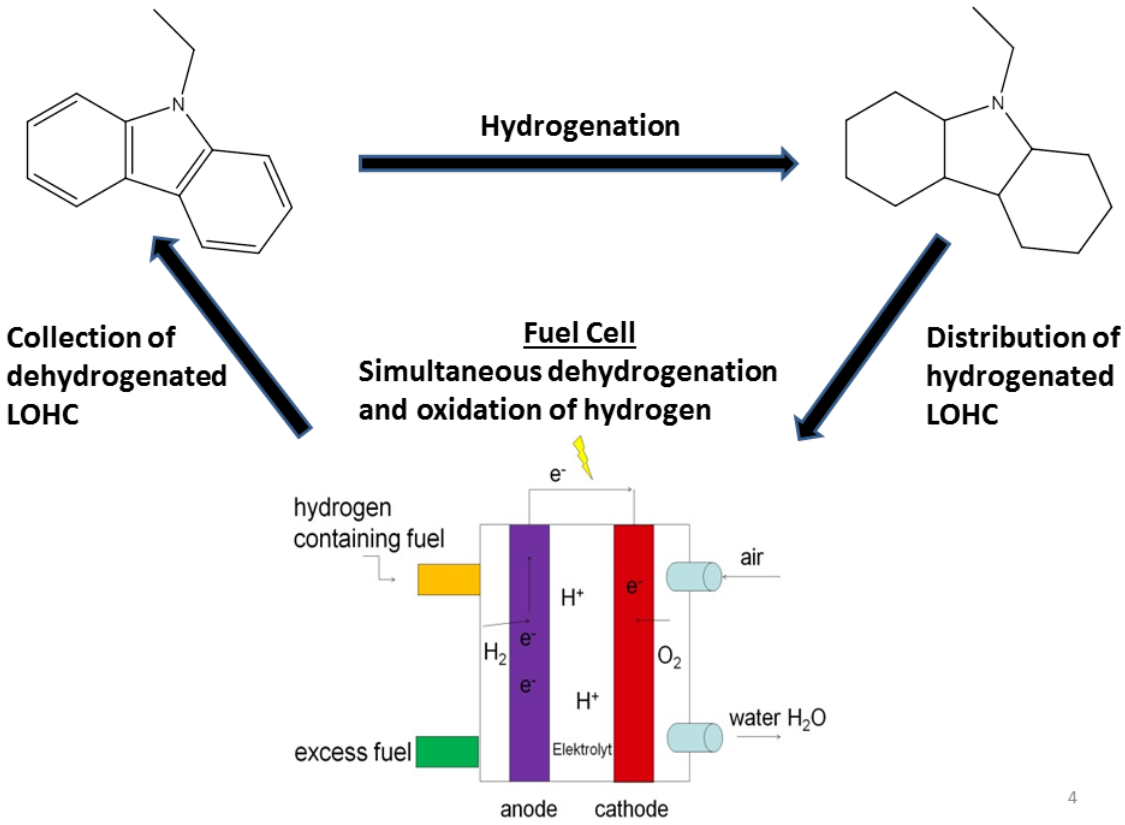

Figure 2: LOHC scheme: Hydrogenation from unsaturated to saturated molecule, distribution and finally dehydrogenation/oxidation of hydrogen in a DLFC. The LOHC can be hydrogenated again.

Combination of hydrogen and oxygen finally results in energy and water as the main product as follows:

Anode reaction: $2H_2 + 2O^{2-} \rightarrow 2H_2O + 4e^-$
Kathode reaction: $O_2 + 4e^- \rightarrow 2O^{2-}$
Overall reaction: $2H_2 + O_2 \rightarrow 2H_2O$

The dehydrogenated carrier can be reused and hydrogenated again. The majority of the examined molecules are cyclic $N-$heterocycles like n-ethylcarbazole which get hydrogenated over a heterogenous catalyst like PtRu or Pd/SiO_2 and dehydrogenated thermally in a reactor [6]. From the point of thermodynamics desired hydrogen release temperatures lie between 0 °C and 100 °C regarding the transport sector [7]. Hydrogen release temperatures of pure hydrocarbons like cyclohexane are far away from this aim. A big advantage of N-heterocycles over molecules consisting only of cyclic hydrocarbons are the thermodynamic and kinetic properties of the hydrogenation and dehydrogenation process. Nitrogen included in a cyclic molecule weakens the adjacent C-H bonds [7]. But not only the stability (thermodynamics) of the molecule also the reaction rate (kinetics) of the dehydrogenation process is altered. N-heterocycles adsorb through their N-atom on the metal (catalyst) surface which results in a higher turn over frequency (TOF) for a dehydrogenation reaction [6]. Another way to influence the reaction rate of the hydrogenation/dehydrogenation reaction is the choice of the catalyst. Various inter-metallic compounds like palladium-gallium or aluminum-palladium are known to be effective towards dehydrogenation/hydrogenation reactions [8]. Since the dehydrogenation kinetics are mostly governed by metal-hydrogen bond strength (Sabatier principle) an alteration of the main element d-band could turn metal-hydrogen interaction favorable. Several intermetallics were synthesized by our collaboration partners (I. Antonysyn, Y. Grin Max Planck Institute for Chemical Physics of Solids, Dresden) as a part of the LOHC project including $PtAl_2$, $MoSi_2$ and others. In previous works they proved to be suitable and selective catalysts for the oxidation and reduction of many molecules [9]. Some of the tested hydrogenated molecules like dodecahydro-

carbazole (H12-NEC) were provided by the institute of chemical engineering (Prof. Wasserscheid, Erlangen). Until now LOHCs were dehydrogenated thermally [10, 11]. Another possibility besides the thermal dehydrogenation is the electrochemical dehydrogenation. A hydrogen release with a subsequent hydrogen oxidation by the application of a certain potential is a possible way. Application of electrochemistry has proven to be a valuable method for the oxidation or reduction of various compounds [12]. Furthermore electrochemistry provides immense amounts of reaction energy to reactants by application of a few volts. 1V of electrochemical energy amounts to a thermal activation equivalent to around 500 °C. A direct electrochemical dehydrogenation of a LOHC in a DLFC would be a great achievement.

1.3 CO_2 capture on N-heterocycles and electrochemical reduction

The idea to turn the greenhouse gas like CO_2 into syngas and fuels has been of tremendous interest [13]. Due to the possibility of potential controlled reactions, the electrochemical reduction of CO_2 is a very attractive method for the synthesis of these compounds [9]. It has been possible to reduce CO_2 electrochemically to obtain chemicals like methanol and methane [14, 15, 16]. One of the major challenges in turning CO_2 into reduced products happens at the source. Concentration of CO_2 in the atmosphere is very small and one has to rely on the source of CO_2 production like a coal burning power plant to capture and create significant concentrations of CO_2. Amines are known to be some of the best CO_2 capturing agents like methylamine and other. Besides this CO_2 reduction in aqueous medium has to deal with the significant issue of low solubility. The idea this paper presents is to use the CO_2 captured by amines as carbamates directly to reduced products still tied to the amine scaffold. This idea allows CO_2 obtained from CO_2 capturing technologies (in the form of carbamates) to be directly utilized to form reduced products and also allows a method to bypass solubility issues by tailoring the amine backbone. Choice of non aqueous solvent allows to avoid significant faradaic efficiency issues arising out of competing hydrogen

evolution reaction. Recently Suraprakash et. al. have shown the reduction of CO_2 bound to a polyamine in an ethereal solvent on a Ru catalyst thermally [17]. For our studies we have chosen piperazine, which is a saturated diamine compound. Saturated amines are known to be non reactive to electrochemical oxidation/reduction as the sp^3 backbone of carbon atoms is not attacked and all chemistry happens through N lone pairs which in carbamates have already been blocked. This allows for the chemistry to happen only at the carbamate site. Acetonitrile was chosen as the solvent and Pt was chosen as the catalyst. Electrochemical reduction of CO_2 in acetonitrile on Pt is known and results in formation of oxalic acid [18].

2 Techniques and theorie

2.1 Kinetics of electrode reactions and rotating disc electrode (RDE) theory

The rate constant k of a chemical/electrochemical reaction is given by the Arrhenius equation :

$$k = A \cdot e^{\frac{-E_A}{RT}} \tag{1}$$

With E_A the activation energy, R as the universal gas constant 8.3144598 $[\frac{J}{molK}]$, T [K] as temperature and A called the pre-exponential factor. Every reaction has to reach the energy E_A to start. For electrochemical reduction or oxidation reactions this energy is reached by applying a potential called the activation overpotential η. In other words η is the kinetic barrier for the electron transport in an electrochemical reaction. To predict how the current changes by variation of the overpotential the Butler-Volmer equation (2) is used.

$$i = i_0 \cdot \left\{ exp\left[\frac{\alpha_a z F \eta}{RT}\right] - exp\left[-\frac{\alpha_c z F \eta}{RT}\right] \right\} \tag{2}$$

With i as electrode current density [A/m^2], i_0 as exchange current density, z number of electrons involved in the electrode reaction, F as Faraday constant and α_c/α_a as cathodic/anodic charge transfer coefficient. Equation (2) only describes the rate of the electron transfer and neglects other physical processes that contribute to the overall kinetics. Mass transport in form of diffusion, convection and migration have to be taken into account. Theoretically only a non moving bulk solution would give exact results for i or i_0. A widely used static approach for a forced convection method is the Rotating Disc Electrode (RDE) . The electrode is rotated with speeds until a laminar flow is reached. Figure 3 shows how a steady state near the electrode surface is reached. A electrode tip rotates with constant speed in solution which results in a vortex on the the surface of the electrode. The center of the electrode can be compared with the center of a tornado where everything around the it rotates but only the objects in the center are completely motionless.

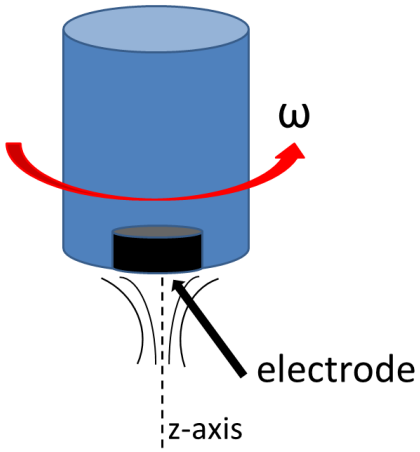

Figure 3: Rotating electrode tip rotation at a constant angular rotation rate w

Mathematically the situation is very simple, the convective stream has only one direction showed as the dotted line (z-axis). With D as the diffusion coefficient $[m^2 s^{-1}]$, ν_z as the velocity component along the z-axis $[w^{\frac{3}{2}} n^{\frac{-1}{2}}]$, t [s] as time and c [mol/l] as the concentration of molecules in solution :

$$\frac{\partial[c]}{\partial t} = D\frac{\partial^2[c]}{\partial z^2} - \nu_z \frac{\partial[c]}{\partial z} \tag{3}$$

A layer where no convection occurs is formed on the surface of the disc which is called diffusion layer as it is shown in figure 4.

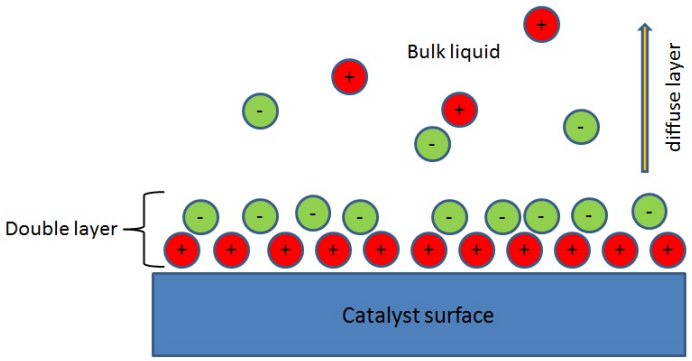

Figure 4: Scheme of the double layer for an electrochemical reaction

The thickness of the diffusion layer depends on the mass transport rate J $[mol \cdot m^{-2} s^{-1}]$ in the direction (z axis in figure 3) of the catalyst surface which can be changed by the rotation speed of the RDE.

$$J = -\frac{D(c_0 - c_s)}{\delta} \tag{4}$$

with c_0 as the concentration of the ions in bulk solution, c_s as the concentration of the ions on the disc and δ $[m]$ as diffusion layer thickness which is described by:

$$\delta = 1.61 D^{\frac{1}{3}} \nu^{\frac{1}{6}} \omega^{-\frac{1}{2}} \tag{5}$$

As we know the current has to pass resistances when it flows. In this case there is a charge transfer resistance (R_k) and the mass transport resistance (R_d). According to the Ohm's law we get:

$$I = \frac{V}{R} = \frac{V}{R_d + R_k} \tag{6}$$

When $R_k \ll R_d$ the kinetics are very fast and the reaction is mass transfer limited and (6) becomes:

$$I = I_d = \frac{V}{R_d} \tag{7}$$

To calculate the amount of substance n [mol] which is deposited after time t [s] during the electrolysis the law of Faraday is used :

$$n = \frac{It}{zF} \tag{8}$$

For I_d we get :

$$I_d = -zFAJ = zFAD\frac{c_0 - c_s}{\delta} \tag{9}$$

with A as the electrode area [cm^2]. In the case of the RDE and a mass transport limited current c_s is zero, because every reactant approaching the catalyst is instantly consumed. The current that flows is called the limiting current I_L and is calculated by the following equation by Levich:

$$I_L = 0.620 nFA(D)^{\frac{2}{3}} v^{\frac{-1}{6}} c w^{\frac{1}{2}} \tag{10}$$

v as the kinematic viscosity [$m^2 s^{-1}$]. With the reciprocal value of the total current of equation (6) the kinetic current density i_K ($i = \frac{I}{A}$) [A/m^2] can be calculated with the so called Koutecky Levich equation.

$$\frac{1}{i} = \frac{1}{i_k} + \left(\frac{1}{0.620nFAD^{\frac{2}{3}}\nu^{-\frac{1}{6}}C}\right)\omega^{-\frac{1}{2}} \tag{11}$$

The kinetic current corresponds to the catalytic activity of the oxidized or reduced molecules in the absence of mass-transport limitations. Equation (11) takes into account that both mass transport and kinetics contribute to the overall reaction rate. Plotting the logarithmic i_k against potential gives the exchange current density i_0 at a temperature T. The exchange current density is the current during a reduction/oxidation reaction when at equilibrium. As it is already said in the LOHC section a catalyst should be able to dehydrogenate and oxidize hydrogen at the same time. Pt is known to oxidize hydrogen and therefore hydrogen oxidation was measured on a polycrystalline Pt disk and results were compared to literature data (chapter 4).

2.2 Nuclear Magnetic Resonance (NMR)

2.2.1 Magnetism and nuclear spin

Every atom possesses a nuclear spin quantum number I ($I \geq 0$) which can be any multiple of $\frac{1}{2}$. All nuclei with $I \neq 0$ possess a nuclear spin and are NMR active. Often measured NMR active nucleis are ^{1}H and ^{13}C which have an angular momentum m and a nuclear magnetic moment µ and are correlated as follows:

$$\mu = \gamma m \tag{12}$$

γ is the gyromagentic ratio of the nucleus which is correlated to the frequency ν of an absorbed photon of a particle (with a net spin) placed in a magnetic field B.

$$\nu = \gamma B \tag{13}$$

The resonance or Larmor frequency is the frequency in which the absorbed photon changes from low to high and from high to low energy state.

$$E = h\nu \tag{14}$$

with h as the Planck constant (h = 6.626x10^{-34} Js). The change between the two spin states initiates an absorption of energy. The number of the energy levels is determined by the number of spin states ($2I$+1). The energy difference between high and low spin state is directly proportional to the magnetic field B:

$$\Delta E = h\gamma B \tag{15}$$

When no magnetic field is applied the ratio between low state and high state spin is given by the Boltzmann statistics:

$$\frac{N^{-}}{N^{+}} = e^{-\frac{\Delta E}{kT}} \tag{16}$$

k is the Boltzmann's constant ($1.3805 \cdot 10^{-23}$J/K) and T the temperature. Because spins make transition from low to high states and vice versa the NMR signal is proportional to the population difference of spins (and energy ΔE) in high and low spin states given by equation (16). The sensitivity of NMR comes from the exchange resonance frequency between the spins in their original state and the spectrometer where B is applied. In an NMR experiment the applied field B will be perturbed with an radiofrequency (RF) pulse which creates a transverse pulsed magnetic field B_1. The spins which were aligned to field B will rotate in the direction of the of the new field B_1 through an angle Θ which is proportional to the duration τ and the power of the RF pulse and so the magnitude of B_1.

$$\Theta = 2\pi\gamma\tau B_1 \tag{17}$$

The induced precession generates a current which is detected by a coil in the NMR spectrometer. After the signal gets amplified and referenced against a known frequency it gets digitised as **F**ree **I**nduction **D**ecay known as FID. Fourier transformation of the FID results in a spectrum.

2.2.2 Chemical shift and spin-spin coupling

The position of a peak in a spectrum is defined by chemical shift. Each nucleus is shielded differently by its electron cloud. According to the bonds

in a molecule or the type of a nuclei the shielding effect varies. Some enhance the B field (deshielding) and some weaken the B field (shielding). A deshielding effect (higher chemical shift) can be observed when the measured nuclei is bonded to an electron rich atom or functional group (COOH, NO_2, aromats...). Shielding (lower chemical shift) effects occur when no electron rich species is around like in alkanes. The shift is standardized against a reference like tetramethylsilane (TMS) and given in ppm:

$$d = \frac{(n - n_{Ref}) \cdot 10^6}{n_{Ref}} \tag{18}$$

Nuclei with the same chemical shift are equivalent and nuclei with different chemical are nonequivalent. Nonequivalent nuclei which are close to each other influence their magnetic field in such a way that this effect shows up in the spectra. It is called indirect dipole dipole or J coupling and can be observed when the distance of the nuclei is equal or less than three bonds ($J_1,\ J_2,\ J_3$). The indirect dipole coupling is responsible for the observed multiplet structure in a ^{1}H-NMR spectrum. Hydrogen atoms have a nucleus spin of -$\frac{1}{2}$ which splits into two when coupled to another hydrogen nucleus which is bonded to the adjacent atom. According to the energy levels always two possibilities of spin transitions are possible. In one case a nucleus changes its spin from up to down (nucleus A) in the other case its spin changes from down to up (nucleus B). The more the number of nucleus B increases the more the splitting pattern in a spectrum increases:

Table 1: Pascal's triangle

Configuration	Peak ratios
A	1
AB	1:1
AB_2	1:2:1
AB_3	1:3:3:1

The coupling constant J gives information about connectivity, distance (higher J value = less distance between the nuclei) and angles of a molecule.

2.2.3 Relaxation

The net magnetization is changed during the exposure of the spin system under a RF pulse. Between the pulses the system relaxes and returns to its equilibrium. The time for relaxation is governed by the nuclei physical environment, molecular motion and variations of the applied magnetic field B. Relaxation is categorized in longitudinal (spin-lattice relaxation) and transversal (spin-spin relaxation). The spins and the surrounding environment exchange energy. This energy exchange is responsible for longitudinal relaxation in which the magnetization relaxes to its equilibrium M_0. Figure 5 shows schematically the relaxation to equilibrium.

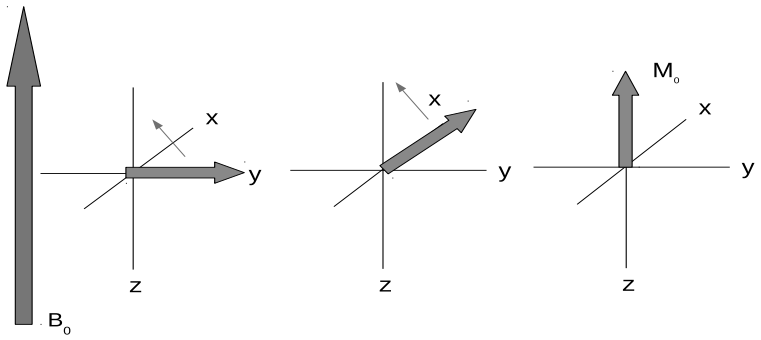

Figure 5: Longitudinal relaxation in an magnetic field B

The magnetization relaxation can be seen as a slow decay with time T_1 from the y-axis back to the z-axis.

$$M_0 - M_z(\tau) = [M_0 - M_z(0)]e^{\frac{-\tau}{T_1}} \tag{19}$$

Chemical shift anisotropy (the electronic environment around a nucleus is anisotropic), dipole-dipole interactions and paramagnetic interactions provide longitudinal relaxation. The transversal relaxation is independent from the environment. This type of relaxation takes into account that not every spin experiences the same net magnetization. Spins have to be regarded as group of spins (spin packets) experiencing the same magnetization. Each spin packet rotates at its own Larmor frequency and results in a phase difference

between the spin packets.

2.3 NMR spectroscopy techniques

The techniques used in this work are ^{1}H, ^{13}C-BB , ^{13}C-dept (distortionless enhancement of polarisation transfer), **HMBC** (Heteronuclear Multiple Bond Correlation) and **HMQC** (Heteronuclear multiple quantum correlation). They will be (except ^{1}H NMR) described in this chapter.

2.3.1 ^{13}C-BB (CPD) and ^{13}C-dept

^{13}C-BB is a technique in which the spin-spin coupling is suppressed, the spectra are broadband decoupled which results in spectra only consisting of singlets. The decoupling method used in this work is "Composite Pulse Decoupling" (CPD) which consists of sequenced pulses with a specific flip angle and re-phase. Radio frequency power and pulse width have to be adjusted before measurement. To get more information of the measured carbon atom ^{13}C-dept (distortionless enhancement of polarisation transfer) is used. It distinguishes between signals of CH_3, CH_2 and CH by using pulses in different angles (45°, 90° and 135°) with frequencies in the range of ^{1}H and ^{13}C. Quaternary carbons don't show up in a dept spectra because the one bond C-H J-coupling is needed for polarization transfer. Primary and tertiary carbons will show up as positive peaks and secondary carbons as negative peaks.

2.3.2 HMQC and HMBC

The correlations between two different nuclei separated by one bond is detected by HMQC (Heteronuclear multiple quantum correlation) . In other words $^{1}J_{CH}$, $^{1}J_{NH}$ or coupling with other heteroatoms can be measured. The spectra is plotted with two traces, the vertical trace shows the heteroatom or ^{13}C spectra and the horizontal trace the ^{1}H spectra. HMBC (Heteronuclear Multiple Bond Correlation) is the correlation of heteroatoms and protons with couplings separated by more than one bond (^{2}Jor ^{3}J). Figure 6 shows

schematically how a HMQC (left) and HMBC (right) spectra has to be interpreted.

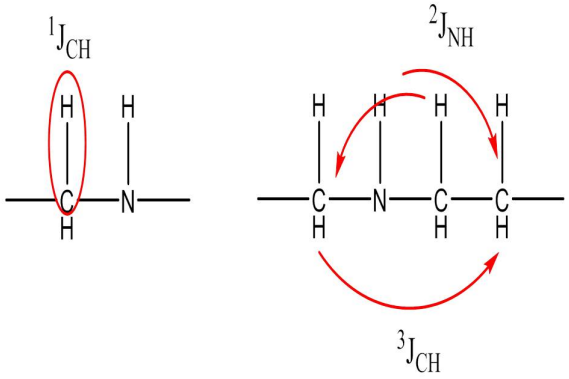

Figure 6: left: HMQC couplings right: HMBC couplings

2.4 Infrared spectroscopy (IR)

Infrared spectroscopy also called vibrational spectroscopy is a method which makes use of the absorbency of characteristic frequencies of molecules. A beam of infrared light is passed through a sample and molecules start to vibrate. Only if the frequencies of the excited molecules match the frequency of the incoming IR light energy is absorbed. The frequency υ energy E and the wavelength λ of the incoming light are related as follows:

$$E = h\upsilon = \frac{hc}{\lambda} \tag{20}$$

with h as the Plancks constant and c the speed of light. The strength of a bond and the type of stretching is correlated to the absorbed energy. For two atomic molecules only stretching vibration will occur and molecules with three atoms experience stretching and bending vibration. Furthermore stretching can be asymmetric or symmetric (figure 7).

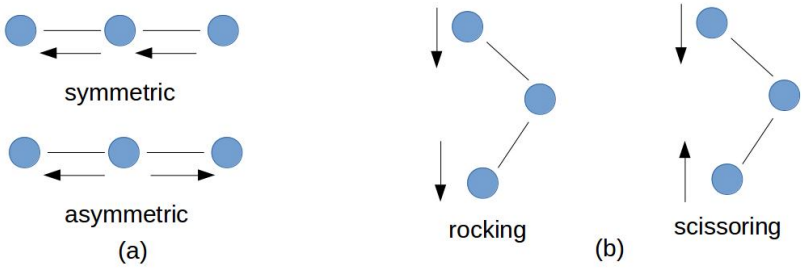

Figure 7: (a) stretching vibrations (b) bending vibrations

Besides the shown stretching modes in figure 7 there are out of plane modes called wagging and twisting. Each excited mode is reached when a molecule is irradiated with a light of a specific frequency. These frequencies are shown as absorption bands in the IR spectra. Intensities of the bands are the result of the dipole moment changes of the bonds. Bond length and the different charges of the atoms are responsible for the dipole moments. Molecules like N_2 have no dipole and are IR inactive and water with a very high dipole is IR active. Band positions are determined by the different energies of the absorption frequencies. The strength of a bond and the masses of the corresponding atoms are directly related to the frequencies as described in Hooke's law:

$$\nu = \frac{1}{2\pi c}\left[\frac{k(m_1 + m_2}{m_1 m_2}\right]^{\frac{1}{2}} \tag{21}$$

with k as the force constant of the bond. Due to their characteristic frequencies the structure of the molecules and the types of functional groups can be determined.

2.5 Ultraviolet-visible absorption (UV-Vis)

Electronic transitions from the ground state to the excited state are caused by ultraviolet or visible radiation. The promotion from one state to another requires the absorption of a photon which falls in the energy range of UV/Vis. Only π to π^* and n to π^* transitions occur in this range. These are molecules containing π-electrons (double bonds) or non bonding electrons like

the electrons of oxygen of a carbonyl group. Depending on the energy gap between HOMO (**H**ighest **O**ccupied **M**olecule **O**rbital) and LOMO (**L**owest **O**ccupied **M**olecule **O**rbital) the length of the emitted wavelength of the photon changes.

3 Experimental

A Biologic VSP 300 potentiostat with EC-Lab 13.04 software was used for every electrochemical measurement. If not mentioned in the text measurement temperature was always between 23-24 °C.

3.1 Electrochemical setup for hydrogen oxidation (HOR) on Pt and procedure

Measurements were carried out in 0.1 M KOH solution, prepared with Milli-Q water (18 MΩcm) and KOH pellets (Sigma Aldrich, 85 %). Solutions were saturated with argon (5.0 Prax air) before measurements. A jacketed 250 mL glass cell (Pine Instruments) was connected to a temperature-controlled water circulating thermostat (Lauda edition 2000). The potentiostat was connected to a rotator (Pine Instruments) and a Pt(pc) disk (Alfa Aeasar 99.99 % metal basis $\varnothing = 0.4$ cm, area = 0.5 cm^2) was mounted in a teflon® RDE holder (Pine Instruments). A RHE (Gaskartel) served as reference electrode and a Pt wire (Pine Instruments) as counter electrode. The Pt disk was cleaned electrochemically by cycling between 0 V and 1.8 V vs RHE in 0.5 M H_2SO_4 until a clear CV was visible and rinsed with Milli-Q water three times. After immersing the electrode into the argon saturated solution CVs at 294 K were recorded between 0.08 and 1.0 V vs RHE with a scan rate of 50 mV/s until steady state. For the measurements of the HOR the KOH solution was saturated with pure hydrogen (Air liquide) and polarization curves were taken between -0.08 V and -1.0 V vs RHE with different rotation rates (400, 900, 1600, 2500 rpm) at a scan rate of 10 mV/s. This was repeated for every temperature (275 K, 294 K, 314 K) with freshly prepared KOH solutions for each measurement.

Impedance measurements

After the RDE measurements at different temperatures the cell resistance was measured. The electrochemical impedance spectroscopy with potentio control (PEIS, frequency range from 0 Hz to 100 kHz and a sine amplitude of 10 mV) was used.

3.2 Electrochemical setup for LOHC measurements and procedure

Electrochemical measurements for the tests of LOHC molecules were almost the same for all tested substances. If an alteration was done it is stated in the appropriate chapter. A 250 mL airtight RDE glass cell (100 mL teflon® beaker for measurements in basic solutions) from PINE was used and cleaned with Milli-Q water/Mucosolvan® mixture and rinsed at least three times with water. For measurements in organic solvents the cell was rinsed with acetonitrile (99.98%, Alfa Aeasar) and dried in an oven at 350 K. As counter electrode a platinized platinum wire (Alfa Aeasar 99.99 % metal basis) was used. Measurements in acetonitrile were referenced against a self made $Ag/AgNO_3$ reference electrode. Therefore a silver wire was immersed into a glass tube filled with a solution of acetonitrile and 0.01 M $Ag/AgNO_3$. A vycor frit (Ø=0.2 cm, Gamec) was used to establish ionic conduction between bulk solution and reference electrode. The electrode was referenced against the ferrocene/ferrocenium (Fc/Fc^+) couple in acetonitrile and 0.1 M $NaClO_4$. For measurements in H_2O a standard RHE (reversible hydrogen electrode, Gaskartel) was used. Electrolytes and working electrodes (WE) used in this work are listed below:

WE's

- Pt disk (Alfa Aeasar 99.99 % metal basis Ø = 0.4 cm, area = 0.5 cm^2)
- Pt foil (Alfa Aeasar 99.99 % metal basis, area = 1.2 cm^2)
- glassy carbon disk (Pine, Ø = 0.4 cm)

- the inter metallic phases MoSi, $Mo_{46.15}Co_{41.85}Si_{12}$, $Mo_{33.33}Co_{46.67}Si_{20}$, Mo_6Co_7, MoCoSi, $MoAl_{12}$, $ReAl_{12}$, WAl_{12} (from Max Planck institute for chemical physics of solids, Dresden, chemical materials science department)

Electrolytes

- sodium perchlorate hydrate (99.99 %, Sigma aldrich)
- lithium tetrafluoroborate (98 %, Sigma aldrich)

Chronoamperometric measurements were carried out at a fixed potential for about 15 hours. After the measurement finished the solvent was removed with a rotary evaporator at 180 mbar and a temperature of 310 K. The residue was collected and analyzed by the described methods below. The $Ag/AgNO_3$ reference electrode used for measurements in acetonitrile was referenced against Ferrocene on Pt. Ferrocene is known to be a metallocene which can be reversibly oxidized and reduced [19, 20]. The IUPAC recommendation says that every reference electrode used in organic solvents should be referenced against the half wave potential $E_{1/2}(Fc^+/Fc)$ of the ferrocene/ferrocenium redox couple [21]. Therefore CV's at different scan rates were done (figure 8).

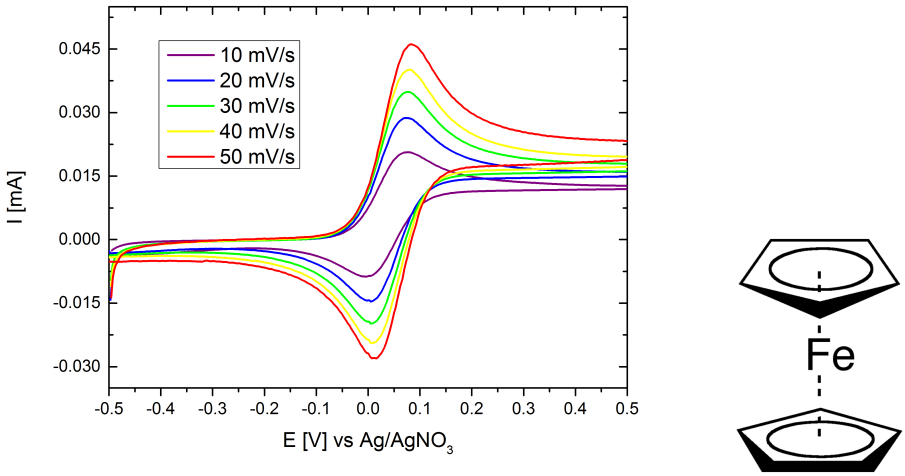

Figure 8: CV's of 1 mM Ferrocene on Pt in acetonitrile and 0.1 M $NaClO_4$

The half wave potential is $E_{1/2}(Fc^+/Fc) = +35\ (\pm 3)$ mV against $Ag/AgNO_3$ (595 mV vs NHE [18]) with an anodic/cathodic peak separation of 0.07 V.

3.3 CO_2 capture measurements with piperazine

Electrochemical measurments were carried out at 295 K and atmospheric pressure in a 250 mL glass cell from PINE which was cleaned with a water (Milli-Q 18 MΩcm)/Mucasol (Sigma Aldrich) mixture, rinsed two times with acetonitrile (99.98%, Alfa Aeasar) and dried in an oven at 350 K. As supporting electrolyte 0.1 M sodium perchlorate hydrate (99.99 % trace metal basis, Sigma aldrich) was used. Piperazine (99.9 % Sigma Aldrich) was used without any purification. For the formation of piperazinecarbamate ($PipCOO^-$) 5% CO_2 in argon was bubbled through a solution of acetonitrile and 40 mM piperazine until the solution changed from transparent to a white liquid. After the formation of the carbamate was completed the solution was bubbled with argon until no unreacted CO_2 remain in solution. The Pt working (disk, Alfa Aeasar 99.99% metal basis Ø = 0.4 cm, area = 0.5 cm^2) and the platinized Pt counter (wire, Alfa Aeasar 99.99% metal basis) electrode were cleaned electrochemically by cycling it from 0 to 1.8 V (scan rate = 0.5 V/s) in 0.5 M H_2SO_4 against a RHE reference electrode. The procedure of the carbamte formation, electro-reduction and the product analysis is shown below.

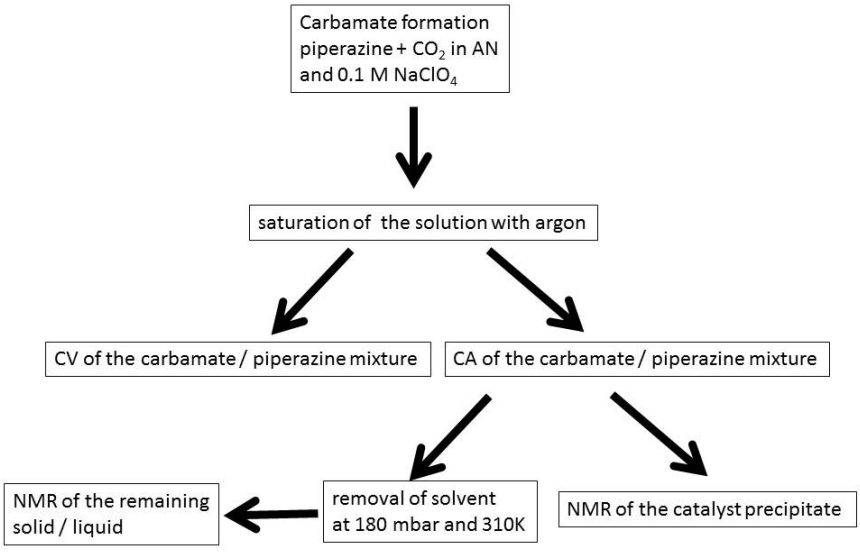

Figure 9: "Workflow" for the piperazinecarbamate reduction measurements (AN = acetonitrile)

The reference electrode for the chronoamperometric measurements and the CVs in acetonitrile was the already mentioned $Ag/AgNO_3$ electrode. After electrochemical reduction at a constant potential the solvent was removed at 180 mbar and a temperature of 313 K until a white solid and a transparent to yellow liquid remained. Liquid and solid were analyzed simultaneously.

3.4 Hydrogenation of guaiazulene on Pd(10%)/C

0.2 g of guaiazulene (Sigma Aldrich, 99 % 1,4-dimethyl-7-isopropylazulene) was diluted under stirring in deaerated MeOH (MERCK, 99.99 %) in a schlenk tube. Then 0.1 g of activated Pd (10%)/C (MERCK) was added and the tube was closed with a balloon. Hydrogen was filled in the closed schlenk tube until the balloon reached a decent size. This was done three times until the balloon and the tube were full of hydrogen and the valve was closed. The mixture was stirred for about 5 h until the color changed from blue to colorless. The Pd/C catalyst was filtered out and the solvent was removed with a rotary evaporator at 180 mbar and a temperature of 313 K.

3.5 NMR

A Bruker Avance III HD Ascend^{TM} 500 (^{1}H-NMR at 500 MHz) equiped with a sample Xpress and Top Spin Version 3.2 was used. For ^{1}H-NMR measurements a frequency of 500 MHz and for ^{13}C-NMR a frequency of 125 MHz was applied. The data evaluation software was MestReNova 10.0.2. with the possibility to simulate ^{1}H and ^{13}C-NMR spectra. Deuterated solvents were chloroform-D (Deutero, 99.80 %), deuterium oxide (Deutero, 99.90 %), methyl alcohol-D4 (Deutero, 99.80 %) and acetonitrile-D3 (Deutero, 99.80 %).

3.6 IR

An Ir-Nicolet iS50 with a ATR diamond probe was used. Pulvers or liquids were directly placed on the probe and spectra were taken. A background

spectra was taken before every measurement and substracted from the sample spectra.

3.7 UV-Vis

A SHIMADZU double beam UV-Vis scanning spectrophotometer "UV-2102 PC" was used. Acetonitrile was used as solvent in every measurement. The measured range was 190 nm to 400 nm.

4 Results and discussion

4.1 Hydrogen oxidation kinetics on Pt in alkaline media

As it is already stated in the introduction an anode-catalyst used in a DLFC should be able to dehydrogenate a molecule and oxidize the released hydrogen at the same time. A hydrogen carrier which is soluble in water that shows electrochemical dehydrogenation and oxidation behavior is the most desirable system. A very well known catalyst for the HOR (**H**ydrogen **O**xidation **R**eaction) is Pt which was used as a model catalyst in this work. Due to the fact that all *N*-heterocycles are alkaline in aqueous media, measurements were done in alkaline media. Furthermore HOR exchange current densities on Pt in acidic media are extremely high, a quantification of the kinetics in acidic media are nearly impossible [22]. Several attempts have been made but with HOR exchange current densities i_0 varying from 1 mA/cm² to 50 mA/cm² depending on the Pt electrode used [23]. The fact that HOR has much smaller current densities in alkaline media makes it possible to measure kinetics with the RDE. Temperature-dependent HOR current densities are measured and corrected by impedance measurements. Obtained values were used to compensate resistances in solution and correct the measured currents.

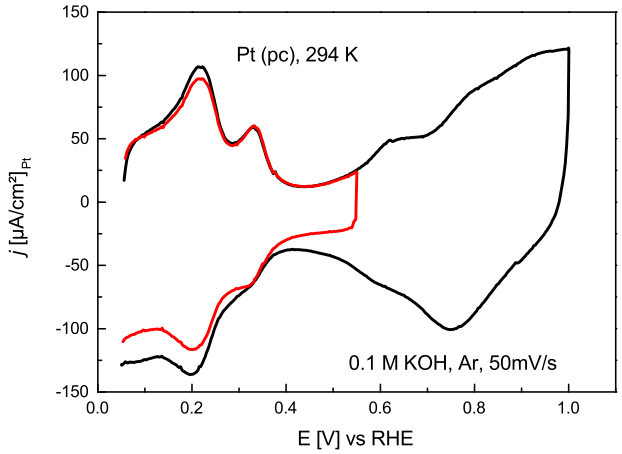

Figure 10: CVs of argon saturated 0.1 M KOH on Pt with two different potential limits.

The CVs in figure 10 shows clearly the two hydrogen oxidation peaks in the

typical Pt-H underpotential region of 0.08 to 0.45 V which were a result of Pt-H interaction on two different Pt planes (Pt(110) and Pt(100)) [24]. The double layer region can be found between 0.45 and 0.6 V and the Pt-oxide region above 0.6 V. The current density was referenced to the Pt surface area which was calculated by integration of the H adsorption region and subtraction of the double layer currents. Figure 11 shows the HOR at different rotation rates at a constant temperature (294 K). The part with the rising current is limited by kinetics and mass transport. When the curve reaches the flat part (above 0.15 V) currents are only mass transport limited.

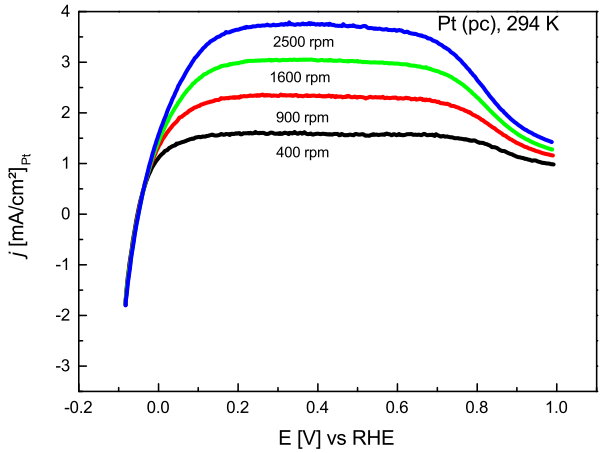

Figure 11: HOR current densities at T = 294 K at different rotation rates, scan rate 10 mV/s. Currents were corrected by a resistance of 46 Ohm which was measured by the PEIS method (electrochemical impedance spectroscopy under potentio control)

Temperature dependent HOR current densities are shown in figure 12. Higher temperatures result in higher currents as it is expected and written in the Arrhenius equation (1).

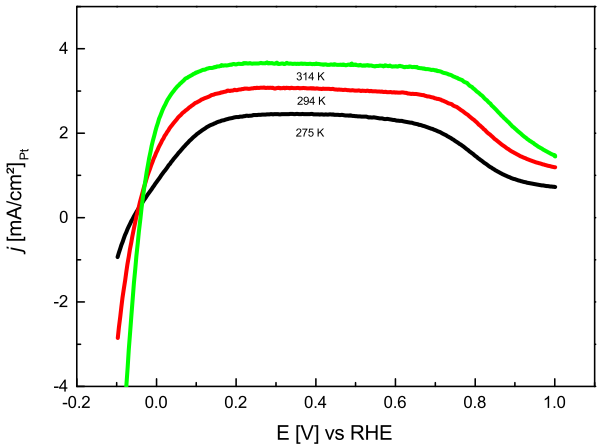

Figure 12: HOR current densities (1600 rpm) at different temperatures, 275 K (67 Ohm), 294 K (46 Ohm) and 314 K (34 Ohm), scan rate 10 mV/s

Figure 13 shows the Levich plot for T = 294 K. The intercept at 0.02 mA/cm^2 shows that there is only a little deviation from a perfect mass transport limited current. The limiting current of 2.51 mA/cm^2 at 294 K and 1600 rpm is in good agreement with the reported value in [25].

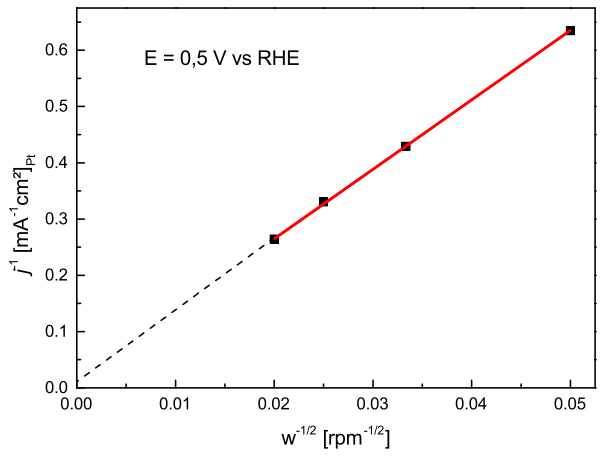

Figure 13: Levich plot for T = 294 K, values for the HOR current densities were taken from figure 14 at 0.5 V

For the rising portion of the voltammogram in figure 11 and 12 the mass transport is limited by the kinetics on the electrode surface. By extrapolation

back like shown in figure 14 the kinetic current density i_k at a certain potential was obtained.

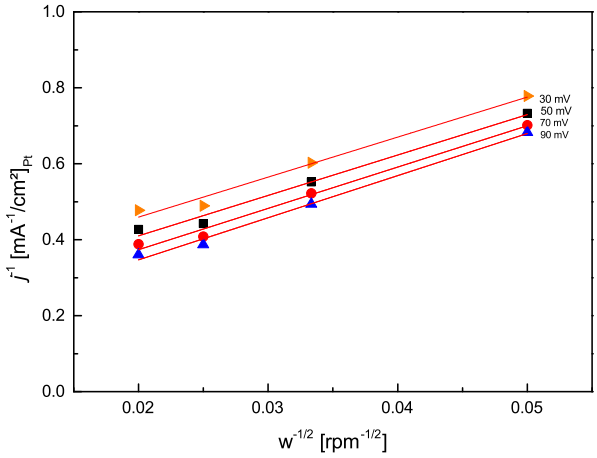

Figure 14: Kinetic current density plot for 294 K. Reciprocal current densities were plotted against reciprocal square root of the angular rotation rate for various potentials in kinetic limited area shown in figure 12. The intercept with the y-axis gives the i_k according to its potential.

The constant k in the Arrhenius equation (1) defines the rate in which a reaction attains its equilibrium. In other words, the higher the value of k the better the electrode. The exchange current density i_0 is directly proportional to k.

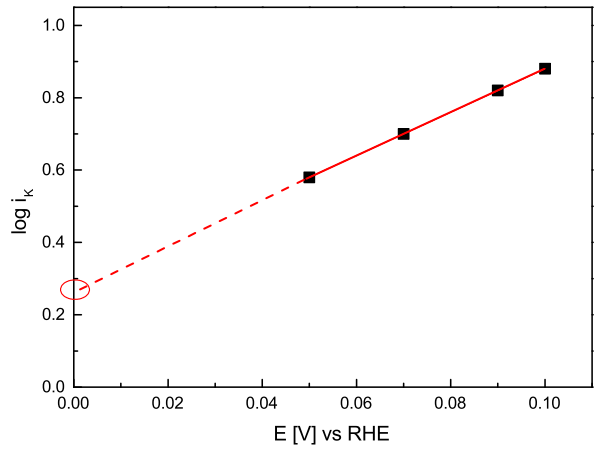

Figure 15: Plot of logarithmic i_k (294 K) versus their corresponding potentials. The intercept with the y-axis is log i_0.

In table 2 the exchange current densities are listed and compared with literature data [25]. As it can be seen the values are in good agreement with the literature data.

Table 2: Exchange current densities i_0 for different temperatures compared to literature data [25] (right). Logarithmic kinetic currents were plotted against their corresponding potentials. The intercept at the y-axis gave the logarithmic values of i_0 at each temperature.

i_0	self [mA/cm$^2{}_{Pt}$]	lit. [mA/cm$^2{}_{Pt}$]
275 K	0.32 (+/- 0.09)	0.25 (+/- 0.01)
294 K	0.69 (+/- 0.06)	0.69 (+/- 0.03)
314 K	1.25 (+/- 0.2)	1.26 (+/- 0.3)

The activation energy can be obtained by plotting the inverse temperature against the exchange current densities following the Arrhenius equation 1.

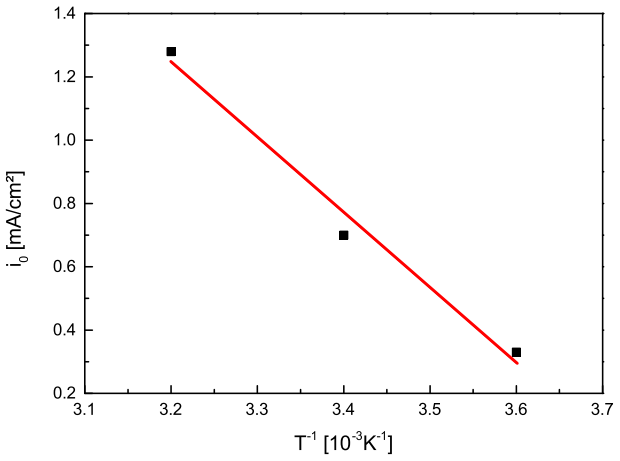

Figure 16: Representative Arrhenius plot of the HOR exchange current densities on Pt(pc) in 0.1 M KOH. The HOR activation energy E_a is 23.1 kJ/mol.

The activation energy of 23.1 kJ/mol (5.5 kcal/mol) is 5.8 kJ/mol less than the energy found in literature (E_A= 28.9 kJ/mol [25]). The fact that this energy is very small (C-H dissociation energies (alkane) lie between 370 and 550 kJ/mol) and that the literature error is 4.3 kJ/mol the value found in this work is accurate.

4.2 Electrochemical tests of possible LOHCs on Pt

The fundamental idea of a LOHC is to bind gaseous hydrogen chemically in form of a liquid which is easy to reversibly dehydrogenate, store and transport. These molecules consist of a hydrocarbon backbone $C_{backbone}H_x$ on which a certain number n of hydrogen are chemically bound $C_{backbone}H_{x+n}$. Once the hydrogen is released on site, the remaining $C_{backbone}H_x$ is reversibly recharged (hydrogenated) back to $C_{backbone}H_{x+n}$. Until now the dehydrogenation was tested at high temperatures which implies a loss of energy when used in a conventional Carnot type heat engine [3, 10]. Much higher efficiency can be obtained by using hydrogen in a hydrogen fuel cell (HFC) where chemical energy is converted to electrical energy which is again turned into mechanical energy. In a HFC hydrogen and oxygen can be combined chemically at room temperature by application of an electric potential (efficiency 50%-90% presently). The combination of LOHC and a HFC (in this case DLFC "direct liquid fuel cell") is of great interest. Therefore a system containing LOHC, solvent and catalyst need to be tested electrochemically to see if a dehydrogenation can be obtained without the formation of side products .

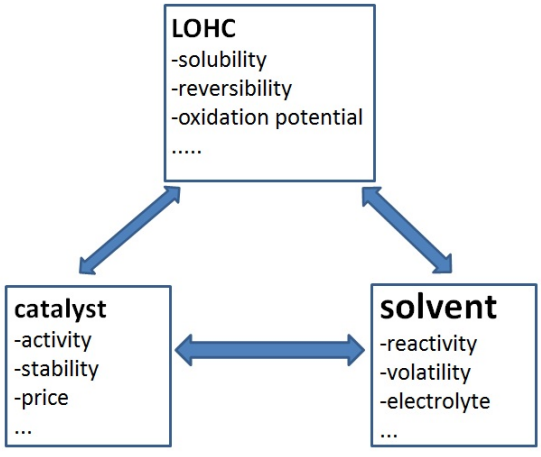

Figure 17: Relationship between solvent, LOHC and catalyst

Figure 17 shows the relationships between LOHC, solvent, catalyst and the parameters which have to be considered. A LOHC needs to carry hydrogen but it also needs to be soluble in the chosen solvent and the dehydrogena-

tion from saturated to unsaturated molecule needs to be reversible. The amount of energy needed for the oxidation of these molecules should be as low as possible, therefore molecules with low oxidation potentials are preferred. Solvents should not react under electrochemical conditions neither react with the LOHC. Activity of the catalyst as well as stability and price are only two more features of a long list which have to be dealt with. To start with the investigations solvent and catalyst were fixed components and only the LOHC was varied. Therefore Pt a known hydrogen oxidation catalyst and already used in HFC was used. As solvent acetonitrile is known to be a nonreactive solvent on a broad electrochemical potential window. All the LOHCs were soluble in this solvent. As it is already stated in the introduction the advantage of *N*-heterocycles over hydrocarbons are the weakened C-H bonds and the ability to bind to the metal surface. The most known LOHC is Dodecahydro-n-ethylcarbazole (H12-NEC) which was tested as the first molecule. Based on the experiences made with the measurements of H12-NEC ideas for other molecules were derived.

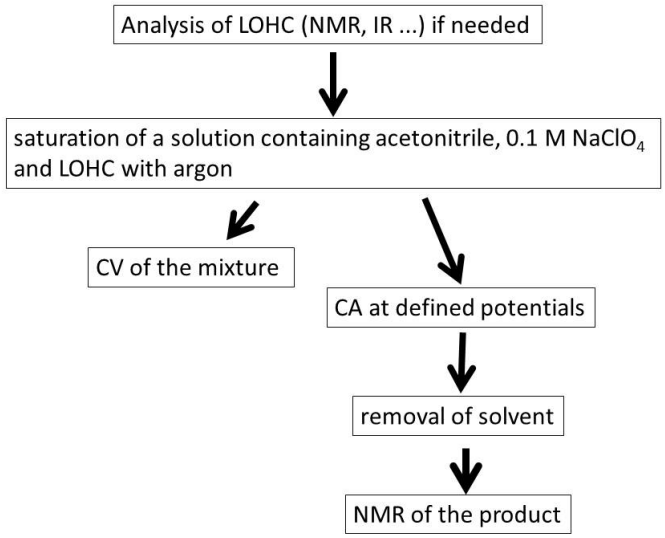

Figure 18: "Workflow" for the LOHC oxidation measurements

Partially saturated carbazoles as well as smaller molecules like pyrroldine were tested. After the measurements on Pt some molecules were tested on intermetallic phases (IMCs) to see if they show activity for an oxidation reaction. Besides *N*-heterocycles the bicyclic hydrocarbon guaiazulene which

changes its color upon hydrogenation/dehydrogenation was tested. Figure 18 shows roughly how the molecules were electrochemically tested and analyzed at room temperature. The idea is to carry out an electrochemical reaction $C_{backbone}H_{x+n} \rightarrow C_{backbone}H_x + nH^+ + ne^-$inside a DLFC.

4.2.1 Carbazoles

The following scheme in figure 19 shows the desired electrochemical dehydrogenation of a hydrogenated carbazole.

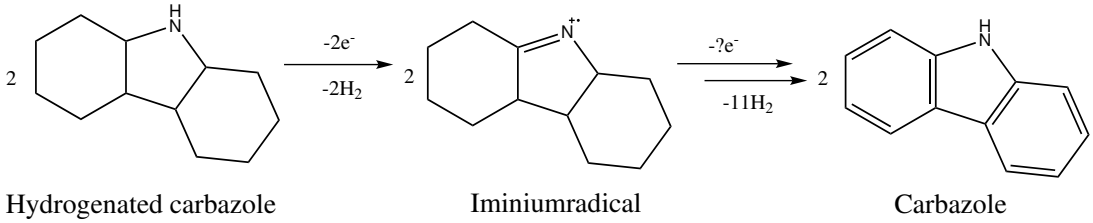

Figure 19: Electrochemical dehydrogenation of hydrogenated carbazole

Electrochemical oxidation of an amine results in a cationic radical. Further oxidation of the formed iminiumradical should result in a full dehydrogenation of the carbazole. The mechanism for this reaction and the number of electrons transfered are unknown. A carbazole with an ethyl protecting group at the nitrogen was tested.

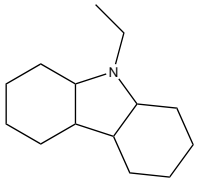

Dodecahydro-n-ethylcarbazole (H12-NEC)

Due to the fact that carbazoles became important chemicals for optoelectronics their electrochemical oxidation behavior was intensively investigated [26]. Besides optoelectronics carbazoles became popular for their use in the field of LOHC. In 2006 the DOE hydrogen program started with the investigation of LOHC which have a gravimetric hydrogen capacity of at least 7 wt% [27]. One of the first molecules tested was n-ethylcarbazole (5.7 wt%) which was

hydrogenated at 150 °C and dehydrogenated at temperatures around 150 °C on a Pd catalyst [28]. Not only that dehydrogenation temperatures were too high the formation of decomposition products could be observed. The search for other molecules with lower dehydrogenation temperatures is still going on. As already discussed electrochemical oxidation is another possibility to reach the needed energy for a dehydrogenation reaction at room temperature. This was tested with the above mentioned hydrogenated n-ethylcarbazole made by our partners (Prof. Wasserscheid, Erlangen). It was a yellowish viscous liquid which didn't dissolve immediately in acetonitrile, around 20 minutes of stirring was necessary. One part of the liquid dissolved faster than the other, so that a mixture of more than one compound was assumed. The hydrogenated composite solution was analyzed with NMR. The HMQC (figure 20) shows the couplings between the nitrogen and the adjacent (J_1 couplings) hydrogen atoms of H12-NEC. It shows a mixture of more than one product. The main product (peak at 71 ppm in the ^{15}N-NMR spectra, y-axis) shows couplings with the ethylene group at 2.65 ppm.

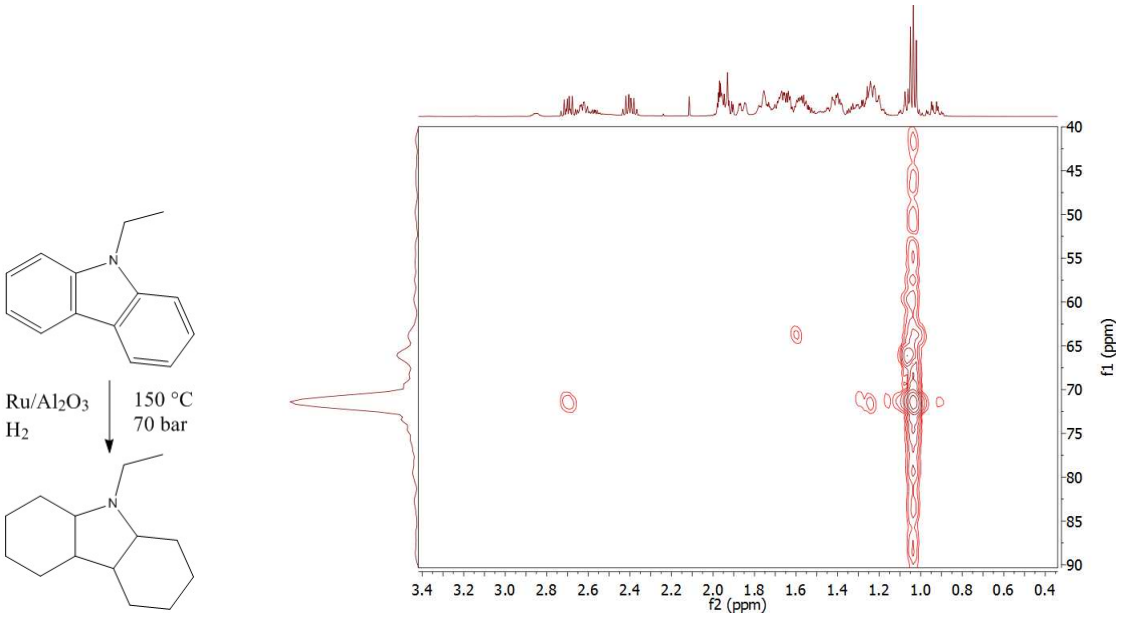

Figure 20: Left: scheme of the hydrogenation process of n-ethylcarbazole (Prof. Wasserscheid, Erlangen) Right: HMQC (in CD_3CN) of the products (x-axis (f2): ^{1}H-NMR, y-axis (f1): ^{15}N-NMR)

Also J_1 couplings of the CH groups near the nitrogen in the pyrrolidine ring are visible at 1.25 ppm. The methyl group is the most intense triplet signal

at 1.1 ppm. Methyl groups with smaller concentrations are also visible and show up near 1.1 ppm or are overlapped. A conglomeration of CH_2 signals which represent the two cyclohexane rings of H12-NEC can be seen between 1.2 ppm and 2.1 ppm in the ^{1}H-NMR spectra. The couplings of the CH_2 of the ethylene group are shown in figure 21 which result in two sextet signals and give rise to a symmetrical molecule.

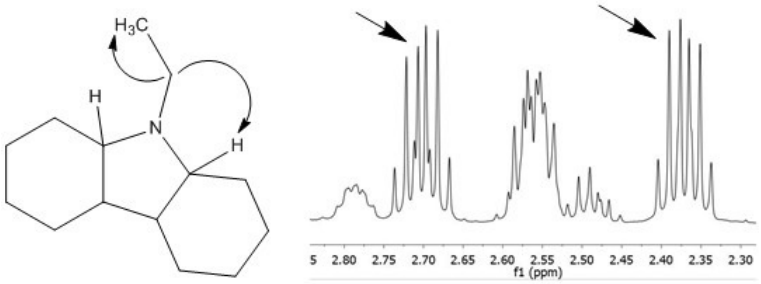

Figure 21: ^{1}H-NMR (CD_3CN, 500 MHz, TMS) of hydrogenated n-ethylcarbazole. Couplings of the hydrogen are marked with arrows.

In the middle of the two sextets (2.55 ppm) another sextet appears, it is the signal of the CH adjacent to the nitrogen atom in the pyrrolidine ring. To have a better overview of the product distribution the ^{13}C-dept spectra in figure 22 shows the carbon peaks of the H12-NEC isomers mixture.

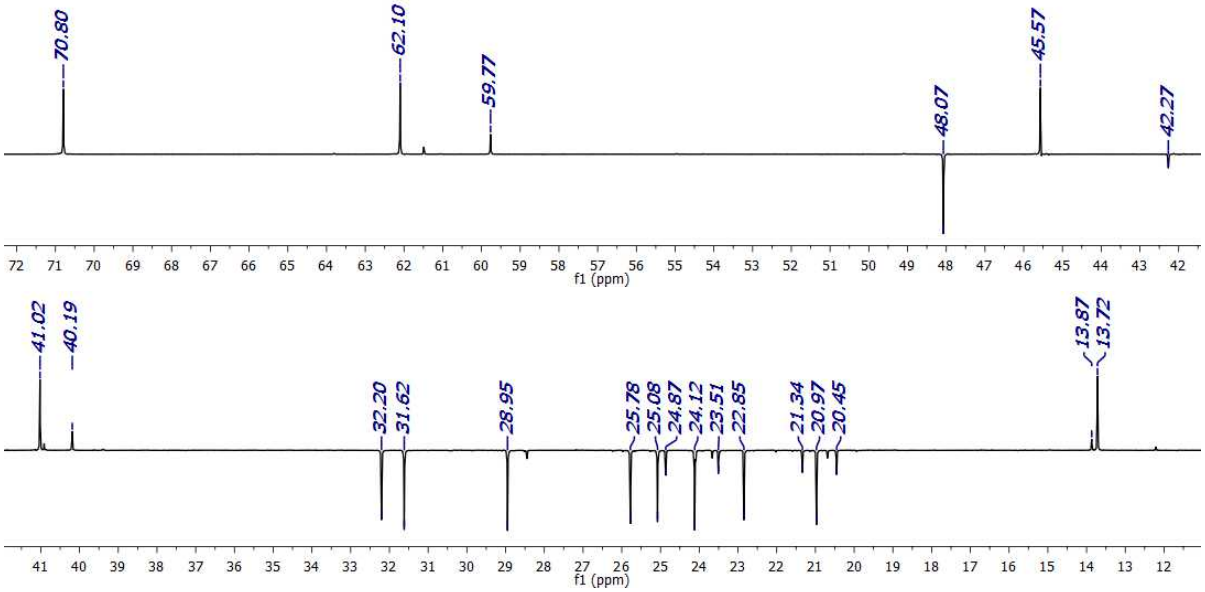

Figure 22: ^{13}C-dept NMR (125 MHz, $CDCl_3$, TMS) of H12-NEC

It shows the signals for three different isomers of H12-NEC with different concentrations. In literature 6 isomers were found upon hydrogenation of n-ethylcarbazole with an 5 wt% Ru/Al_2O_3 catalyst [29]. Three of the six isomers could be identified in the mixture (figure 23) used in these measurements.

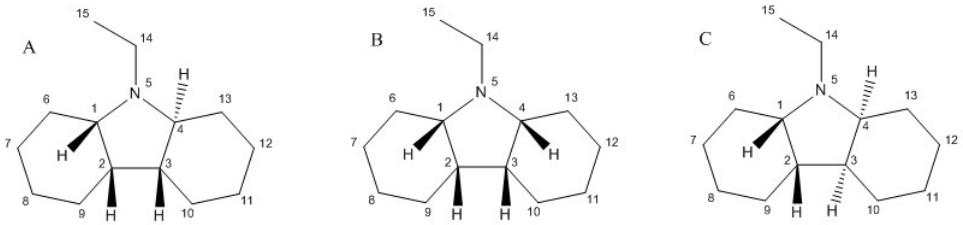

^{13}C-NMR (125 MHz, $CDCl_3$, ppm) : (**A**)δ= 70.80; 48.07; 45.57; 31.62; 25.78; 24.12; 20.97; 13.72; (**B**)δ= 62.10; 41.02; 32.20; 28.95; 25.08; 22.85 (**C**) δ= 42.27; 24.87; 23.51; 21.34; 20.45; 13.87

Figure 23: isomers of hydrogenated n-ethylcarbazole found in the mixture, A is asymmetric, B and C are symmetric molecules.

Small peaks in the gc data (supporting information figure 99) shows that besides the fully hydrogenated n-ethylcarbazole eventually partly hydrogenated n-ethylcarbazole existed in the mixture. IR measurements (supporting information figure 98) show the broad NH peak at around 3300 cm^{-1} and signals of saturated C-H vibrations between 2700 and 3000 cm^{-1}. A small shoulder at around 3000 cm^{-1} could be an IR stretch band of an alkene.

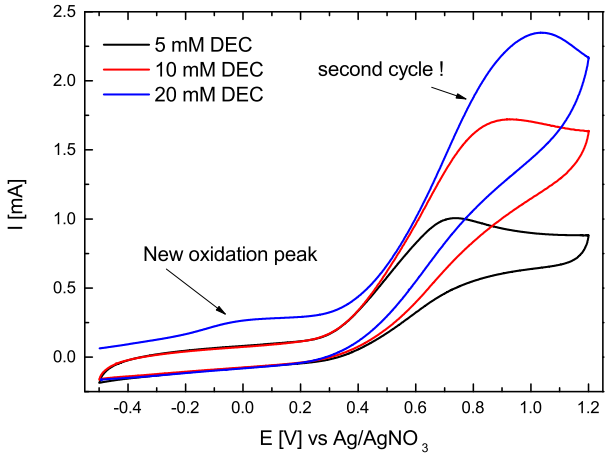

Figure 24: CVs of H12-NEC in acetonitrile and 0.1 M $NaClO_4$ on Pt, scan rate 50 mV/s. Concentrations of H12-NEC were doubled for each cycle. In case of 20 mM the second cycle of the CV is shown.

The CV of H12-NEC in figure 24 shows an irreversible reaction. Increase in concentration of H12-NEC resulted in higher currents and a shift of the current maximum. When cycled a second time a new oxidation peak became visible at around 0 V. This indicates that H12-NEC gets oxidized and forms a new compound with a lower oxidation potential. The CA measurement (figure 25) at a constant potential of 0.8 V for about 18 hours resulted in the formation of a colorless/yellowish precipitate on the catalyst surface which could be the reason for the current drop which is visible in the figure.

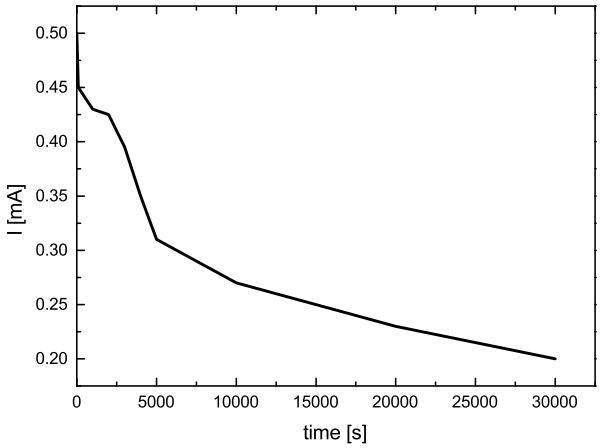

Figure 25: CA at 0.8 V on Pt of H12-NEC in CH_3CN, 0.1 M $NaClO_4$ on Pt

The shift of the ^{1}H-NMR peaks to higher ppm is a sign for the formation of a cationic radical which is a typical reaction for the electrochemical oxidation of amines (see full ^{1}H-NMR spectra in figure 89 in the supporting information).

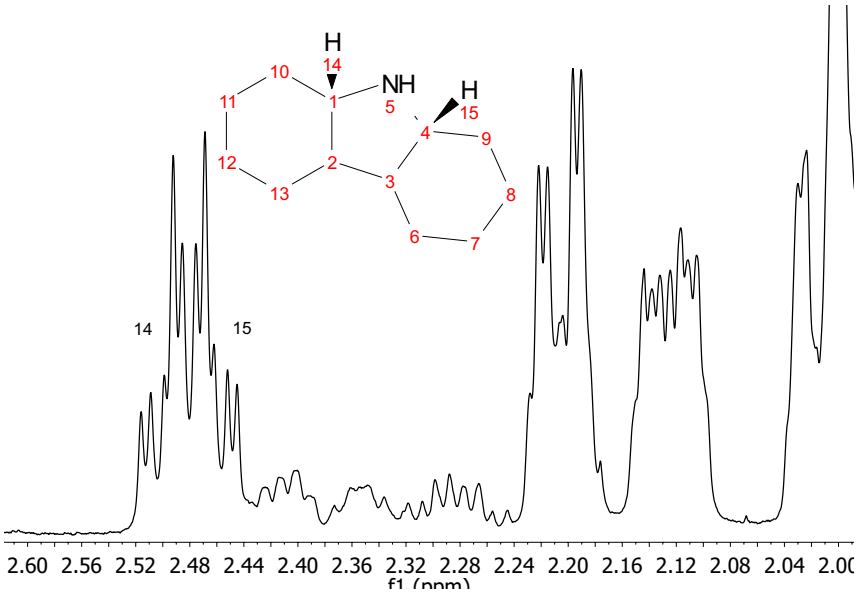

Figure 26: ^{1}H-NMR ($CDCl_3$, 500 MHz, TMS) of oxidized H12-NEC

A closer look to the NMR of the oxidized H12-NEC shows the signals for the H-atoms adjacent to the amine group of the pyrrolidine ring between 2.1 ppm and 2.7 ppm in figure 26. The additional peaks are a result of an isomeric mixture of H12-NC (dodecahydro-carbazole) which show up in the same shift region as H12-NEC. Decrease of current which is visible in the CA could be the result of the deethylation of H12-NEC and an adsorption of H12-NC on the surface of the catalyst. Formations of cationic radicals with a dealkylation of tertiary *N*-heterocycles by electrochemical oxidation could already be observed with molecules like a substituted tertiary tropane [30].

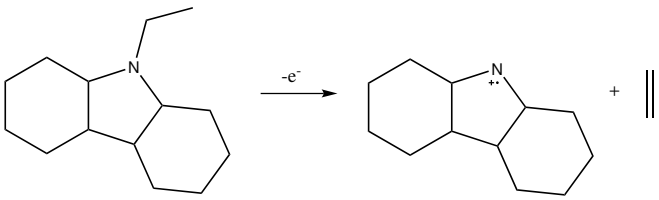

Figure 27: Scheme of the deethylation of H12-NEC to H12-NC

The ^{13}C-NMR and ^{1}H-NMR (figures 89 and 90 in supporting information) of the product shows no sign of a dehydrogenation of H12-NC or H12-NEC to a unsaturated molecule. Only the mentioned product on the surface of the catalyst could be found which was yellow and insoluble in acetonitrile. Upon oxidation the chemical peak shift moved upfield so that a cationic

aminiumradical is supposed. The formation of an iminiumradical could not be detected. If a dehydrogenation of H12-NC/H12-NEC would have been successful at 0.8 V a direct formation to a green product would have followed which will be discussed for the case of octahydro-n-ethylcarbazole later on [31]. The cause for the undesired reaction and no dehydrogenation could be a result of the the molecule being fully saturated. The fact that only the nitrogen is affected by electrochemical oxidation supports the assumption. The reactivity towards electrochemical oxidation of unsaturated carbazoles on Pt seems to be very low so that a partially saturated carbazole was tested. Carbons which are sp^2 hybridized are easier to attack than sp^3 ones. Therefore 1,2,3,4-tetrahydrocarbazole (H4-NEC) was bought and tested.

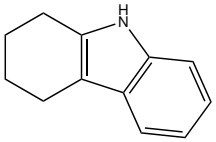

H4-NEC can be seen as one of the possible intermediates of the electrochemical oxidation of H12-NEC which loses its ethyl group. H4-NEC was already electrochemically oxidized in aqueous acetonitrile at 0.7 V (vs SCE) with the result of different dimers postulated [32]. Measurements in unaqueous acetonitrile were not done and it would be of great interest if the partially saturated ring gets dehydrogenated or not. If this part of the molecule doesn't take part in any reaction during the electrochemical oxidation on Pt, electrochemical oxidation of hydrogenated carbazoles on Pt could be the wrong choice for a LOHC system. In contrast to the ethylcarbazole H4-NEC has no nitrogen protecting group, a stronger nitrogen metal interaction was expected. CVs in acetonitrile (figure 28) show three oxidation peaks. The first peak is visible at 0.6 V (vs $Ag/AgNO_3$) and is higher than the oxidation potential in aqueous acetonitrile [32]. The second oxidation peak and the third oxidation peak are visible at 0.75 V and 0.9 V respectively.

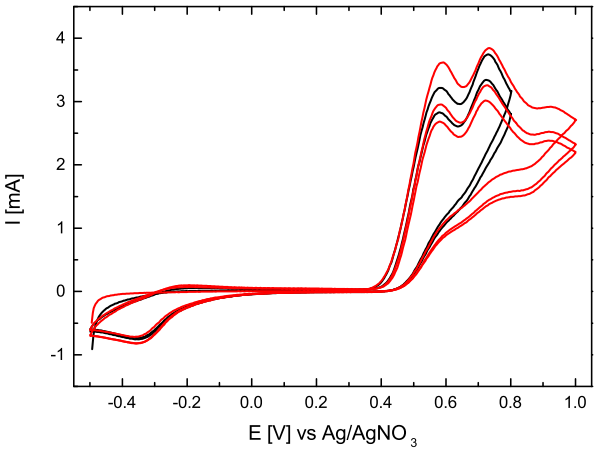

Figure 28: CVs (two potential ranges) of H4-NEC in acetonitrile and 0.1 M $NaClO_4$ on Pt, scan rate 50 mv/s

Besides the three oxidation peaks a reduction peak is visible at around -0.4 V vs $Ag/AgNO_3$. The oxidation at 0.6 V for about 16 hours showed no sign of adsorption on the catalyst surface or a change in the molecule color.

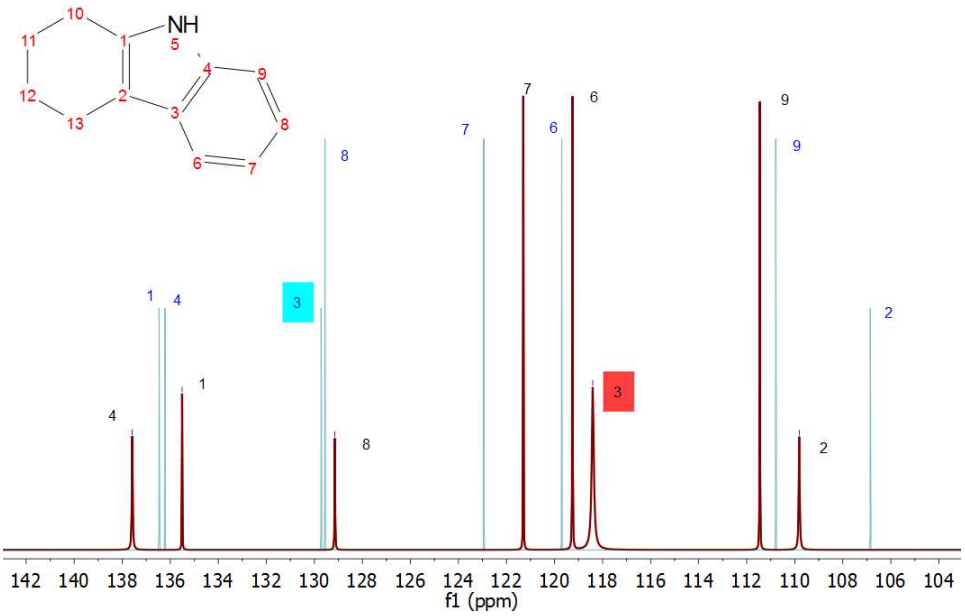

Figure 29: ^{13}C-NMR (MeOD, 125 MHz, TMS) of oxidized H4-NEC at 0.6 V for 15 hours (red) and H4-NEC unoxidized (blue)

^{13}C-NMR in figure 29 shows a change in the shifts of the pyrrole carbon atoms with nearly no change of the aromatic carbon shifts. The lack of a

quaternary carbon in the range of 50 to 80 ppm shows that no dimerisation occurred during the electrochemical oxidation process (CA shown in figure 100 in supporting informatiom). Oxidation at 0.6 V turned the H4-NEC molecules into cationic radicals which are stabilized via mesomerism like it is shown in figure 30.

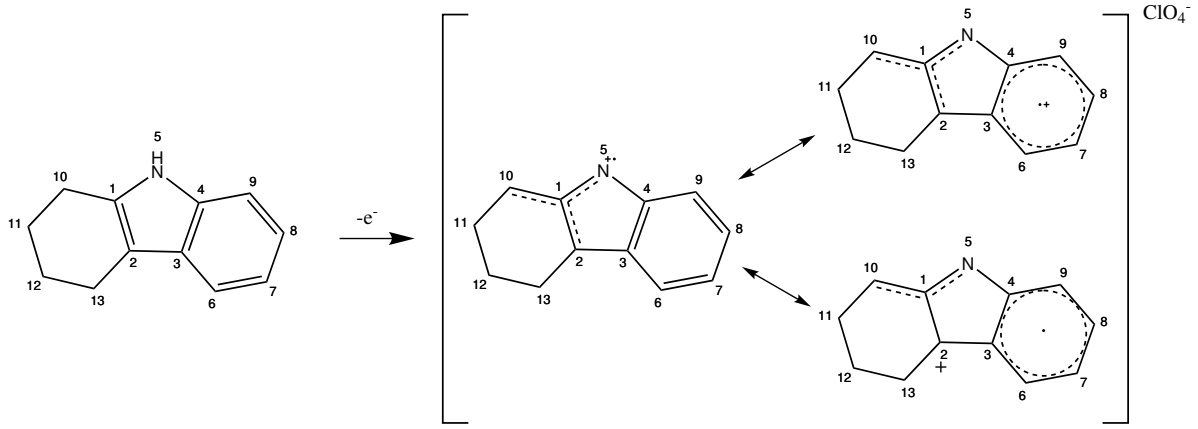

Figure 30: Oxidation of H4-NEC at 0.6 V to a cationic radical

A drastic change of the chemical shift of carbon in 3rd position shows a change in the reactivity of the pyrrole ring. As it is shown in the scheme the carbon in 2nd position forms a cation which is favored for a nucleophilic attack upon further oxidation.

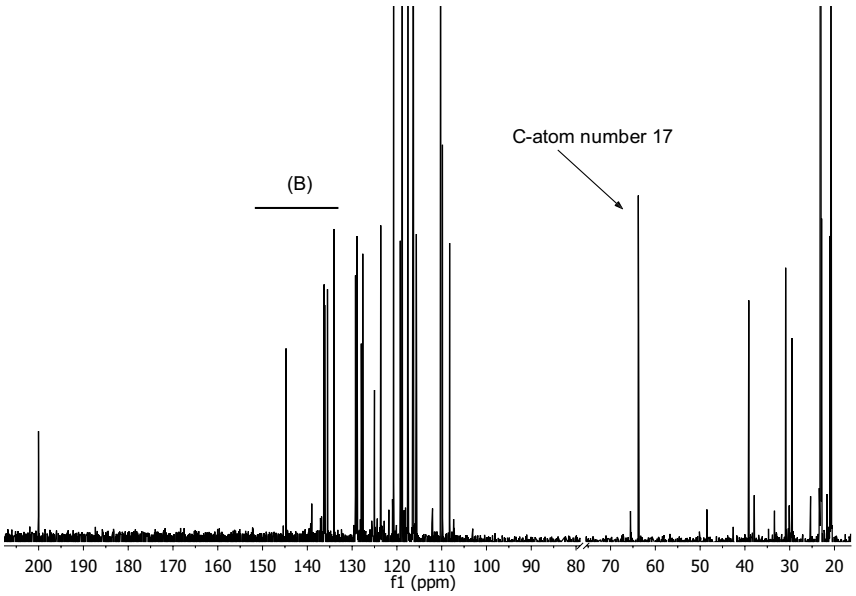

Figure 31: ^{13}C-BB of oxidized H4-NEC at 0.75 V (MeOD, 125 MHz, TMS)

The ^{13}C-BB NMR in figure 31 of H4-NEC oxidized at a potential of 0.75 V

shows a new peak at 62 ppm which is not visible in the ^{13}C-dept (figure 32) spectra.

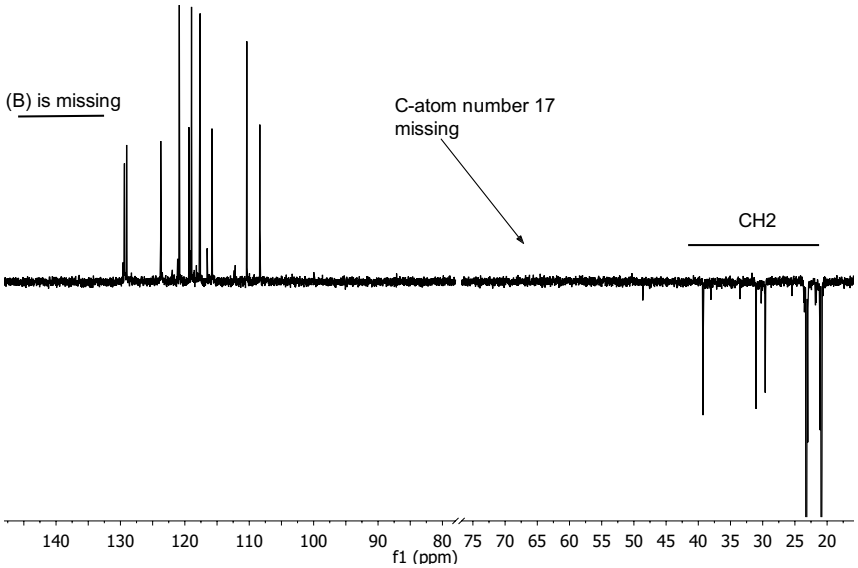

Figure 32: ^{13}C-dept of oxidized H4-NEC at 0.75 V (MeOD, 125 MHz, TMS)

As we know only quaternary C-atoms are not visible in a ^{13}C-dept spectra. Calculations of every possible dimer have shown that a quaternary C signal in this shift region belongs to C-17 (circled red in figure 33). Compared to unoxidized H4-NEC the quaternary C signals in the range between 135 and 145 ppm (group B) have doubled and shifted upfield. All other signals for the aromatic ring as well as for the saturated ring have also doubled and show up in the same shift region as the unoxidized H4-NEC.

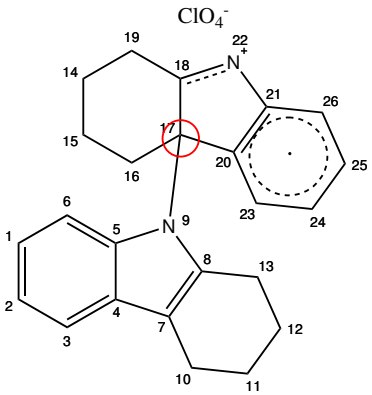

Figure 33: Radical dimer formed at 0.75 V

The cationic radical dimer formed via a nucleophilic attack of the nitrogen lone pair of an unoxidized H4-NEC molecule at the cationic carbon in 2nd

position of an oxidized H4-NEC. It has been shown that an oxidation of H4-NEC in acetonitrile shows a different dimer when water is absent [32] but a dehydrogenation could only partially be achieved. The change from fully saturated to a partially saturated carbazole did not change the reactivity as wanted. As already seen with H12-NEC the saturated ring is not affected by electrochemical oxidation on Pt. Other than H12-NEC the unprotected amine in H4-NEC shows reactivity which leads to a head to tail dimerisation. A dehydrogenated H12-NEC would lead to a tail to tail dimerisation as it will be discussed in the case of octahydro-n-ethylcarbazole (H8-NEC) in chapter 4.3.1.

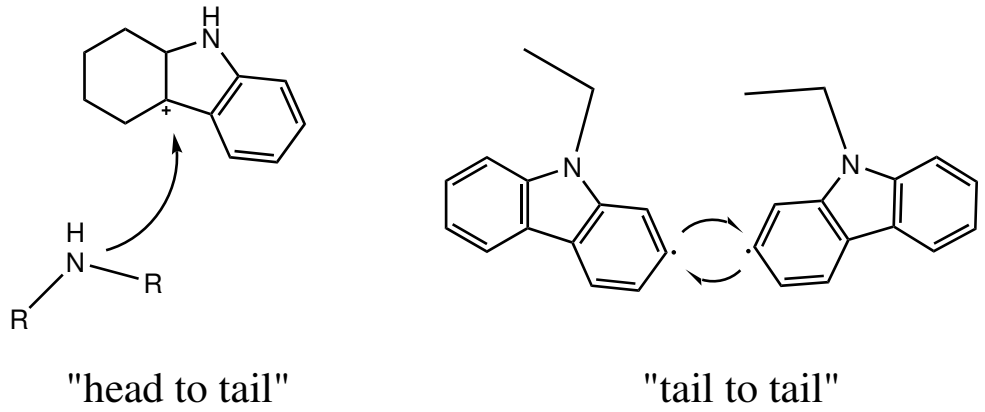

Figure 34: Scheme of carbazole dimerisation

Figure 34 shows the two possible dimerisation reactions. The two tested carbazoles showed no dehydrogenation reaction when electrochemically oxidized on Pt. Therefore simpler and smaller *N*-heterocycles were tested.

4.2.2 Simple *N*-heterocycles

Due to the fact that electrochemical oxidation of carbazoles on Pt only resulted in different unwanted products, simpler molecules with only one ring were measured. The electrochemical oxidations should result in more predictable reaction products. Like it is shown for carbazoles the dehydrogenation should be initiated by the formation of iminiumradicals. Piperidine which was already electrochemically oxidized on Pt and Hg electrodes in aqueous solutions formed *N*-oxides in water [33].

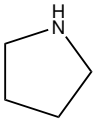

Pyrrolidine

Measurements in this work were done in deareated acetonitrile with the aim to avoid the formation of *N*-oxides. Pyrrolidine which has a five membered ring should be easier to dehydrogenate than piperidine which is a six membered ring [7]. Furthermore a dehydrogenation to pyrrole should be visible immediately due to polymerization to polypyrrole. The polymerization potential of pyrrole is expected to be lower than the dehydrogenation potential of pyrroldine. A polymerization (figure 35) is an unwanted reaction but the reaction of pyrrole to polypyrrole is a very well known one [34] and would be a good indicator for a dehydrogenation reaction of pyrrolidine.

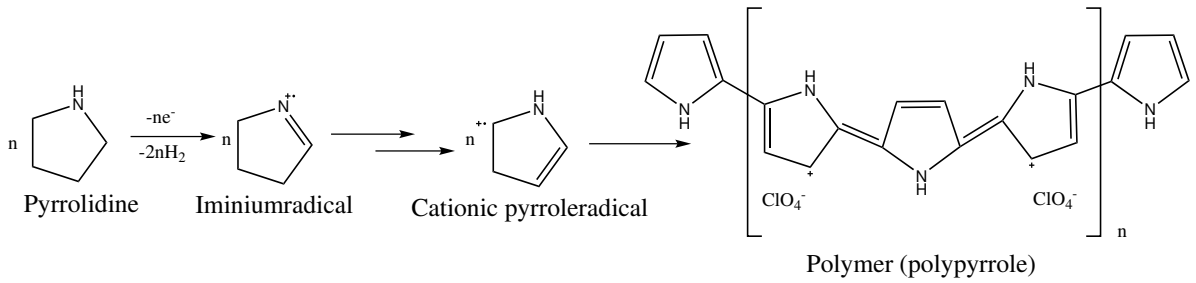

Figure 35: Possible dehydrogenation of pyrrolidine to pyrrole with following polymerization to polypyrrole scheme

Measurements in acetonitrile and $NaClO_4$ under argon showed only negligible activity. A change in color from yellowish/colorless to yellow was visible when oxidized at 0.8 V and 1 V vs $Ag/AgNO_3$. The peaks in the ^{1}H-NMR (500 MHz, D_2O, TMS δ ppm : 1.95 (4H, t); 3.23 (4H, t)) and in the ^{13}C-NMR (125 MHz, D_2O, TMS δ ppm : 23.40; 45.60) remained almost unchanged in chemical shift. It seems that this molecule interacted very strong with the catalyst surface and formed a strong passivating layer which was visible after 5 minutes regardless which oxidation potential applied. Much more interesting was the oxidation/reduction under air which will be discussed later (CVs and discussion in chapter 4.6). The next tested molecule, a seven membered *N*-heterocycle, showed different behavior when electrochemically oxidized.

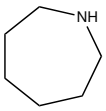

Azepane

No polymerization or dimerisation reactions are known for azepane. With around 6 wt% hydrogen capacity it is not far away from the DOE standards of 7 wt%. A thermal dehydrogenation leads to 1H-azepine which is in equilibrium with an aziridine derivate [35].

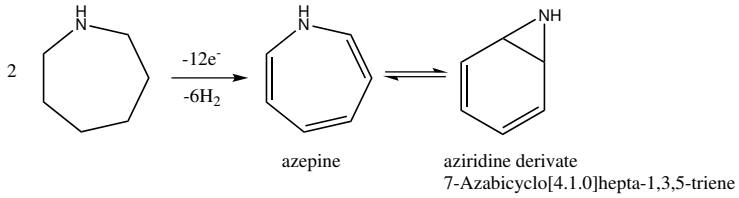

Figure 36: Possible electrochemical dehydrogenation of azepane scheme

The fact that azepane could dehydrogenate to two different molecules (figure 36) makes it difficult to hydrogenate it back to azepane. A mixture of reactants or products is unwanted. Nevertheless the reactivity and its affinity towards a ring opening reaction makes azepane an interesting molecule for an electrochemical oxidation which could lead to different reaction pathways and to a dehydrogenation.

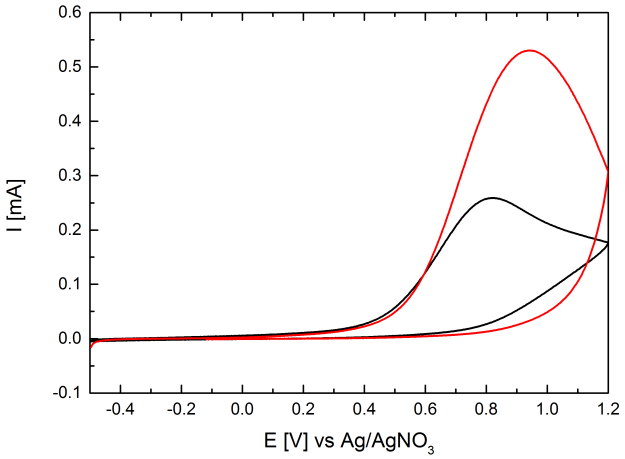

Figure 37: CVs of azepane (black: 10mM; red: 20 mM) in acetonitrile/0.1 M $NaClO_4$ on Pt, scan rate 50 mV/s

The CV in figure 37 shows two cycles with different concentrations of azepane. Clearly visible the increase of current due to a higher concentration of azepane.

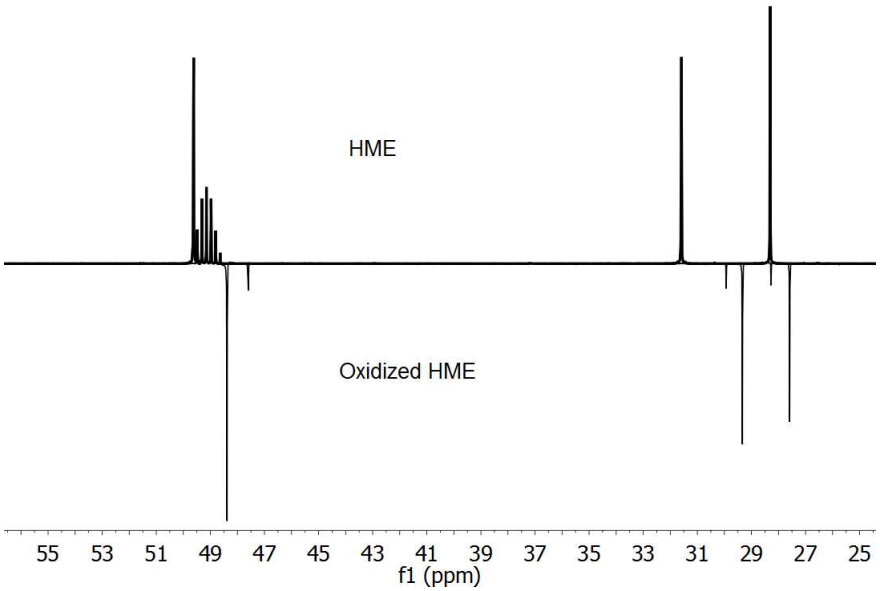

Figure 38: top: ^{13}C-BB ($CDCl_3$, 125 MHz, TMS) of unoxidized azepane (HME) down: ^{13}C-Dept of azepane oxidized at 0.8 V

CA measurements at 0.8 V vs $Ag/AgNO_3$ for around 16 h gave a cation and a cationic radical species. As it is shown in the ^{13}C-NMR spectra in figure 38 a shift to lower ppm of all ^{13}C signals could be observed. In figure 39 the ^{13}C signals are assigned to the CH_2 of azepane. The numbers in brackets represent the loss of shift due to electrochemical oxidation. Three additional peaks (47.60 ppm, 29.93 ppm, 27.59 ppm) with lesser intensity is azepane as a cation or a cation radical. It is not sure if the radical nature of the oxidized molecule remains after the electrochemical oxidation. Other than tetrahydrocarbazole azepane has no aromatic ring to stabilize a radical by mesomerism.

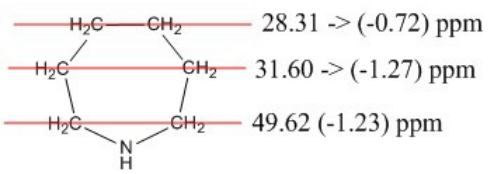

Figure 39: Azepane ^{13}C-NMR shifts before and (after) oxidation

Only the nitrogen atom is involved in the electrochemical oxidation, a reac-

tion at the ring could not be detected. Like carbazoles smaller $N-$heterocycles are affected the same way by electrochemical oxidation on Pt. Only the nitrogen lone pair is involved in a reaction. In this chapter different molecules were tested, in the next chapter different catalysts are tested for their electrochemical behavior towards dehydrogenation of N-heterocycles.

4.3 Electrochemical tests of possible LOHCs on Intermetallic Phases (IMC)

The previous results have shown that electrochemical dehydrogenation of N-heterocycles is not an easy task. Pt has shown currents but only the formation of cationic radicals, dimers or polymers resulted. As it is known from a lot of reactions in chemistry, different catalyst can drive reactions into different pathways. Intermetallic compounds (IMC) have special physical and chemical properties which makes them interesting and useful materials for a variety of applications. Also on the field of heterogenous catalysis IMCs have become an important material. Semi-hydrogenation of acetylene and methanol steam reforming are some of the applications in which IMCs are useful [36]. The IMCs MoSi, $Mo_{46.15}Co_{41.85}Si_{12}$, $Mo_{33.33}Co_{46.67}Si_{20}$, Mo_6Co_7, MoCoSi, $MoAl_{12}$, $ReAl_{12}$, WAl_{12}, $PtAl_2$ and $PtSn_4$) were used as working electrodes. Unit cells for $PtAl_2$ and $MoSi_2$ are shown in figure 40.

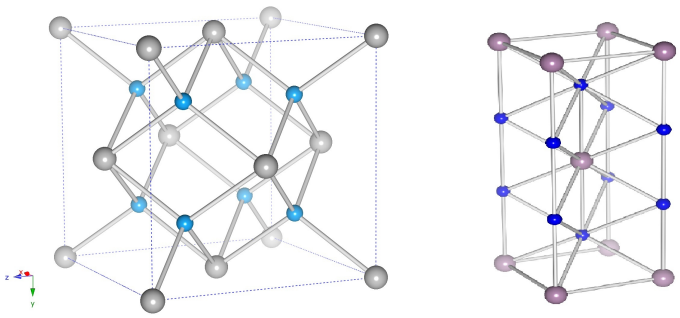

Figure 40: Crystal structures of $PtAl_2$(left) and $MoSi_2$ (right)

The structure type for $PtAl_2$ is $CaF_2$where each Pt (blue) atom is tetrahedrally coordinated by four Al atoms and each Pt atom cubical by eight Al atoms. There is no Pt-Pt or Al-Al bonds unlike in bulk Pt or Al. The $MoSi_2$

structure shows some Mo-Mo bonds but most of the bonds are Mo-Si. Other compounds like $MoAl_{12}$ or $ReAl_{12}$ or WAl_{12} which are isostructural (structure prototype W_6Fe_7) show similar bonding situations where Mo-Mo or Re-Re bondings are non existent. Electronic structures compared to bulk metals are changed and so the catalytic properties. All IMCs were synthesized and characterized at the MPI Cpfs (Max planck institute for chemical physics of solids) by the group of Prof. Yuri Grin. catalysts were tested concerning the electrochemical oxidation of *N*-heterocycles.

4.3.1 Octahydro-n-ethylcarbazole (H8-NEC)

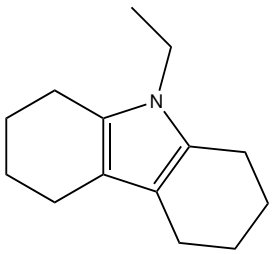

As it was shown electrochemical oxidation of H12-NEC resulted in a deethylation to H12-NC. H8-NEC which is only partly saturated is one possible dehydrogenation product of H12-NEC but also an intermediate of the hydrogenation from n-ethylcarbazole to H12-NEC (figure 41). Double bonds in the pyrrole ring may lead to a different reaction rather than a deethylation.

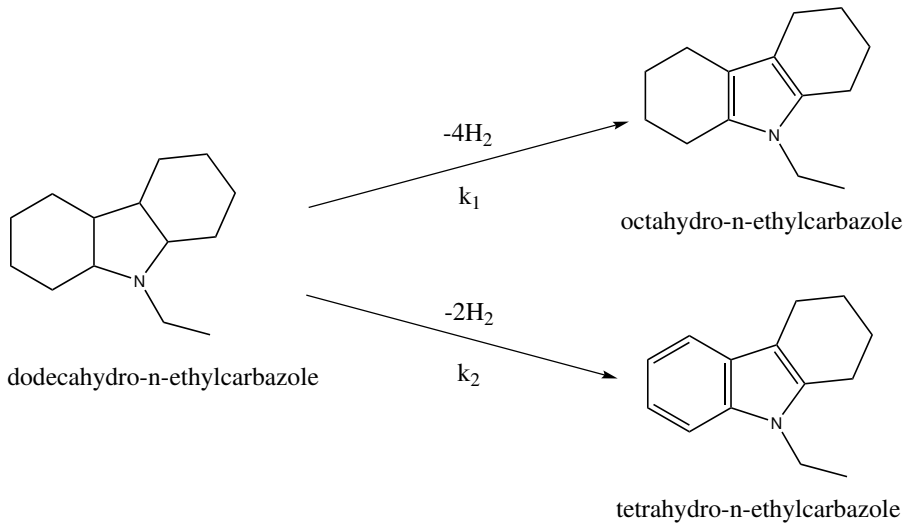

Figure 41: Two dehydrogenation intermediates for the thermal dehydrogenation of H12-NEC

H8-NEC was found to be a stable intermediate and is the main product of the dehydrogenation at temperatures between 140 and 170 $°C$ [28]. The dehydrogenation process of H12-NEC can be summed up like this: H12-NEC $\rightarrow$ H8-NEC + H4-NEC (in minor concentration)$\rightarrow$ H4-NEC $\rightarrow$ NEC. A thermal dehydrogenation to the full saturated molecule was possible but needed high temperatures and the formation of decomposition products on the catalyst surface could be observed [37]. An electrochemical approach to overcome the energy barrier for the full dehydrogenation is tested with various catalysts. As it is known it is much easier to attack a sp^2 hybridized carbon atom than a sp^3 hybridized one, therefore the partially unsaturated character of H8-NEC could help the dehydrogenation process. Tests with the fully unsaturated n-ethylcarbazole in acetonitrile/$NaClO_4$ have shown that it formed a green film which moved from anode to cathode. If a dehydrogenation of H8-NEC would succeed it would immediately form the green film which is known in literature [38]. Electrochemical measurements (figure 42) showed activity for all catalysts tested. Glassy carbon (gc) was by far the best catalyst for the oxidation reaction. With an onsetpotential of around 0.1 V and very high electron transfer kinetics (steep rise of current) it was much better than all the other catalysts. The noisy behavior of the linear sweep starting at 0.4 V is an indicator for drastic reactions happening on the catalyst surface.

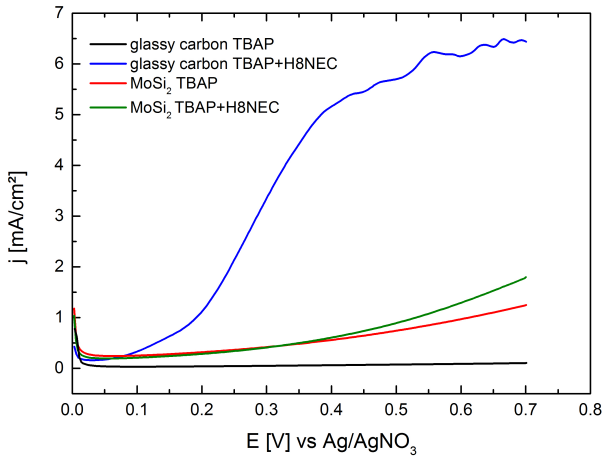

Figure 42: Linear sweep voltammetry of acetonitrile/0.1 M TBAP on gc and $MoSi_2$with and without H8-NEC, scan rate 10 mV/s

A green film formed immediately when the potential of 0.4 V on a gc pellet was achieved. The film emigrated from the anode in the direction of the cathode as it was observed when n-ethylcarbazole was electrochemically oxidized on gc. After the electrochemical oxidation the green film dissolved. $MoSi_2$ and other IMCs showed minor currents and also no reaction. In literature a green cationic radical associated to ClO_4^- (figure 43) is proposed [38]. Depending on the substitution at the amine group of the carbazole, the choice of solvent and electrolyte the color of the dimer can be changed.

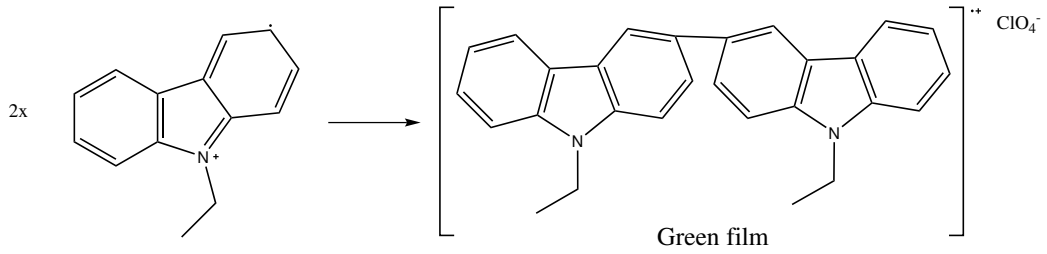

Figure 43: Electrochemically induced radical dimerisation of n-ethylcarbazole

The radical dimer was stable for around 1 to 2 hours depending on the concentration and the oxidation time. Further analysis was not possible due to decomposition when the solvent was removed. The formation of the dimer was certainly due to some n-ethylcarbazole which was not hydrogenated or only partly saturated during the hydrogenation process [39]. The IMCs showed activity but no formation of a film. Compared to the IMCs the gc anode showed high currents which are the result of a fast electron transfer between surface of the gc to the molecule.

4.3.2 2-Methylpiperidine in water

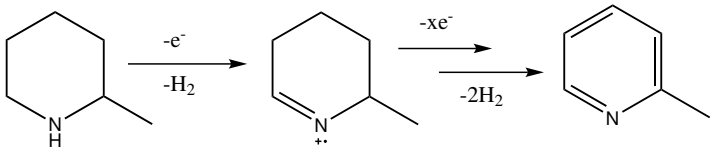

Piperidine with a methyl group in α position was measured. The inductive effect of the methyl group changes the reactivity of the amine group compared to piperidine but also the reactivity of the ring. As it was already shown

simple *N*-heterocycles like pyrrolidine sticked to the surface of the catalyst and no dehydrogenation could be achieved. In the work of D. Wechsler [40] an introduction of a sterical hindering group near the amine functional group increased the thermal dehydrogenation rate. Furthermore a catalyst poisoning or autoinhibition by the strong binding of *N*-heterocycles on the metal surface would be less likely [41]. 2-methylpiperidine is soluble in water and was measured in a 0.1 M $NaClO_4$ solution (4 mM, pH = 9.6).

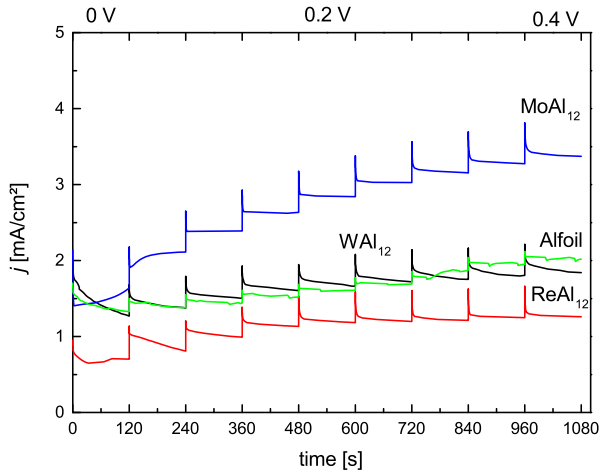

Figure 44: Stepwise CA of 4 mM 2-methylpiperidine in H_2O/ 0.1 M NaClO on Al containing catalysts

Figure 44 shows the Al containing catalysts which all show activity, even at open circuit potential a current was visible. The formation of Al_2O_3 on the surface of the catalyst, which is known for Al in alkaline solution, was the reason for the currents observed. Al_2O_3 was visible as a black powder which formed on the catalyst surface. Al foil was also tested and showed the same behavior in this solution. The CV of a $Mo_xCo_ySi_z$ catalyst showed a different behavior. Other than the Al containing catalysts the $Mo_xCo_ySi_z$ catalysts showed degradation at higher oxidation potentials which is visible at around 0.5 V in figure 45. The surface of the catalyst changed to a black powder at this potential. Metal oxides like Mo oxides are known to form in H_2O and electrochemical oxidation certainly enhanced the formation.

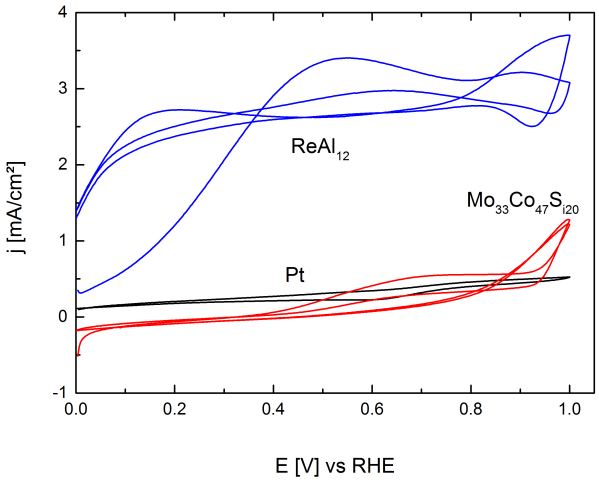

Figure 45: CVs of 4 mM 2-methylpiperidine in H_2O/0.1 M $NaClO_4$ on different IMCs and Pt, scan rate 50 mv/s

$PtAl_2$ was examined by X-ray Photoelectron Spectroscopy (XPS). The near surface depth profiling of $PtAl_2$ in figure 46 showed that the metal surface is essentially made of $Al_2O_3 > 15A$ of depth.

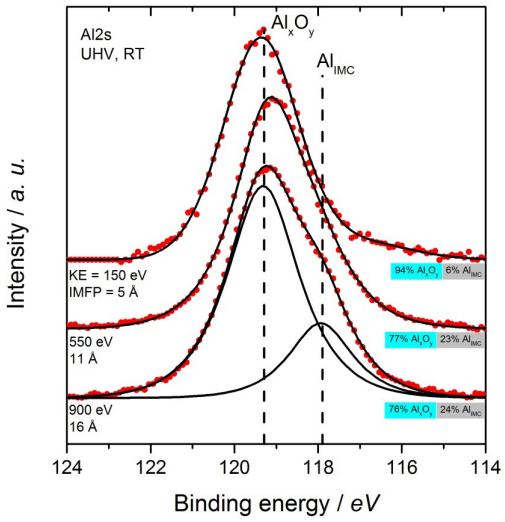

Figure 46: XPS of $PtAl_2$ IMC (untreated)

The annealed and etched (in 25 % ammonia/H_2O solution) $PtAl_2$ is shown in figure 47 showing lower amounts of Al_2O_3 but still most of the surface was covered by the oxide.

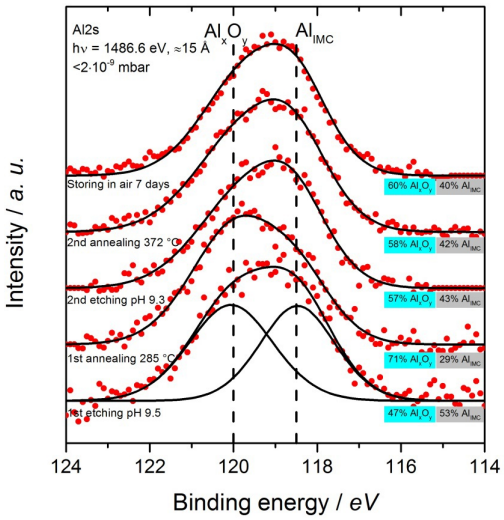

Figure 47: XPS of $PtAl_2$ IMC (annealed and etched)

The surface of the catalyst was composed of Al_2O_3 and Pt metal and the bulk was $PtAl_2$. All of the IMCs showed no activity or only small currents which could be attributed to the formation of a cationic radical. Electrochemical oxidation on Pt showed the formation of *N*-oxides in water which was visible by a yellow coloration of the mixture. The measurements have shown that the IMCs are not stable in aqueous medium.

4.3.3 2-Methyldecahydroquinoline (MDQ)

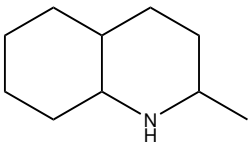

MDQ has a methylene group in second position to protect the nitrogen lone pair like it is the case for 2-methylpiperidine. Due to a second six membered ring it carries much more hydrogen than piperidine. NMR data (shown in the supporting information, figure 93 and 94) shows a mixture of more than two substances in the mixture. Due to the lack of signals in the double bond shift area in ^{1}H-NMR and ^{13}C-NMR spectra fully saturated molecules are expected in the mixture. MDQ was made by a reduction of quinaldine

by our partners in Erlangen. From literature a partly hydrogenation of 2-methylquinoline is known [42] and in another work a fully hydrogenation was tried but product isolation failed [43]. From the data in literature and the NMR spectra side products cannot be excluded. Electrochemical oxidation was tested on different IMCs using CV technique (figure 48). The most active IMC is $ReAl_{12}$ followed by the $Mo_xCo_ySi_z$ compounds. Most of the CVs show oxidation and reduction currents which eventually implies a partial oxidation of MDQ on the IMC surface. As we discussed before the informations about chemical properties and hydrogenation of 2-methylquinoline to MDQ is extremely scarce in literature so that the currents during the electrochemical oxidation could be the result of the formation of a MDQ cationic radical coupled with the degradation of the IMCs.

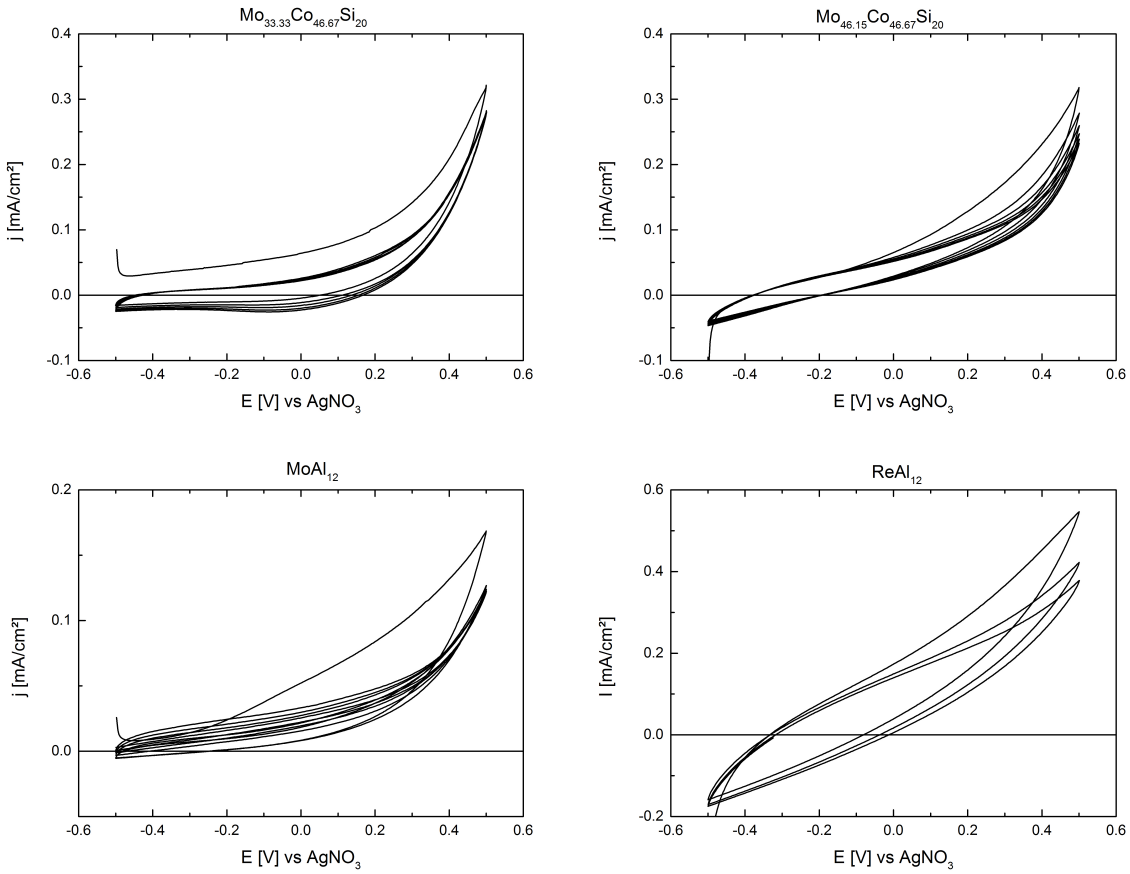

Figure 48: CVs of MDQ in acetonitrile/0.1 M TBAP on different IMCs, scan rate 50 mV/s

Compared to the CVs of the $Mo_xCo_ySi_z$ catalysts the Al containing catalysts

show high current resistance. Obviously the dielectric Al_2O_3 formed of the surface of the catalysts. Measurements to higher potentials (figure 49) shows that Pt was the most active catalyst. The Mo based catalysts showed a formation of black precipitate on the surface which was a oxidative degradation of the catalyst surface.

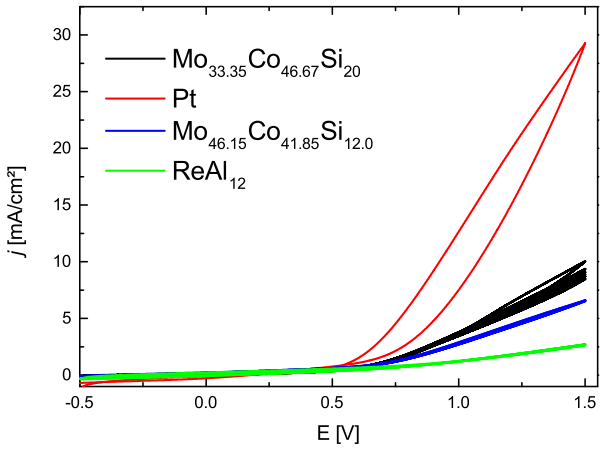

Figure 49: CVs of MDQ in acetonitrile/0.1 M TBAP on different IMCs, scan rate 200 mV/s

As it is already shown with azepane or H4-NEC an unstable cationic radical formed during the electrochemical oxidation on Pt and the IMCs. The IMCs didn't show any reaction towards a dehydrogenation reaction like it was the case for Pt.

4.3.4 Indoline

Due to the fact that electrochemical dehydrogenation of indoline on Pt or Pd is known it was tested on the Pt consisting IMC $PtAl_2$. The electrochemical dehydrogenation should be visible because of a direct polymerization of indole [44, 45, 46].

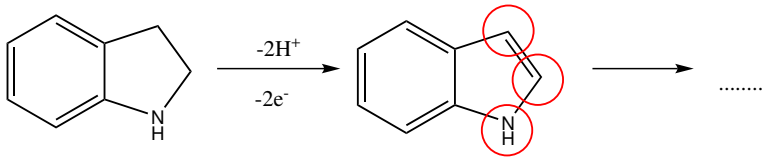

Figure 50: Electrochemical dehydrogenation of indoline to indole and possible attack sites for a polymerization reaction

In figure 50 the possible attack sites for a electrochemical oxidation reaction are marked with a circle. A dehydrogenation should be easy visible due to a colorless polymer forming on the catalyst surface. Indoline is a good choice to test if IMCs are capable of dehydrogenation reactions or not.

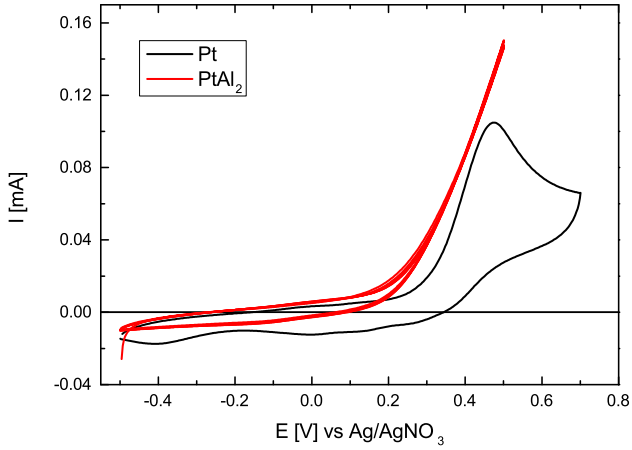

Figure 51: CVs of 10 mM indoline in acetonitrile/0.1 M $NaClO_4$, 50 mV/s

The CV on Pt in figure 51 shows an oxidation peak at around 0.4 V. A polymer was visible on Pt after 1 h of chronoamperometric measurement at 0.5 V (supporting information figure 101). Some smaller reduction peaks were visible due to the formation of the polymer on the catalysts surface. $PtAl_2$ showed an oxidation peak but CA measurements didn't show any formation of a polymer. Due to degradation of the catalysts surface no more measurements were done in indoline. It cannot be ruled out that some water remained in the indoline so that it acted as a base and degradation of the surface set in. Nevertheless the measurements have shown that the oxidation potentials in acetonitrile are too high for the IMCs. Degradation was visible in water and even in acetonitrile, catalysts like the $Mo_xCo_ySi_z$ IMCs showed

a surface change. Therefore molecules with lower oxidation potentials had to be tested. Diaza-heterocycles could be a solution for this problem.

4.3.5 Diaza-heterocycles

Piperazine and DABCO (1,4-Diazabicyclo[2.2.2]octane) were chosen as heterocycles with two nitrogen in their structure. The existence of another nitrogen atom in the ring weakens C-H bonds and should simplify dehydrogenation even more than one nitrogen does [7]. A formation of side products, polymerization or dimerisation is unknown for these molecules.

As we will see piperazine and DABCO are *N*-heterocycles which differ in properties as well as in electrochemical behavior. If electrochemical dehydrogenation of piperazine succeeds a rehydrogenation of 1,4-Dihydropyrazine or pyrazine can be done easily over a ruthenium based catalyst under mild conditions [47].

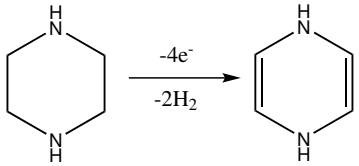

Figure 52: Possible electrochemical dehydrogenation of piperazine to 1,4-dihydropyrazine

The CVs in figure 53 show oxidation of piperazine on various IMCs and Pt with an unusual behavior for secondary amine oxidation.

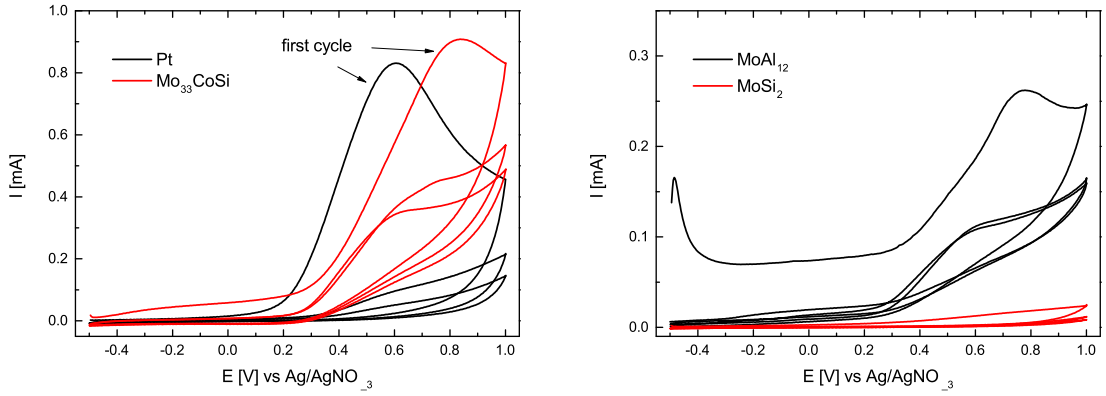

Figure 53: CVs of 10 mM piperazine on Pt and different IMCs in acetonitrile/0.1 M $NaClO_4$, scan rate 50 mV/s

When cycled the high current oxidation peak at around 0.5 V only appears at the first cycle. The second and the third cycle show only an oxidation peak with a quarter of current. During the first cycle a white cloudy substance appeared in the bulk solution which could be the result of a carbamate formed due to the reaction of piperazine with remaining CO_2 in solution as we will see in chapter 4.6. The decrease in current was due to a formation of a cationic radical which covered the surface of the catalyst in form of a white powder. Further current decrease can be seen in the second and third cycle. Chronoamperometric measurements have shown that the decrease in current continued until it reached nearly 0 A. The formation of the passivating layer made piperazine a bad choice as LOHC but a good choice as a CO_2 catcher which will be discussed in chapter 4.6.

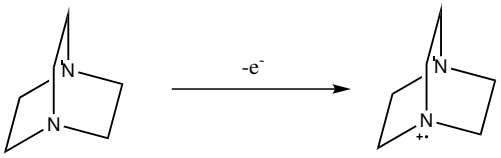

Figure 54: Electrochemical oxidation of DABCO

Other than piperazine electrochemical oxidation of DABCO didn't show the formation of a passivating layer. DABCO is known to form stable cationic radicals without side products upon electrochemical oxidation [48]. This property made DABCO a good probe molecule to check whether the IMCs

were undergoing a surface change, oxidizing the molecule or doing both. A dehydrogenation was unlikely to happen but the formation of the cationic radical should be clearly visible at potentials comparable to piperazine. In organic chemistry DABCO is used as a catalyst for a variety of chemical reactions [49] and is used in anionic exchange membranes in form of a quaternary ammonium cation [50].

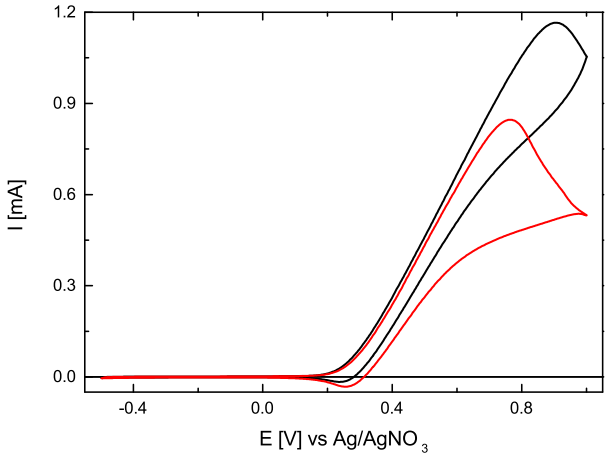

Figure 55: CVs of DABCO (red: 10 mM, black: 15 mM) in acetonitrile/0.1 M $NaClO_4$ on Pt, scan rate 50mV/s

Figure 55 shows the CVs on Pt with different concentrations of DABCO. One oxidation peak maximum around 0.8 V and a small reduction peak at 0.25 V. Other than piperazine it didn't stick to the surface but a slow constant decrease in current was visible. The decrease of current occured due to a formation of a stable ammonium salt which didn't got oxidized further. Other than Pt the IMCs showed an oxidation current maximum at 0.4 V (figure 56). As it has been shown with DABCO and other molecules a current increase was visible at around 0.2 V for most of the IMCs. It seems that these catalysts undergo a surface change before oxidation of the *N*-heterocycle.

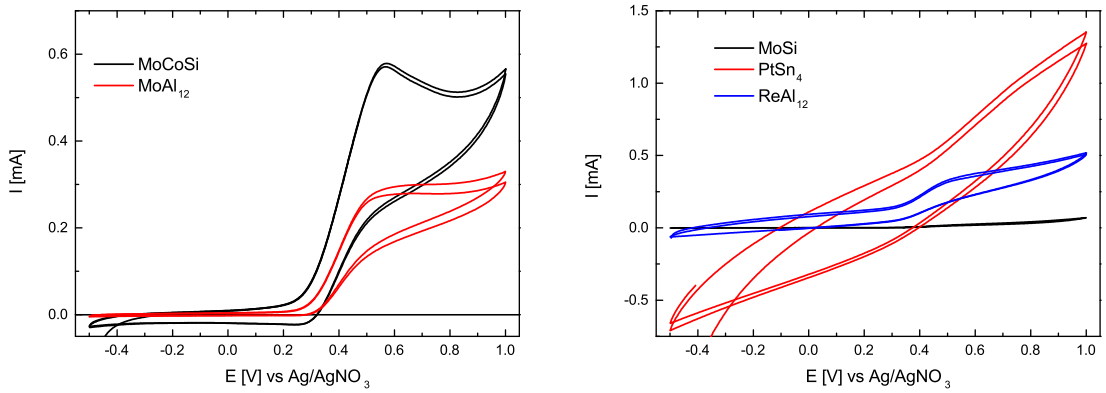

Figure 56: CVs of 15 mM DABCO in acetonitrile/0.1 M $NaClO_4$on different IMCs, scan rate 50 mV/s

DABCO was the only molecule besides the H4-NEC dimer which formed a stable radical on Pt in this work. The stability and the importance of a stable radical for a dehydrogenation reaction will be discussed.

4.3.6 Conclusion

Analysis of the oxidation products of all N-heterocycles have shown that an electrochemical dehydrogenation could not be achieved. NMR spectra showed cationic salts when fully saturated molecules were oxidized and dimerisation for partly unsaturated molecules like H4-NEC. Only the lone pair of the nitrogen was affected by the electrochemical oxidation of *N*-heterocycles on Pt. In the case of H12-NEC a deethylation reaction could be observed which makes the idea for n-ethylcarbazole as a LOHC in context of electrochemical oxidation obsolete. Another big problem of the electrochemical dehydrogenation of organic molecules is the fact that oxidation potentials for the unsaturated compounds are close or even below the oxidation potentials of their saturated counterparts. A dehydrogenation would also imply an oxidation of the product to another product like dimers or polymers like it was shown in the case of indoline which formed polymers. Electrochemical measurements of IMCs in the electrochemical oxidation of saturated *N*-heterocycles didn't show activity of dehydrogenation or hydrogen oxidation reaction. Currents observed were mostly due to the catalysts surface

degradation. Only molecules with lower oxidation potentials like DABCO showed clearly electrochemical activity with IMCs but coupled with a surface change. In most of the cases oxidation potentials higher than 0.4 V seem to degrade the catalysts surface. *N*-heterocycles have to bring special properties to achieve a full dehydrogenation through electrochemical oxidation. All electrochemical oxidations always form cationic radicals. The molecule should be able to stabilize the radical which is formed during the first electron transfer. In the second step a dehydrogenation of the ring could follow due to an abstraction of the radical through further electrochemical oxidation. The only possibility to fully dehydrogenate a LOHC by electrochemical oxidation is a step by step dehydrogenation with a multi electron transfer. Some thoughts how a molecule could look like are presented. The case of H4-NEC has shown that a partly dehydrogenation of the electrochemically formed stable cationic radical occured. The formation of unstable radicals which was the case for the electrochemical oxidation of azepane in acetonitrile and $NaClO_4$ resulted in an aminium salt and didn't react further. An example of electrochemical dehydrogenation is shown in figure 57 **[51]:**

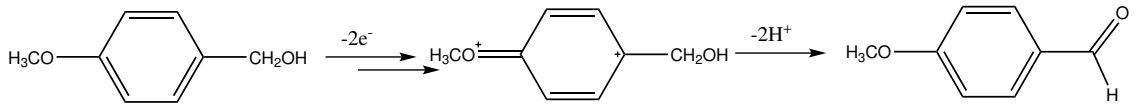

Figure 57: Electrochemical dehydrogenation of anisyl alcohol to anisaldehyde in CH_3CN

The cationic radical (not shown) which is formed after the first electron withdraw is stabilized through resonance system build up by the aromatic ring and the methoxy group. The second electron withdraw forms a dication which results in a removal of two protons. Reactions with a radical that is not stable enough will not result in a dehydrogenation reaction. This can be seen in most of the saturated *N*-heterocycles measured in this work. Only H4-NEC undergoes a deprotonation because of a long lasting stable radical that is formed after the first electron withdraw. The radical could be stabilized by resonance structures with electron-defiency like shown in figure 58, which could induce a dehydrogenation of the ring.

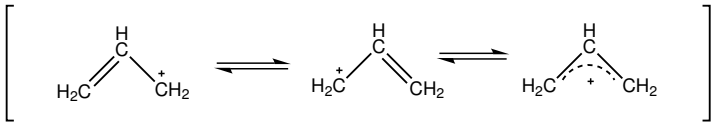

Figure 58: Resonance structure

In the case of *N*-heterocycles the first step for a dehydrogenation a reaction to an iminium cation which form cationic enamines by further oxidation would be desirable but could not be detected. Therefore a stable radical which doesn't react with the solvent neither with another radical for every dehydrogenation/oxidation step is needed. A molecule which builds a stable radical is TEMPO which can be modified in α position by replacement of the methyl group(s) with hydrogen (figure 59). A disproportionation occurs with one of the molecules being dehydrogenated to a nitrone:

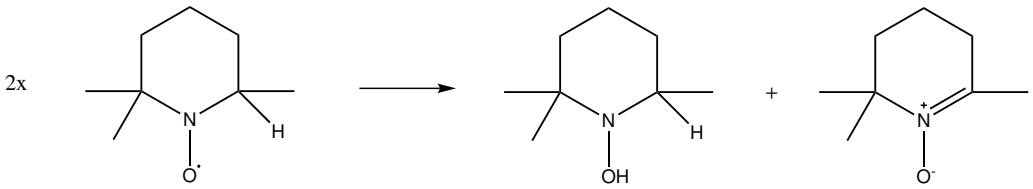

Figure 59: TEMPO with hydrogen in α position (TEMPO-H), disproportionation to an nitrone and hydroxy species

The possibility to achieve a nitrone and to oxidize the hydrogen in α position could start a elechtrochemical dehydrogenation. A possible mechanism for a electrochemical oxidation of TEMPO-H is shown below (figure 60). The TEMPO-H radical is oxidized to a nitrosonium cation which is in equilibrium with a hydrogenated nitrone. Another electron withdraw results in a deprotonation to a nitrone radical.

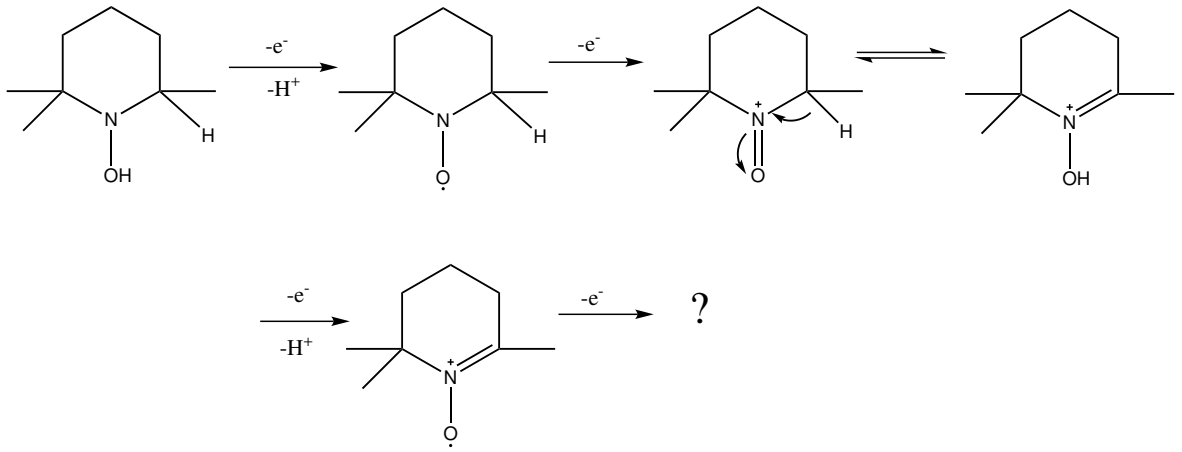

Figure 60: Electrochemical "step by step" dehydrogenation of TEMPO-H

Further mechanistic speculations about the mechanism are far away from reality because nobody knows what would happen with a nitrone radical and the ring has to be functionalized in that way that another stable radical can be formed like it is the case for the anisaldehyde. The above shown example shows that it is extremely difficult to find the right molecule. The fully saturated *N*-heterocycles tested in this work are not to the right type of molecules for the LOHC idea. One attempt of an electrochemical dehydrogenation/oxidation reaction was made with an interesting and reactive cyclic hydrocarbon in the next chapter.

4.4 Hydrogenation of guaiazulene and electrochemical oxidation on Pt

As it has been shown until now no *N*-heterocycle could be dehydrogenated electrochemically. Another interesting class of molecules are azulenes. These intensive blue molecules which are isomers of naphtalene can be found in mushrooms or guaiac wood oil. The reactivity is special because azulenes can be seen as a cyclopentadienyl anion fused with a tropylium cation [52]. Transfer of an electron between the five and seven membered ring give aromaticity to each cycle following the Hückel's rule. This feature gives the molecule a variety of reaction possibilities [53]. Especially guaiazulene is interesting because it is one of the azulenes which doesn't polymerize upon electrochemical oxidation [54] and is easy to hydrogenate [55][53]. Guaiazu-

lene has the big advantage to change its intense blue color into a colorless compound upon hydrogenation. Only a small concentration of guaiazulene is needed to colorize a liquid blue so that dehydrogenation of the saturated molecule will be easy visible. Until now the dehydrogenation of partially hydrogenated guaiazulene has been reported at room temperature by shaking it with platinum black in the presence of air [56].

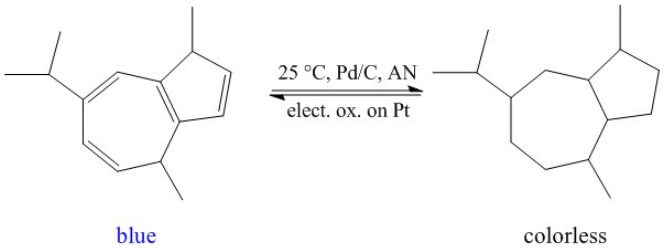

Figure 61: Hydrogenation of guaiazulene and electrochemical dehydrogenation of guaiane

It seemed that an electrochemical dehydrogenation of reduced guaiazulene (GuaH) should be feasible. Even if it produces more than one product a partial dehydrogenation would be immediately visible by the change of color [57]. A hydrogenation of guaiazulene has been already done with γ-ray irridiation and analyzed with different methods like gc, refractometry and UV [58]. The hydrogenation in methanol over a Pd/C catalyst gave a mixture of colorless and yellow liquid. The refractive index for the yellow liquid was n_D=1.488, close to the index given in literature ($n_{DLit.}$=1.4878) for octahydroguaiazulene [58]. The colorless liquid gave a refractive index of n_D=1.481 which was also close to the one in literature ($n_{DLit.}$=1.4758) for decahydroguaiazulene (guaiane) [58]. Higher refractive indexes like n_D=1.4984 for hexaguaiazulene could not be found in the mixture. Ir spectra (figure 62) shows clearly a nearly fully saturated molecule, aromatic signals vanished completely after the hydrogenation process. According to literature octahydroguaiazulene was the main compound [58]. The signals in the double bond area shown in the ^{13}C-NMR spectra at 131, 135, 139 and 140 ppm didn't occur when spectra were taken initially after the hydrogenation process. Both NMR-spectra shown in figure 63 and 64 are measurements of 16 hours old hydrated guaiazulene.

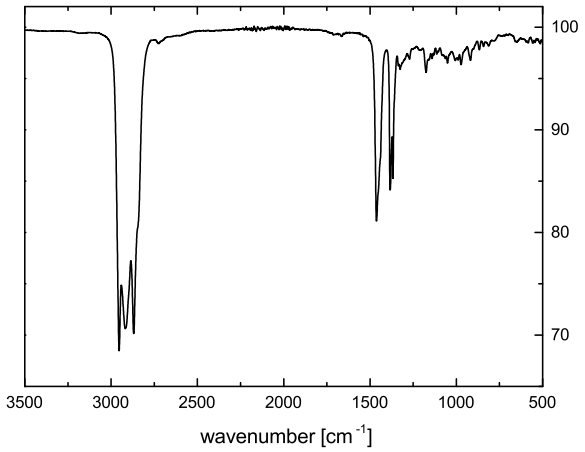

Figure 62: IR spectra of hydrated guaiazulene.

NMR measurements also show signals for a saturated or partially saturated guaiazulene. An interesting fact is that the hydrated guaiazulene changed when left under air for some hours.

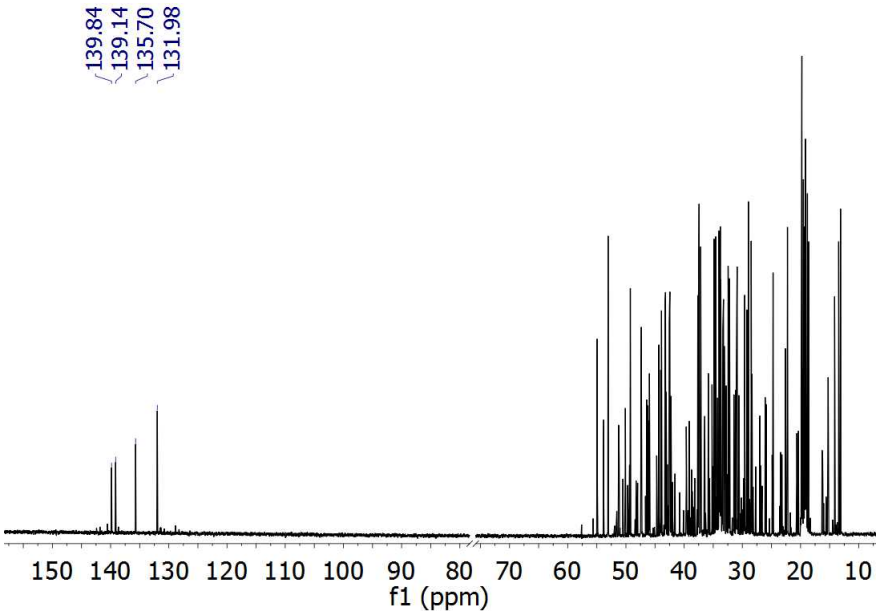

Figure 63: ^{13}C-NMR ($CDCl_3$, 125 MHz, TMS) of GuaH

The peaks in the double bond area between 130 and 140 are peaks due to partial oxidation of decahydroguaiazulene to octahydroguaiazulene in air. Not all of the decahydroguaiazulene were oxidized so that a distribution of the compounds listed in figure 65 could be identified.

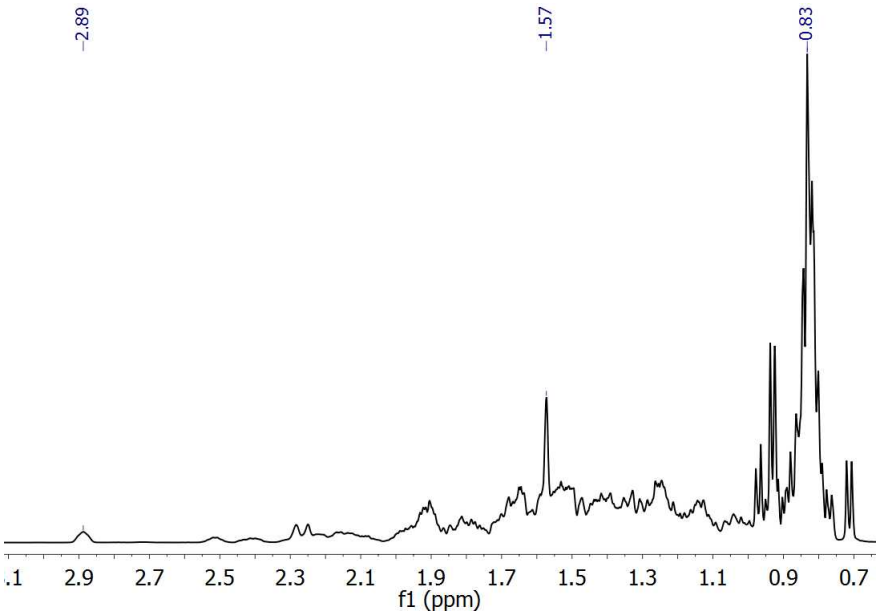

Figure 64: ^{1}H-NMR ($CDCl_3$, 125 MHz, TMS) of GuaH

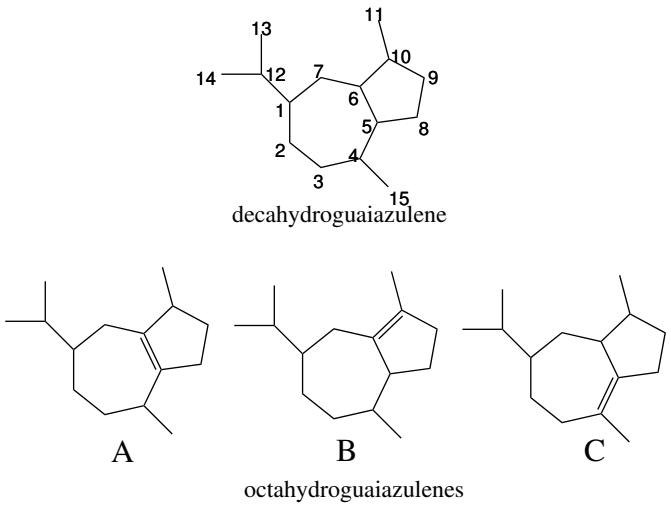

Figure 65: Hydrogenation products of guaiazulene

Other than in literature [57] only isomers with quaternary C atoms in the double bond region could be found in the mixture (see ^{13}C-NMR dept in the supporting information, figure 95).

^{1}H-^{1}H COSY	HMQC (J_{1CH})	HMBC (J_{2-3CH})	C (molecule)
0.71 (d), 0.72 (d) → 1.82	0.71, 0.72 → 13.13	0.71, 0.72 →37.13, 53.05, 131.97	13, 14 (B, CH_3)
0.76 (d), 0.78 (d) → 1.82	0.76, 0.78 → 15.24	0.71, 0.72 →37.13, 53.05, 131.97	13, 14 (A, CH_3)
0.79 (d), 0.80 (d) → 1.90	0.79, 0.80 → 13.44	0.79, 0.80 → 16.20, 16.30	CH_3)
0.91 (d), 0.93 (d) → 1.35		0.91, 0.93 → 31.04	14 (B, CH_3)
0.92 (d), 0.94 (d) → 1.42	0.92, 0.94 →18-20	0.92, 0.94 → 139.13	13, 14 (A, CH_3)
		0.96, 0.98 → 139.84	
1.26 → 1.96	1.26 → 24.71		8 (CH_2)
1.58 → 2.89	1.58 → 14.16	1.58 → 131.97, 135.70	11 (B , CH_3)
1.57 → 0.82	1.57 →30	1.57 → 37.57	
1.82 → 0.71, 0.72	1.82 → 37.13	1.82 → 28.48	12 (B, CH)
1.90 → 1.41	1.90→ 47.35	1.90 → 131.97, 135.70	5 (B, CH) OK
1.92 →1.42	1.92 → 28.50		7 (A, CH_2)
2.25, 2.28 → 0.97	2.25, 2.28 → 37.12, .13	2.25, 2.28 →32.20	(A, CH_2)
2.51 → 0.92	2.51 → 46.45	2.51 → 139.13	
2.89 → 1.57, 1.90	2.89 → 53.05	2.89 →1 3.13	(B, CH_2)
		2.89 → 131.97, 135.70	(B, CH_2)
	0.82 → 19.31		(CH_3)
	1.25 → 24.72		(CH_2)

Table 3: Different NMR couplings of GuaH ($CDCl_3$)

Table 3 shows the couplings from the HMBC and HMQC and COSY measurements. The fourth column represents the carbon number of the structures depicted in figure 65. Due to overlapped signals not all of them could be identified. Furthermore the concentration of molecule C was very low so that it was very hard to identify signals properly. For electrochemical measurements the mixture of isomers was dissoluted in acetonitrile / 0.1 M $NaClO_4$ and CVs (figure 66) were taken on Pt and glassy carbon (gc).

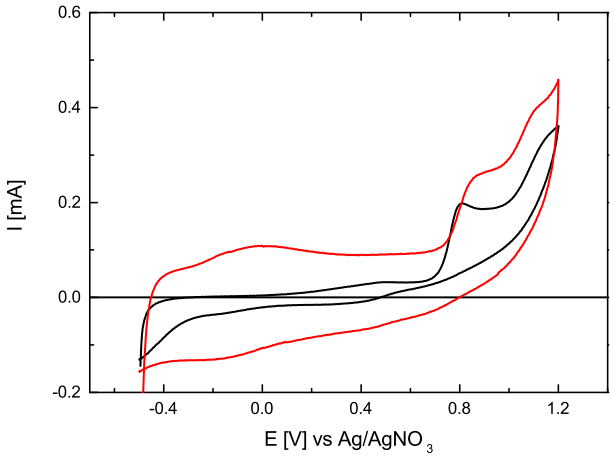

Figure 66: CVs of GuaH on Pt (black curve) and glassy carbon (red curve) in acetonitrile / 0.1 M $NaClO_4$, scan rate 50 mV/s

Both anode materials showed activity and several peaks at different potentials. Other than gc the Pt anode showed a small broad oxidation peak at around 0.4 V and a reduction peak between -0.5 V and -0.4 V. Both anode materials showed activity at 0.8 V and a maximum between 1 and 1.2 V. The different oxidation potentials were a result of the different hydrogenated species in solution. Chronoamperometric measurements shown in the supporting section in figure 102 were done at different potentials with the result that only at potentials higher than 0.9 V a visible change in UV wavelength absorbance was observed. The UV spectra in figure 67 (right) show a mixture of decahydroguaiazulene and octahydroguaiazulene [58].

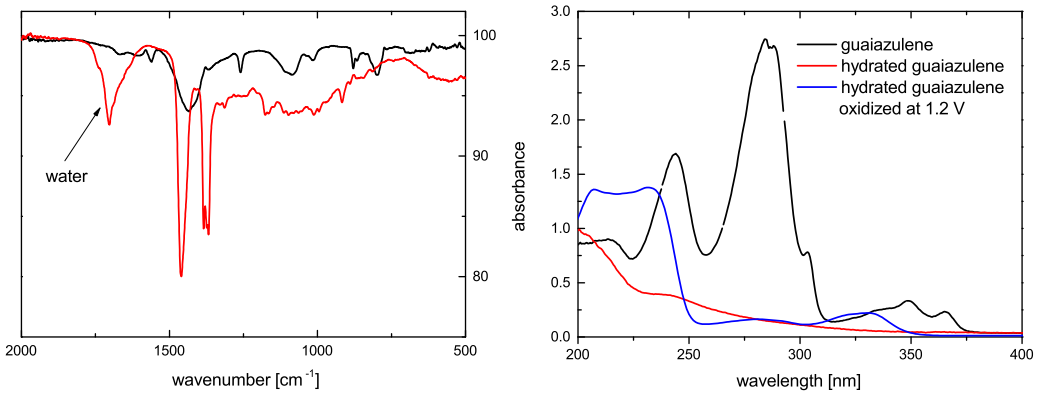

Figure 67: left: IR spectra of oxidized GuaH (red: bulk, black: precipitate of kathode); right: UV spectra of guaiazulene, GuAH and GuaH oxidized

When oxidized at 1.2 V vs $Ag/AgNO_3$ on Pt in acetonitrile the UV spectra shows new peaks which give rise to a new π bond system. The oxidation clearly introduces new double bonds to the molecules but with clear difference in structure from guaiazulene. The color of the product was mangenta which decolorised after some time. When a potential was applied again, the mangenta color reappeared again. Oxidations over long time $>$ 10 h gave a purple mixture which changed to brown color. Higher voltages $>$ 1.2 V gave a red color which also changed to brown color. The IR spectra on the left side of figure 67 shows the product out of the bulk solution after electrochemical oxidation at 1.2 V with nearly no difference to the initial IR spectra before the process (figure 62). The black curve is an IR spectra of a white precipitate which formed on the cathode during the electrochemical oxidation process. It shows different vibrational bands than the spectra of the bulk product. The C-H vibrational stretching bands at around 1300 and 1450 cm^{-1} disappeared and are replaced or overlapped by a broad peak at 1440 cm^{-1}. Vibrational C-H stretching bands at around 2800 to 3000 cm^{-1} (not shown in figure 67) still exist in both bulk and precipitate spectra. It seems that a part of the hydroguaiazulenes were oxidized on the anode and then reduced on the cathode. NMR measurements showed that a big quantity of the substrate stayed unchanged and a CV after the chronoamperometric measurements shows no oxidation peaks at 0.4 V and 0.8 V which may be a result of an oxidation of partly unsaturated hydroguaiazulenes. A change of electrolyte to $LiBF_4$ showed the same results. A hydrogenation of the oxidation product with Pd/C was not possible.

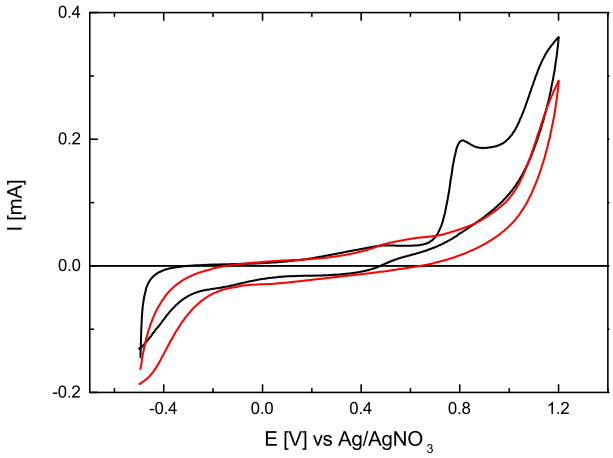

Figure 68: black curve: CV before the CA, red curve: CV after the CA; scan rate 50 mV/s

Only the oxidation of GuaH on Pt showed the color change, the gc and the IMCs only showed some current but no change in color. NMR measurements gave no clear result. Every oxidation experiment gave different spectra which could be attributed to the decay/reaction of a radical to another compound. The mangenta color changed to brown when other solvents than acetonitrile were chosen. It seems that acetonitrile reacted with GuaH during the electrochemical oxidation. Another attempt to dehydrogenate GuaH was done with ferrocene. Ferrocene is known to be an effective cocatalyst for a number of reactions [59, 60]. The CVs in figure 69 show the reduction/oxidation of ferrocene (black curve) and two new peaks when GuaH is added (red curve). It cannot be said if the ferrocene had an effect on the oxidation of GuaH because no new peak arised.

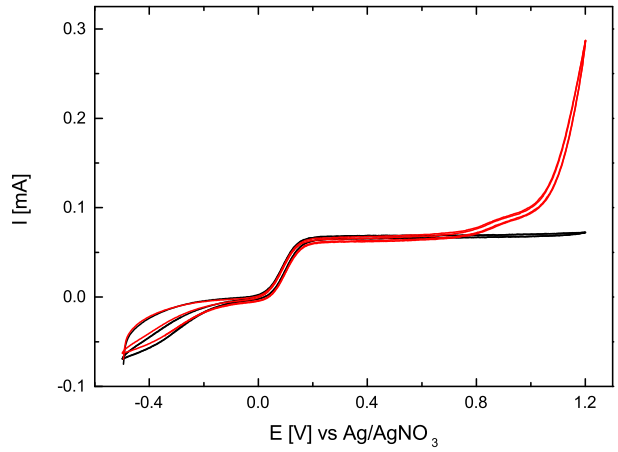

Figure 69: CVs in acetonitrile and 0.1 M $LiBF_4$ on Pt, black curve: 1 mM ferrocene, red curve: 1 mM ferrocene + 1 mM GuaH, scan rate 50 mV/s

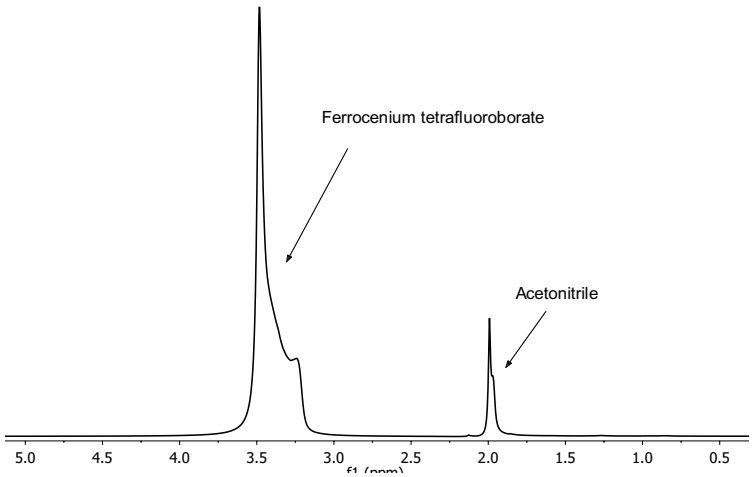

Figure 70: ^{1}H-NMR ($CDCl_3$, 500 MHz, TMS) of oxidized GuAH + ferrocene

Electrochemical oxidation at 1V for 6h showed the desired change of color to blue but not due to GuaH dehydrogenation. ^{1}H-NMR (figure 70) measurements showed that only ferrocene was oxidized and formed the salt ferrocenium tetrafluoroborate which is known to be blue.

4.4.1 Conclusion

The electrochemical oxidation of GuaH showed no signs of a dehydrogenation back to guaiazulene. It seems that a part of the substance got oxidized but also side products were formed. The use of ferrocene as a possible cocatalyst

resulted in oxidation of ferrocene to a blue salt. The two oxidation reactions of ferrocene and GuaH were separately taking place from each other. In literature some attempts to use cocatalysts like DDQ (2,3-dichlor-5,6-dicyano-1,4-benzochinone) were also done and it seems that the results were more or less the same. Cocatalyst and substrate were oxidized separately from each other [44].

4.5 CO_2 capture with saturated N-heterocycles and electrochemical reduction in acetonitrile

The idea of CO_2 capture and electrochemical reduction of the resulting carbamate came when testing pyrrolidine in context of a possible LOHC. When the reaction mixture consisting of pyrroldine, acetonitrile and $NaClO_4$ was left under air and electrochemically reduced/oxidized the following CVs resulted.

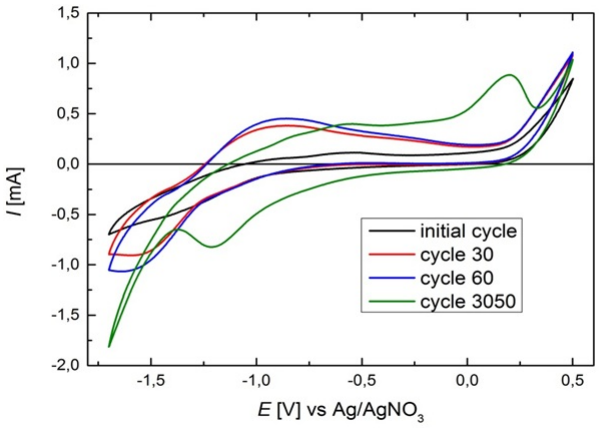

Figure 71: CVs of pyrrolidine in acetonirile/ 0.1 M $NaClO_4$ on Pt, 200 mV/s (under air)

The CVs (figure 71) show clearly oxidation peaks at around 0.25 V, reduction peaks at around -1.5 V and new peaks after 3000 cycles. These new peaks at 0.25 V and -1.25 V were due to a formation of a new compound (figure 72) which was not visible when experiments were done under argon.

Figure 72: Compound which formed upon electrochemical oxidation/reduction under air in a mixture of pyrrolidine, acetonitrile and $NaClO_4$

The ^{13}C-NMR (figure 73) revealed two new peaks between 160 and 170 ppm, the region for carbonyl compounds. Dept NMR spectra showed quaternary C signals for these peaks.

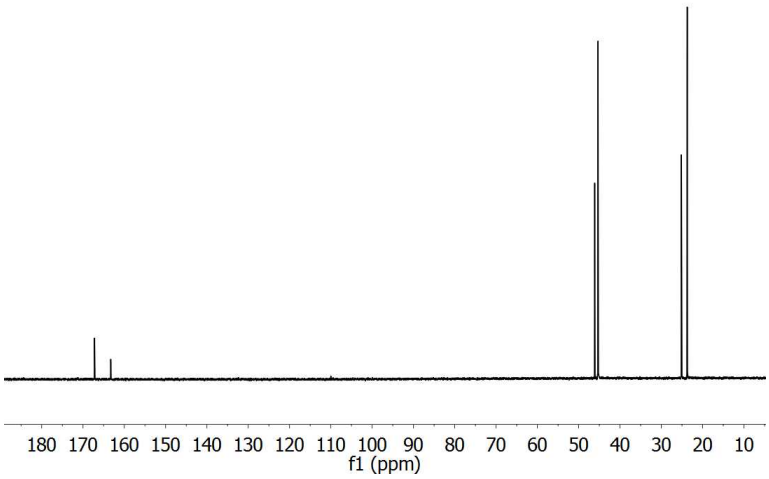

Figure 73: ^{13}C-BB-NMR (125 MHz, D_2O, TMS) of electrochemical treated pyrrolidine

We found out that pyrrolidine reacted with atmospheric CO_2. Two reactions took place during the CVs, when pyrrolidine got oxidized it formed a cationic radical which got reduced when cycled back to negative potentials. A second reaction started when enough carbamate was formed which is visible in the CVs as the new peaks. Amines like pyrrolidine, piperazine or monoethanolamine are known to react with CO_2 to carbamates [61]. The products found after the electrochemical reduction were the salt of n-formylpyrrolidine and 1,1-carbonyldipyrrolidine (figure 74).

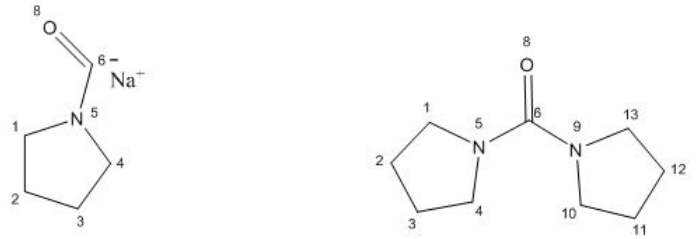

^{13}C-NMR (125 MHz, D_2O, TMS): δ [ppm] 23.7 (2,3) ; 46.1 (1,4); 163.3 (6)

^{13}C-NMR (125 MHz, D_2O , TMS): δ [ppm] 23.7 (2,3,10,11); 45.3 (1,4,9,12); 167.1 (6)

Figure 74: left: salt of n-formylpyrrolidine; right: 1,1-carbonyldipyrrolidine

The carbamate species was reduced electrochemically to formyl compounds. 1,1-carbonyldipyrrolidine could be the result of the oxidation of n-formylpyrrolidine which got attacked by an unreacted pyrrolidine. The white product is a mixture of carbamate, $NaClO_4$ and the reduced carbamate. A molecule which was tested intensively for its CO_2 capture property is piperazine [62, 63]. The electrochemical reduction was tested in this work and results are presented in the next chapter.

4.5.1 Piperazine

As it is described in the experimental section, piperazinecarbamate ($PipCOO^-$) was formed by bubbling CO_2 in a mixture of piperazine, acetonitrile and $NaClO_4$ which was dearated before until a white cloudy liquid resulted.

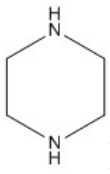

Piperazine

Results of CVs are shown in figure 75. Compared to the carbamate reduction the CO_2 and piperazine reduction currents are very small. The negative sweep of the carbamate shows a current maximum at -1.2 V and the positive sweep shows an oxidation peak at -1.0 V. CA measurements revealed the current potential performance shown in figure 76.

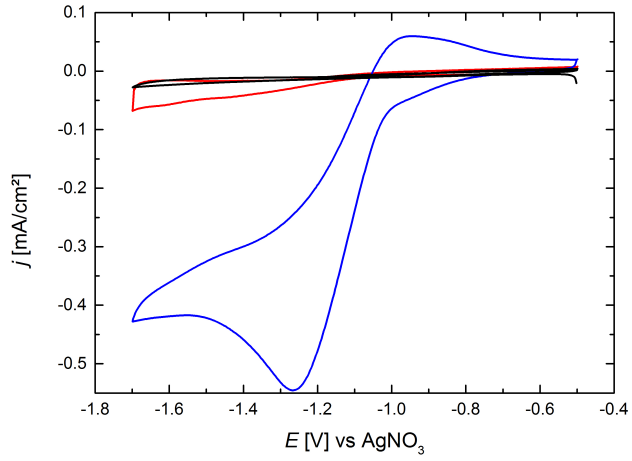

Figure 75: CV's of piperazine (4 mM) in acetonitrile/0.1M $NaClO_4$, scan rate 10 mV/s black: CO_2 on Pt red: piperazine (argon) blue: $PipCOO^-$ (argon)

The data essentially shows that the current producing reactions are different at different potentials. In order to determine the products of the reaction one has to sample the products at various potentials.

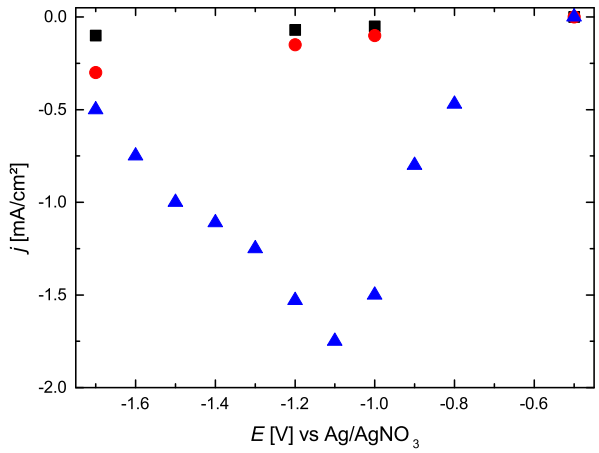

Figure 76: Current potential performance of CO_2 on Pt (black squares), piperazine on Pt (red dots) and piperazinecarbamate on Pt (blue rectangles) in acetonitrile/0.1 M $NaClO_4$.

For CA measurements (figure 77) the potentials were held at -1.2 V and -1.5 V for 40 h and the products of these experiments were collected and analyzed using NMR.

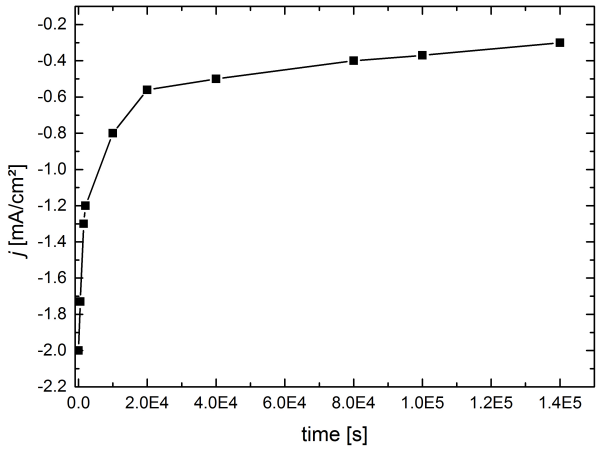

Figure 77: CA of piperazinecarbamate in acetonitrile / 0.1 M $NaClO_4$ at a constant potential of -1.2 V vs $Ag/AgNO_3$ on Pt

With increasing time the amount of white precipitate on the electrode surface increased. NMR data (supporting information, figure 97) of the precipitate showed that the primary molecules in this precipitate were piperazinecarbamate and piperazine.

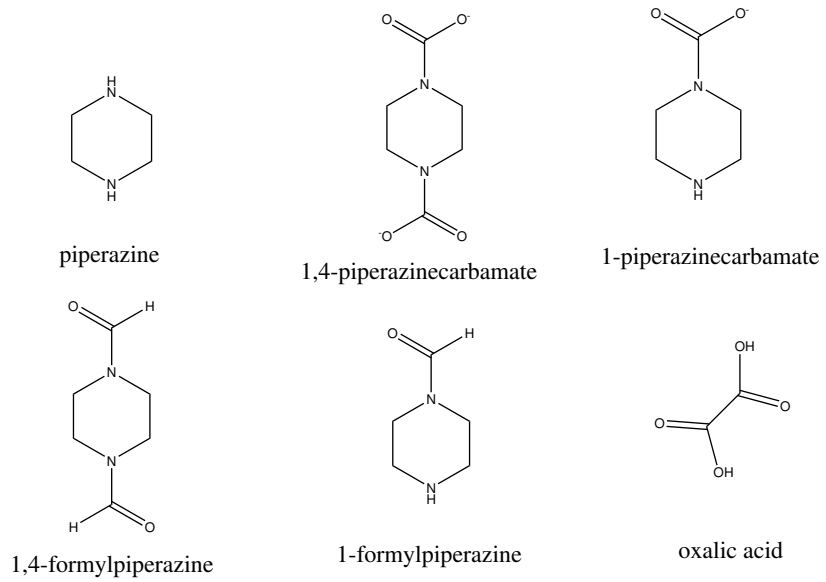

Figure 78: All products found upon electrochemical reduction on Pt at -1.5 V

The NMR data from the yellow liquid and the white solid from the bulk solution are provided in figures 79, 80, 96 (supporting section) and table 4. In figure 78 all molecules obtained from CA measurements are shown. All

of them were confirmed by 1D and 2D NMR measurements shown later in the text. The reported NMR data is discussed below. Figure 79 (reduction at -1.2 V) shows mostly peaks from the carbamate ($PipCOO^-$) species. The NH proton signals of piperazine show up as a singlet at 2.83 ppm. Piperazinedicarbamate shows up at 3.48 ppm as a singlet and as triplets for the monosubstituted piperazinecarbamate. The compound formed at -1.2 V were 1,4-formylpiperazine and 1-formylpiperazine. They appeared as low intensity signals which were close to the carbamate peaks. Reductions at -1.5 V showed formation of oxalic acid in addition to other products discussed above. The nature of the electrochemical reactions are different at the two potentials as the current behavior is different. An important part of the study is that no specific reducing agent (e.g. H_2 or H_2O) was used in the reaction setup.

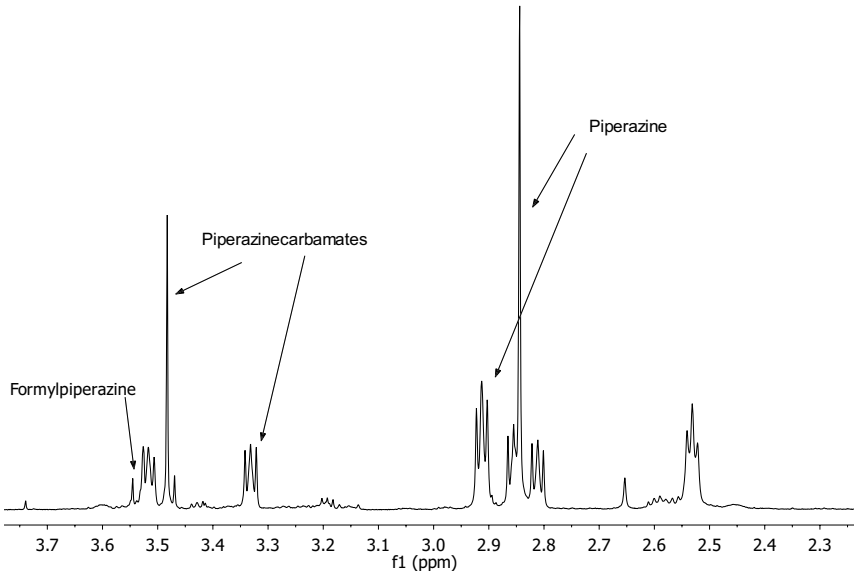

Figure 79: ^{1}H-NMR (500 MHz, $CDCl_3$, TMS) of reduction products found in the bulk solution at -1.2V

Overall the system remained well isolated. The reaction products at -1.2 V showed noticeable quantities of water. Since no oxygen source other than CO_2 was present in the system, it is likely that oxygen species originate from the reduction of CO_2. Pt is a well known catalyst for oxygen reduction reaction, thus partial decomposition of acetonitrile could provide enough hydrogen to form H_2O in presence of Pt at such low potentials. Water definitely had a role to play in this reaction and acetonitrile instead of working as an ideal non participating solvent, reacted. Attempts to get rid of the acetonitrile in

solution after reduction at -1.5 V failed. Even at pressures of 70 mbar and a temperature of 310 K the oily liquid remained. It seems that acetonitrile coordinated or even reacted with piperazine/piperazinecarbamates which can be seen as long range coupling signals at around 3.5 ppm in the HMBC (supporting information, figure 96) which is the region for the CN (115-120 ppm) group of acetonitrile. The HMBC of reduction products at -1.5 V show long range coupling of acetonitrile with carbonyl groups coupled to a hydrogen at 4.19 ppm (singlet) in the ^{1}H-NMR which is marked as "unknown". In comparison to the shifts in the spectra of the reduction products at -1.2 V the chemical shifts for the reduction products at -1.5 V moved downfield in the ^{1}H-NMR for all substances found in the mixture due to a different electrolyte concentration in the NMR probe. Furthermore nearly no water could be identified at -1.5 V which is a result of different reactions taking part alongside the reduction of the carbamates at -1.5 V. The formyl group shows a J_1 coupling, shown in the HMQC in figure 80, due to its hydrogen bonded to the carbonyl carbon. Carbamates don't show J_1 coupling in this region because of the lack of hydrogen connected to the carbonyl group.

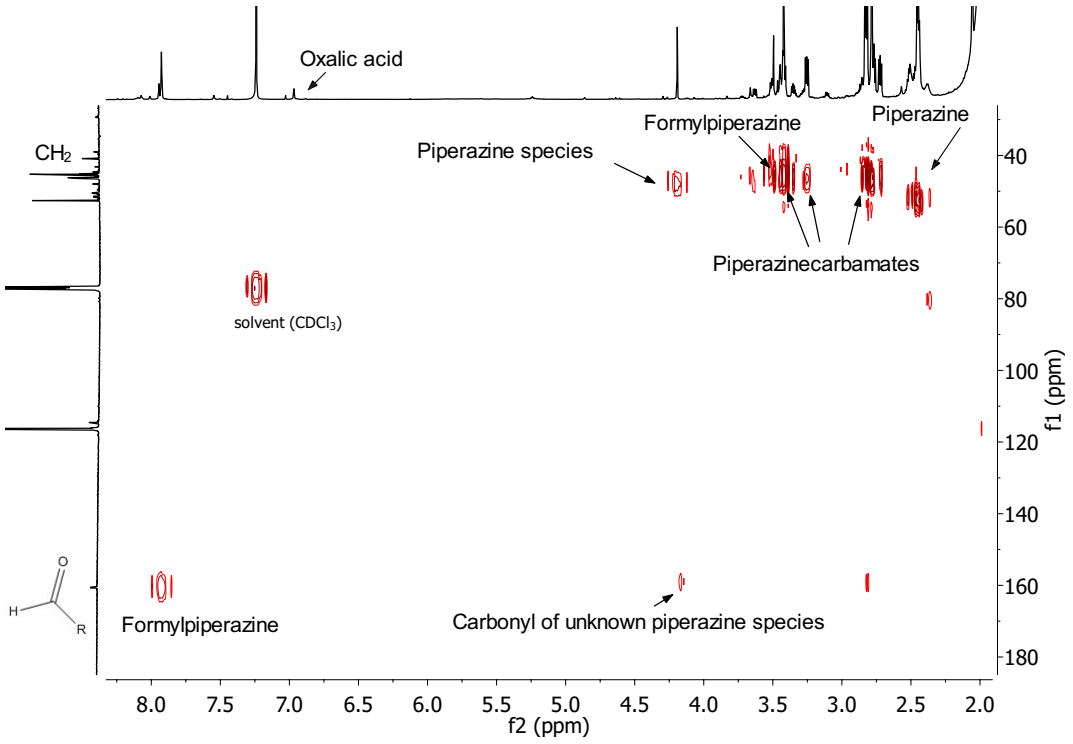

Figure 80: HMQC of reduced piperazinecarbamate at -1.5 V

Table 4 shows the shifts for the products upon reduction at -1.5 V. For some

of the peaks in the HMBC spectrum the signal detected was low in intensity and are marked as "weak". Overlapping signals and small concentrations made it nearly impossible to determine every peak so that only the main product peaks are given. Oxalic acid which showed up at 6.97 ppm in the ^{1}H-NMR had only a small signal so that couplings could not be detected.

Table 4: Substances found upon reduction at -1.5 V, f_1 is the ^{13}C-NMR trace and f_2 the ^{1}H-NMR trace

HMQC (f_2, f_1)	HMBC (f_2, f_1)	Molecule
2.45, 52.60	2.45, 45.26	piperazine
2.82, 45.26	2.82, 52.60	piperazine
2.77, 46.54	weak	piperazine
2.78-2.79, 46.19	2.78-2.79, 46.20	piperazine/carbamate
2.72, 45.12	2.72, 40.82	1-formylpiperazine
3.25, 46.32	3.25, 40.82, 160.48	1-formylpiperazine
not existent	3.35, 160.64	piperazinecarbamate
3.41, 40.82	3.41, 45.12, 160.48	1-formylpiperazine
3.42, 46.20	3.42, 52.60	piperazinecarbamate
3.43, 40.87	3.43, 160.48	1,4-formylpiperazine
3.45, 43.20	3.45, 51.43	piperazinecarbamate
not existent	4.17, 116.40, 159.17	unknown
4.19, 48.01	4.19, 118.13	unknown
7.93, 160.48	7.93, 40.83, 46.32	1-formylpiperazine
7.95, 160.48	weak	1,4 formylpiperazine

4.5.2 Conclusion

We have shown that CO_2 could be captured as carbamates and reduced to formyl compounds electrochemically. This is the first instance in literature where such an attempt at CO_2 reduction has been made. Water and acetonitrile seem to be involved in the overall scheme of reactions. Further exploration of these aspects can be done with either specific reducing agents in the mixture like H_2 or H_2O. Overall target of the reaction should be the formation of compounds like CH_3OH or CH_4 all the way from CO_2. Use of amine based scaffolds can significantly reduce complexities arising out of CO_2 collection and solubility issues.

5 Summary and discussion

A method to store hydrogen in liquid form was presented. Fully and partly hydrogenated molecules were electrochemically oxidized on different metal catalysts. Furthermore CO_2 was catched on *N*-heterocycles and the product was reduced electrochemically. It has been shown that electrochemical oxidation of fully saturated *N*-heterocycles like hydrogenated n-ethylcarbazole or azepane only resulted in a formation of cationic radicals. Compared to the thermal dehydrogenation of hydrogenated n-ethylcarbazole [3], no hydrogen could be released electrochemically. The interaction of nitrogen with the catalyst surface is very strong upon electrochemical oxidation which resulted in absorption of the LOHC on the catalyst surface and partial degradation of the molecules. Electrochemical oxidation of partly saturated heterocycles like tetrahydrocarbazole or indoline resulted in the formation of dimeric and polymeric compounds. The use of IMCs and Pt showed that electrochemical reactions were independent of catalyst choice, only the nitrogen lone pair was affected. Attempt to create a LOHC from guaiazulene failed. The partly hydrogenated guaiazulene was electrochemically oxidized but underwent reactions to unwanted side products which could not be hydrogenated back. All tested IMCs showed degradation when electrochemically oxidized in water and some of them in acetonitrile when potentials higher than 0.4 V were applied. Other systems containing different solvents, catalysts and molecules have to be tested in the future. Initial results with CO_2 reduction when bound to an amine compound like piperazine showed reduction mainly to a formyl compound. Results were comparable to thermal reduction of CO_2 on a polyamine which was studied in literature [17]. We believe choice of other molecules as CO_2 sequesters and choice of different catalysts could result in better selectivities and desired compounds.

5 Zusammenfassung und Diskussion

In dieser Arbeit wurde eine Methode untersucht, die es erlaubt Wasserstoff in flüssiger Form zu speichern. Hierzu wurde der gasförmige Wasserstoff an zumeist *N*-Heterocyclen chemisch gebunden. Die eigentliche Arbeit war das Zurückgewinnen des Wasserstoffs mittels elektrochemischer Oxidation mit verschiedenen Katalysatoren. Platin aber auch intermetallische Phasen kamen zum Einsatz. Aber nicht nur verschiedene Katalysatoren auch diverse Heterocyclen und ein Azulen wurden getestet. Elektrochemische Oxidation der *N*-Heterocyclen führte grösstenteils zu einer Bildung von kationischen Radikalen. Diese konnten auch mit Veränderung des Oxidationspotentials nicht dehydrogeniert werden. Nur das freie Elektronenpaar des Stickstoffs war involviert. Die elektrochemische Oxidation von teilweise hydrogenierten Molekülen wie Tetrahydrocarbazol führten zu Bildung von Dimeren, die zudem die Oberfläche des Katalysators passivierten. Verglichen mit der thermischen Dehydrogenierung von hydrogenierten n-Ethylcarbazol [3], konnte kein Molekül auf elektrochemischen Wege dehydrogeniert werden. Auch das hydrogenierte Guaiazulen zeigte zwar interessante Farbwechsel während der elektrochemischen Oxidation, eine Dehydrogenierung zum gewünschten Guaiazulen blieb aus. Die getesteten intermetallischen Phasen zeigten grössenteils nur geringe Aktivität oder gar Instabilität in wässrigen aber auch organischen Lösungsmittel. Ein ganz anderer Ansatz wurde mit dem Diamin Piperazin untersucht. Dieses Molekül geht eine Reaktion mit CO_2 ein und bildet Carbamate die elektrochemisch auf Pt zu einer Formylverbindung reduziert werden konnten. Die Resultate sind vergleichbar mit Ergebnissen aus der Literatur wo ein Polyamin benutzt wurde [17]. Die Wahl eines anderen Katalysators oder anderen *N*-Heterocyclen könnte die Ausbeute des Reduktionsprodukts noch erhöhen und vielleicht zu wertvollen Produkten wie Methanol führen. Hierzu sind Messungen in Zukunft nötig. Die Frage nach einem geeigneten Wasserstoffträger bleibt nach wie vor ein schwieriges Thema, da viele Komplikationen wie Bildung von Nebenprodukten, Passivierung der Katalysatoroberfläche oder Instabalität des Katalysators noch lange eine Herausforderung sein werden.

References

[1] C. B. Engineer; M. Ghassemian; J. C. Anderson; S. C. Peck; H. Hu and J. I. Schroeder. Carbon anhydrases, EPF2 and novel protease mediate CO_2 control of stromatal development. *Nature*, 513:246–250, 2014.

[2] P. T. Moseley and J. Garche, editors. *Electrochemical Energy Storage for Renewable Sources and Grid Balancing*. El, 2015.

[3] Christoph Gleichweit; M. Amende; S. Schernich; W. Zhao; M. P. A. Lorenz; O. Höfert; N. Brückner; P. Wasserscheid; P. J. Libuda; H.-P. Steinbrück and C. Papp. Dehydrogenation of Dodecahydro-n-ethylcarbazole on Pt (111). *ChemSusChem*, 6:974–977, 2013.

[4] Ferdi Schüth. *Chemical energy storage*. De Gruyter, 2013.

[5] D. J. Durbin and C. Maladier-Jugroot. Review of hydrogen storage for on board vehicle applications. *Int. J. Hydrogen Energy*, 38(34):14595–14617, 2013.

[6] Farnaz Sotoodeh; Benjamin J.M. Huber and Kevin J. Smith. Dehydrogenation kinetics and catalysis of organic heteroaromatics for hydrogen storage. *Int. J. Hydrogen Energy*, 37:2715–2722, 2012.

[7] R. H. Crabtree. Hydrogen storage in liquid organic heterocycles. *Energy Environ. Sci.*, 1:134–138, 2008.

[8] J. Osswald; K. Kovnir; M. Armbruester; R. Giedigkeit; R. E. Jentoft; U. Wild; Y. Grin; R. Schlögl. Palladium-gallium intermetallic compounds for the selective hydrogenation of acetylene. *Journal of catalysis*, 258(1):210–227, 2008.

[9] Daniel Little and Kevin D. Moeller. Organic electrochemistry as a tool for synthesis. *The Electrochemical Society Interface*, 2002.

[10] Christoph Gleichweit. *Dehydrierung von flüssigen organischen Wasserstoffspeichern auf Modellkatalysatoroberflächen*. PhD thesis, Friedrich-Alexander-Universitaet Erlangen-Nuernberg, 2015.

[11] Darrell C. Dean. *Hydrogen Fuel Technologies for Vehicular Transportation.* PhD thesis, Queens University Kingston, 2012.

[12] C.G. Zoski. *Handbook of Electrochemistry.* Elsevier, 2007.

[13] M. M. Halmann and M. Steinberg. Greenhouse gas CO_2 mitigation. *Lewis, New York*, 1999.

[14] J. J. Kim; D. P. Summers and K. W. Frese. *J. Electroanal. Chem*, 245:223, 1988.

[15] R. L. Cook; R. C. Mac Duff and A. F. Sammells. *J. Elektrochem. Soc.*, 134:2375, 1987.

[16] S. Wasmus; E. Cattaneo and W. Vielstich. *Elektrochim. Acta*, 39, 1994.

[17] J. Kothandaraman; A. Goeppert; M. Czaun; G. A. Olah and G. K. Surya Prakash. Conversion of carbondioxide from air into methanol using a polyamine and a homogenous ruthenium catalyst. *J. Am. Chem. Soc.*, 138:778–781, 2015.

[18] Vitaly V. Pavlishchuk and Anthony W. Addison. Conversion constants for redox potentials measured versus different reference electrodes in acetonitrile solutions at 25 °C. *Inorg. Chim. Acta*, 298:97–102, 2000.

[19] Nikos G. Tsierkezos. Cyclic Voltammetric Studies of Ferrocene in Nonaqueous Solvents in the Temperature Range from 248.15 to 298.15 K. *J Solution Chem*, 36:289–302, 2007.

[20] Robert R. Gagne; Carl A. Koval; George C. Lisensky. Ferrocene as an internal standard for electrochemical measurements. *Inorg. Chem.*, 19:2854–2855, 1980.

[21] G. Gritzner and J. Kuta. Recommendations on reporting electrode potentials in nonaqueous solvents. *Pure Appl. Chem.*, 56(4):461–466, 1983.

[22] H. A. Gasteiger; J. E. Panels and S. G. Yan. *J. Power Sources*, 127(162), 2004.

[23] W. Vogel; L. Lundquist; P. Ross and P. Stonehart. *Electrochim. Acta*, 20(79), 1975.

[24] T. J. Schmidt; P. N. Ross and N. M. Markovic. *J. Electroanal. Chem*, 252:524–523, 2002.

[25] Wenchao Sheng; Hubert A. Gasteiger and Yang Shao-Horn. Hydrogen oxidation and evolution reaction kinetics on platinum: Acid vs alkaline electrolytes. *J. Electrochem. Soc.*, 157(11):B1529–B1536, 2010.

[26] K. Karon and M. Lapkowski. Carbazole electrochemistry: a short review. *J. Solid State Electrochem.*, 19:2602–2610, 2015.

[27] A. Cooper; G. Pez; A. Abdourazak; A. Scott; D. Fowler; F. Wilhelm; V. Monk and H. Cheng. Design and development of new carbon-based sorbent systems for an effective containment of hydrogen. *DOE Hydrogen Program*, 2006.

[28] M. Amende; S. Schernich; M. Sobota; C. Papp; C. Gleichweit; P. Wasserscheid et. al. Dehydrogenation mechanism of Liquid Organic Hydrogen Carriers: Dodecahydro-N-ethylcarbazole on Pd(111). *Chem. Eur. J.*, 19:10854–10865, 2013.

[29] K. Eblagon; D. Rentsch; O. Friedrichs; A. Remhof; A. Zuettel; A. J. Ramirez-Cuesta and S. C. Tsang. Hydrogenation of 9-ethylcarbazole as a prototype of a liquid hydrogen carrier. *International journal of hydrogen energy*, 35(20):11609–11621, 2010.

[30] B. L. Laube; M. R. Asirvatham and Ch. K. Mann. Electrochemical oxidation of tropanes. *J. Org. Chem.*, 42(4), 1977.

[31] A. Desbene-Monvernay; P.-C. Lacaze and J.-E. Dubois. Polaromicrotribometric (PMT) and IR, ESCA, EPR spectroscopic study of colored radical films formed by the electrochemical oxidation of carbazoles. *J Electroanal Chem*, 129:229–241, 1981.

[32] K. M. Kadish; K. M. Smith and R. Guilard, editors. *Handbook of porphyrin science*, volume 16-20. World Scientific, 2012.

[33] R. G. Barradas; M. C. Giordano and W. H. Sheffield. Electrochemical oxidation of piperidine at mercury and platinum. *Electrochim. Acta*, 16:1235–1249, 1971.

[34] P. G. Pickup and R. A. Osteryoung. Electrochemical polymerization of pyrrole and electrochemistry of polypyrrole films in ambient temperature molten salts. *J. Am. Chem. Soc.*, 106:2294–2299, 1984.

[35] Römpp online, december 2014.

[36] M. Armbrüster; R. Schlögl and Y. Grin. Intermetallic compounds in heterogenous catalysis-a quickly developing field. *Sci. Technol. Adv. Mater.*, 15, 2014.

[37] F.Sotoodeh and K. J. Smith. Kinetics of hydrogen uptake and release from heteroaromatic compounds for hydrogen storage. *Ind. Eng. Chem. Res.*, 49:1018–1026, 2010.

[38] A. Desbene-Monvernay; P.-C. Lacaze and J.-E. Dubois. Polaromicrotribometric (PMT) and IR, ESCA, EPR spectroscopic study of colored radical films formed by the electrochemical oxidation of carbazoles. *J. E*, 129:229–241, 1981.

[39] K. M. Eblagon; K. Tam; K. M. Yu and S. C. E. Tsang. Comparative study of catalytic hydrogenation of 9-ethylcarbazole for hydrogen storage over noble metal surfaces. *J. Phys. Chem.*, 116:7421–7429, 2012.

[40] D. Wechsler; B. Davis; P. G. Jessop. *Can. J. Chem.*, 88:548–555, 2010.

[41] K. Sotoodeh and J. Smith. *J. Ind. Eng. Chem. Res.*, 49:1018–1026, 2010.

[42] S.-M. Lu; X.-W. Han; H.-Man and Y.-G. Zhou. An efficient catalytic system for the hydrogenation of quinolines. *J. Organomet. Chem.*, 692:3065–3069, 2007.

[43] F. W. Vierhapper and E. L. Eliel. Selective hydrogenation of quinoline and its homologs, isoquinoline, and phenyl-substituted pyridines in the benzene ring. *J. Org. Chem.*, 40(19), 1975.

[44] P. F. Driscoll; E. Deunf; L. Rubin; O. Luca; R. Crabtree; C. Chidsey; J. Arnold and J. B. Kerr. Redox catalysis for dehydrogenation of liquid hydrogen carrier fuel for energy storage and conversion. *ECS Transactions*, 35(28):3–17, 2011.

[45] H. Talbi; G. Monard; M. Loos and D. Billaud. Theoretical study of indole polymerization. *THEOCHEM*, 434:129–134, 1998.

[46] M. Saraji and A. Bagheri. Electropolymerization of indole and study of electrochemical behavior of the polymer in aqueous solutions. *Synthetic metals*, 98(1):57–63, 1998.

[47] Paul Rylander. *Catalytic hydrogenation in organic syntheses.* Academic Press, Inc, 1979.

[48] S. F. Nelsen and P. J. Hintz. Electrochemical oxidation of tertiary amines. the effect of structure upon reversibility. *Journal of american chemical society*, 94(20), 1972.

[49] H. Yang; R. Tian and Y. Li. Organic reaction by 1,4-diazabicyclo[2.2.2] octane (DABCO). *Front. Chem. China*, 3(3):279–287, 2008.

[50] M. M. Di Vona; R. Narducci; L. Pasquini; K. Pelzer and P. Knauth. Anion-conducting ionomers: Study of type of functionalizing amine and macromolecular cross-linking. *Int. J. Hydrogen Energy*, 39:14039–14049, 2014.

[51] H. Lund. *Acta Chem. Scand.*, 11:491, 1957.

[52] A. G. Anderson and B. M. Strecker. Azulene. a study of the visible absorption spectra and dipole moments of some 1- and 1,3-substituted azulenes. *J. Am. Chem. Soc.*, 81(18):4941–4946, 1959.

[53] A. R. Katritzky, editor. *Advances in heterocyclic chemistry*, volume 97. Elsevier, 2009.

[54] R. J. Waltman and J. Bargon. Electrically conducting polymers: a review of the electropolymerization reaction, of the effects of chemical structure on polymer film properties, and of applications towards technology. *Can. J. Chem.*, 64(76), 1986.

[55] Y. Ohtani; N. Itoh; I. Ogura and M. Yamaguchi. The reduction on guaiazulene by the Bouveault-Blanc's method. *Konankako Co. Ltd.*, 13, 1976.

[56] L. Zechmeister. *Progress in the chemistry of organic natural compounds.* Springer Verlag, 1948.

[57] Y. Ohtani; N. Itoh; I. Ogura and M. Yamaguchi. The reduction on guaiazulene by the Bouveault-Blanc's method. *Wakayama Med. Rep.*, 13, 1976.

[58] Y. Otani. Studies on azulenes. The irridation effect on azulenes. The gamma-ray irridiation on Guaiazulene. *Yakugaku Zasshi (Journal of the Pharmaceutical Society of Japan)*, 88(7):795–801, 1968.

[59] K. Fujimura; M. Ouchi and M. Sawamoto. Ferrocene cocatalysis for iron-catalyzed living radical polymerization: Active, robust, and sustainable system under concerted catalysis by two iron complexes. *Macromolecules*, 48:4294–4300, 2015.

[60] B. Sun; Z. Ou; D. Meng; Y. Fang; Y. Song and KM Kadish. Electrochemistry and catalytic properties for dioxygen reduction using ferrocene-substituted cobalt porphyrins. *Inorg. chem.*, 18(53), 2014.

[61] A. Garcia-Abuin; D. Gomez-Diaz; J. M. Navaza and A. Rumbo. CO_2 capture by pyrrolidine: reaction mechanism and mass transfer. *AIChE Journal*, 60(3):1098–1106, 2014.

[62] S.Bishnoi. Absorption of CO_2 into aqueous piperazine: reaction kinetics, mass transfer and solubility. *Chem. Eng. Sci.*, 55:5531–5543, 2000.

[63] G. Seshadri; C. Lin and A. B. Bocarsly. *J. Electroanal. Chem*, 372:145, 1994.

Supporting information

Cyclic voltammetry (CVs)

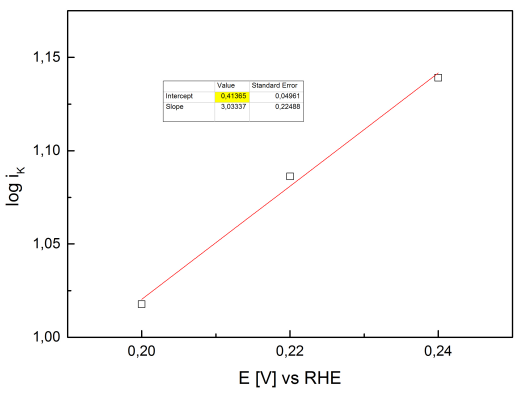

(a) T = 314 K

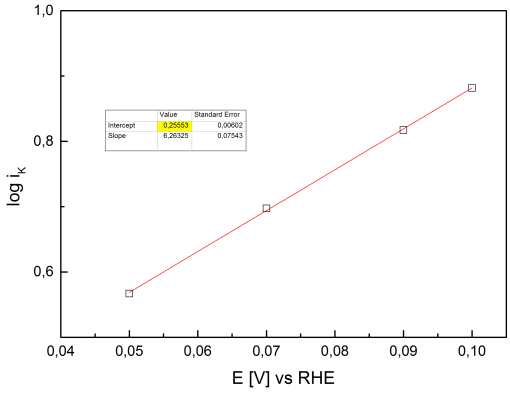

(b) T = 294 K

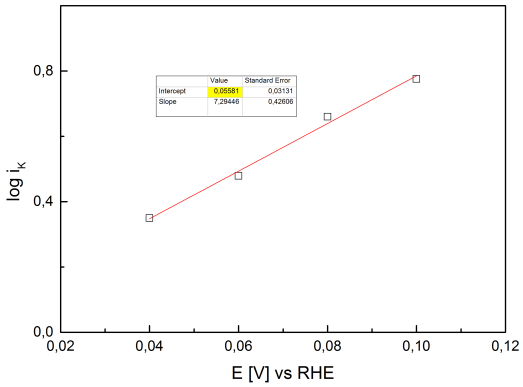

(c) T = 275 K

Figure 81: Exchange current density i_0 plots for (a) T = 314 K, (b) T = 294 K and (c) T = 275 K

CVs in acetonitrile / 0.1 M $NaClO_4$ at 50 mV/s

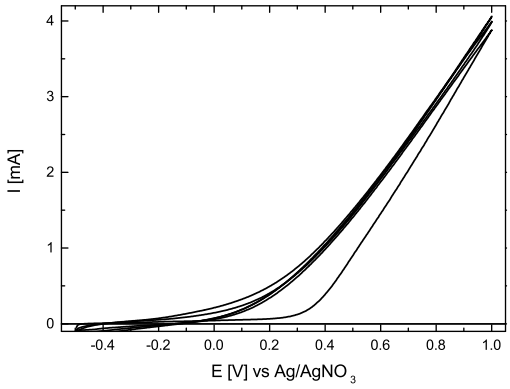

Figure 82: Mo_6Co_7

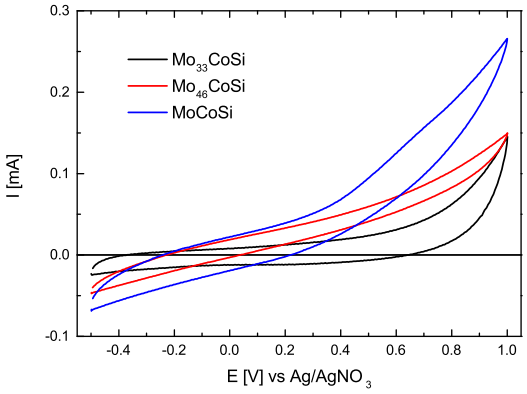

Figure 83: Comparison $Mo_xCo_ySi_z$

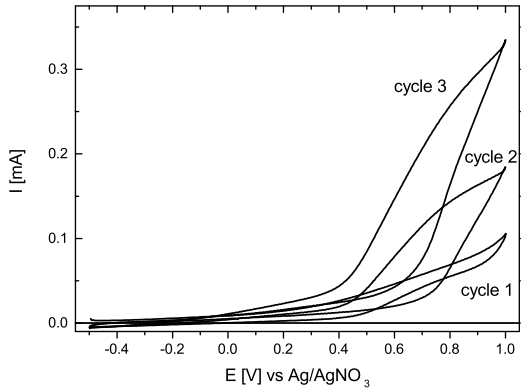

Figure 84: $MoAl_{12}$

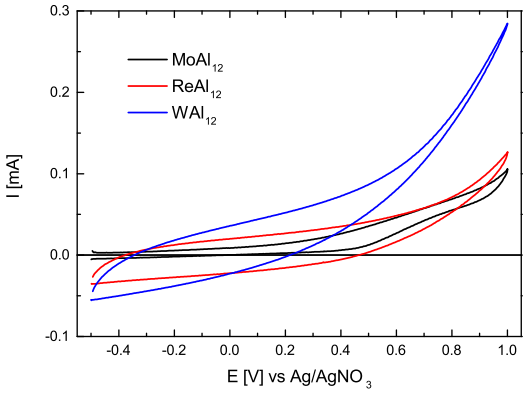

Figure 85: Comparison XAl_{12}

CVs in 0.5 M H_2SO_4, scan rate 50 mV/s

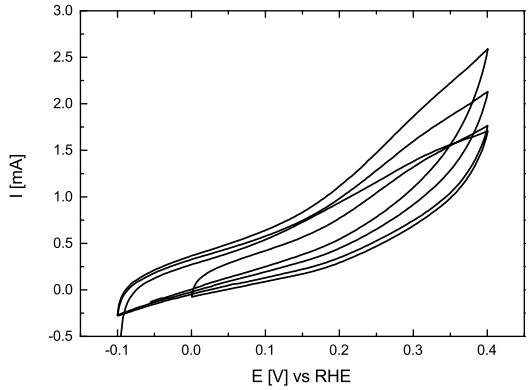

Figure 86: WAl_{12}

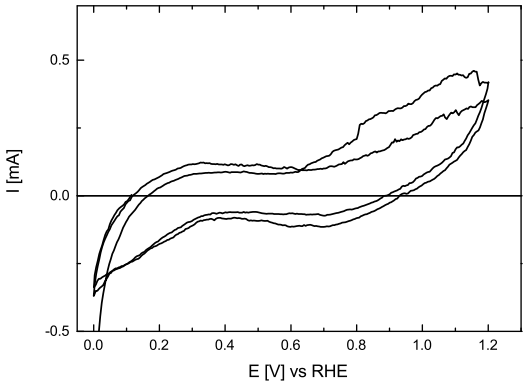

Figure 87: $PtAl_2$

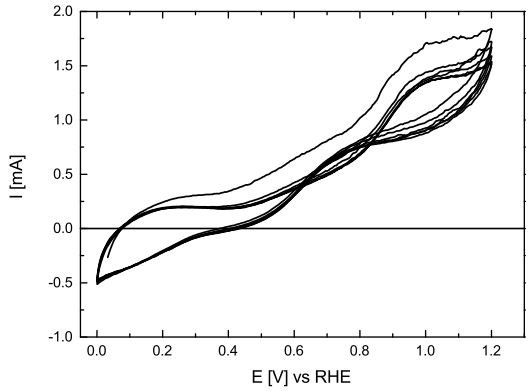

Figure 88: CV $PtAl_2$ in 0.5M H_2SO_4 and 0.05 M MeOH

NMR data

Dodecahydro-n-ethylcarbazole (after oxidation at 0.8V in acetonitrile)

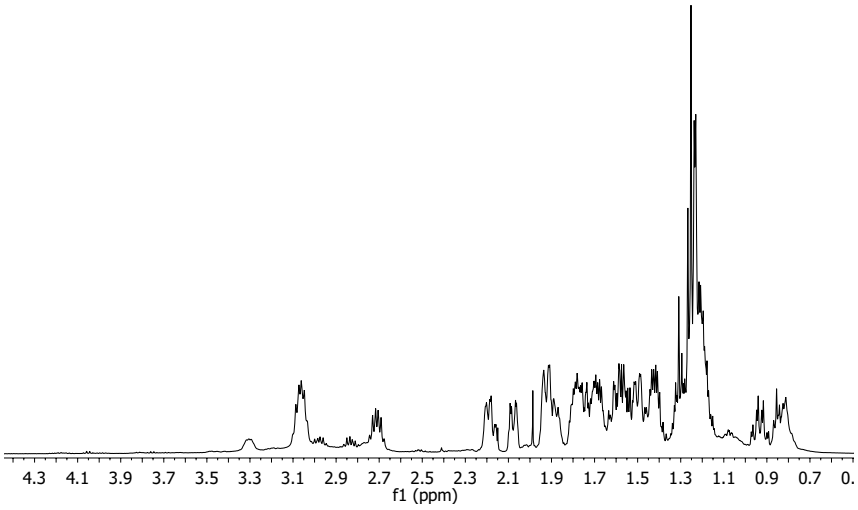

Figure 89: ^{1}H-NMR ($CDCl_3$, 500 MHz, TMS)

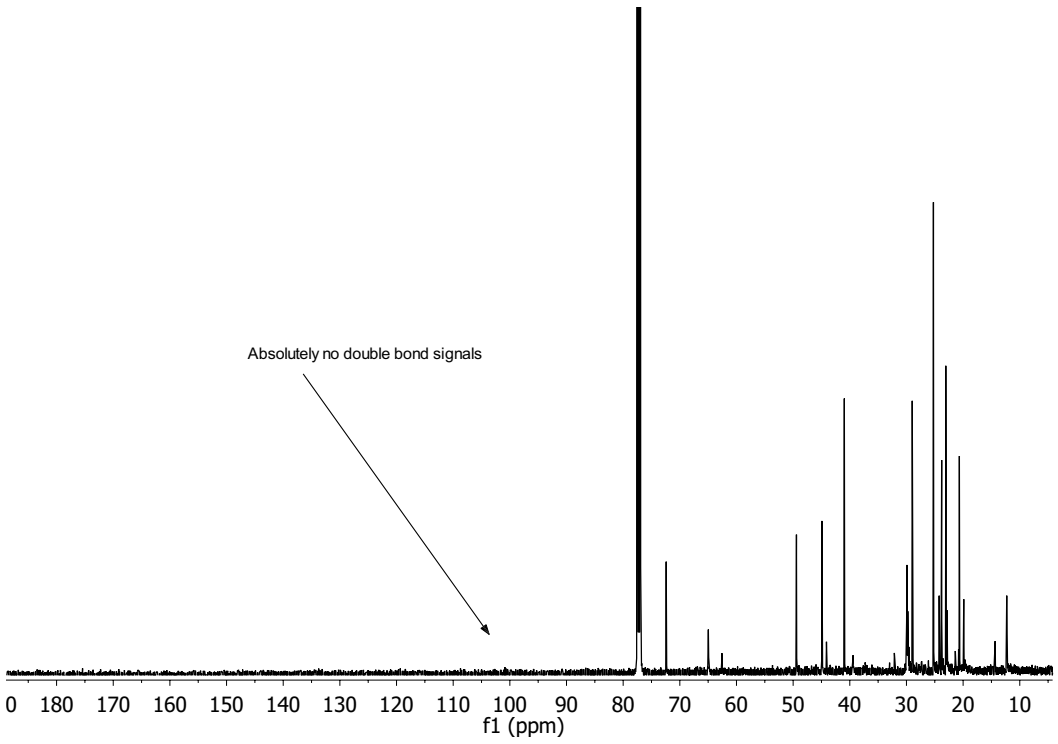

Figure 90: ^{13}C-NMR ($CDCl_3$, 125 MHz, TMS)

Tetrahydrocarbazole (products for different oxidation potentials)

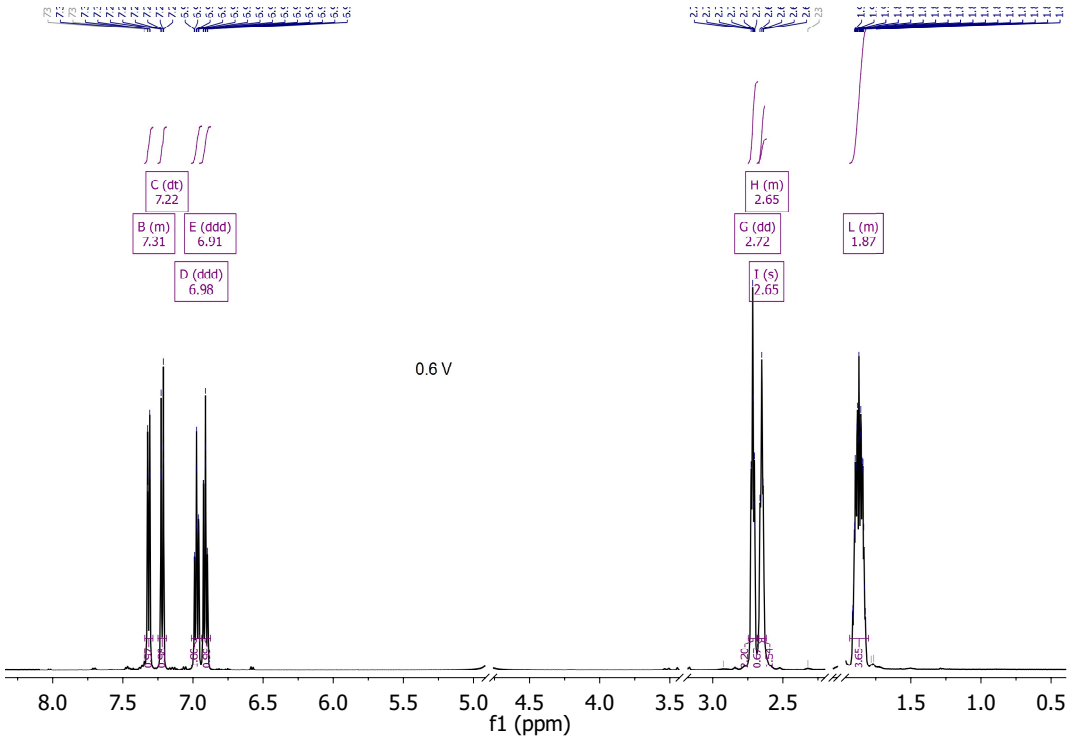

Figure 91: ^{1}H-NMR (MeOD, 500 MHz, TMS) H4-NEC oxidized at 0.6 V

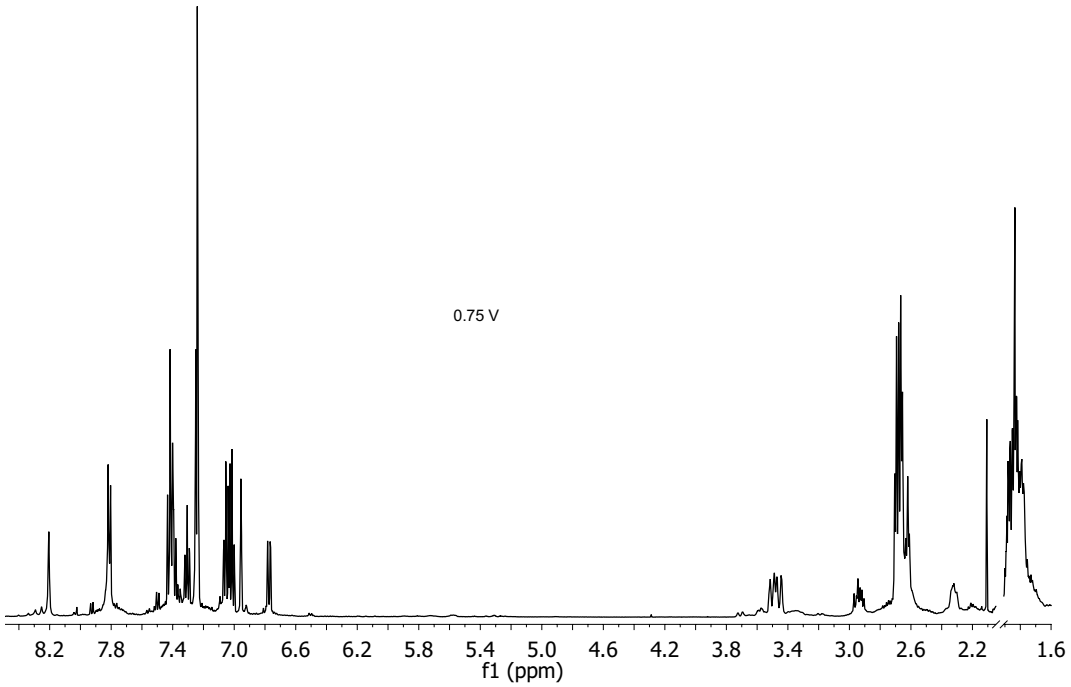

Figure 92: ^{1}H-NMR (MeOD, 500 MHz, TMS) H4-NEC oxidized at 0.75 V

2-methyldecahydroquinoline

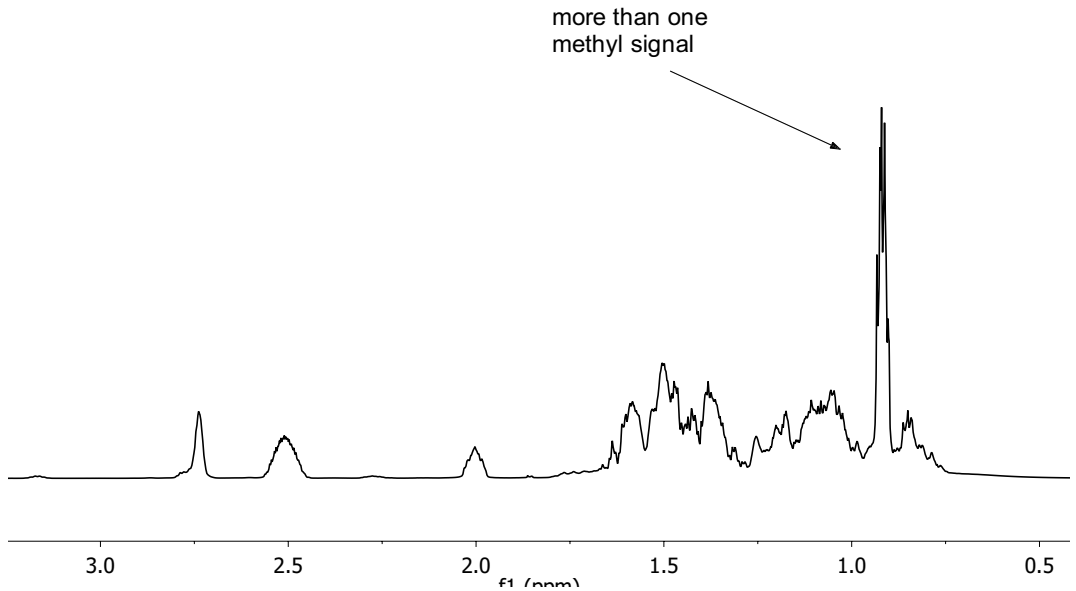

Figure 93: ^{1}H-NMR ($CDCl_3$, 500 MHz, TMS) of 2-methyldecahydroquinoline (MDQ)

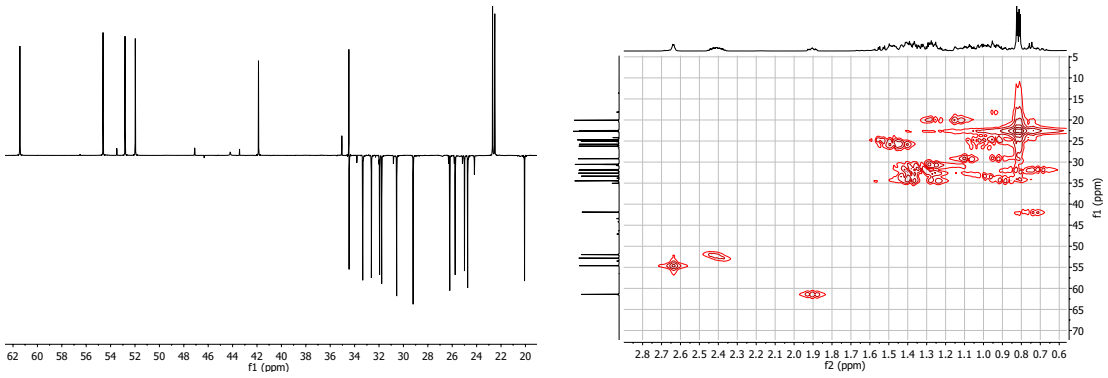

Figure 94: Left: ^{13}C-dept ($CDCl_3$, 125 MHz, TMS) Right: HMQC ($CDCl_3$, 500 MHz, TMS)

Hydrogenated Guaiazulene (GuAH)

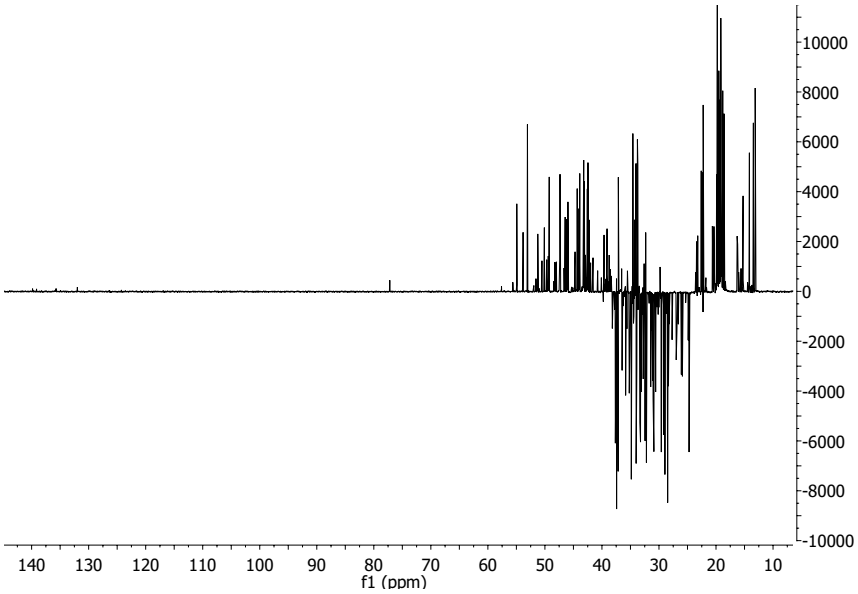

Figure 95: ^{13}C-dept ($CDCl_3$, 125 MHz, TMS)

Piperazinecarbamate

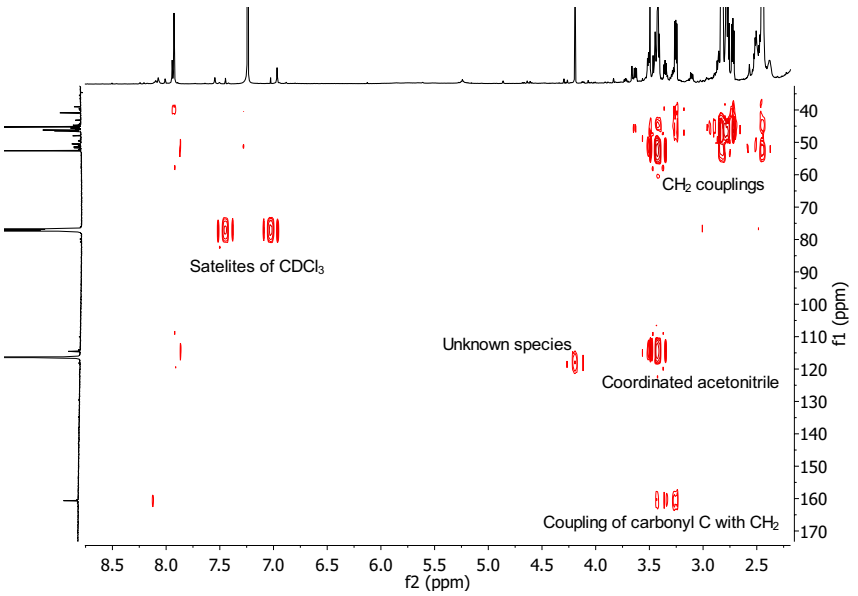

Figure 96: HMBC of reduced piperazine/piperazinecarbamate at -1.5 V

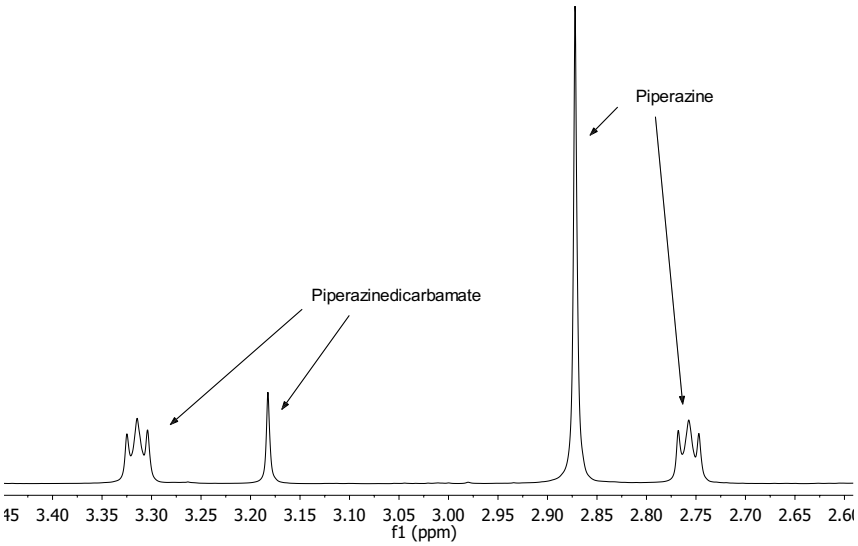

Figure 97: ^{1}H-NMR (500 MHz, $CDCl_3$, TMS) of reduced piperazine/piperazinecarbamate at -1.2V, precipitate from the catalyst surface

IR spectra

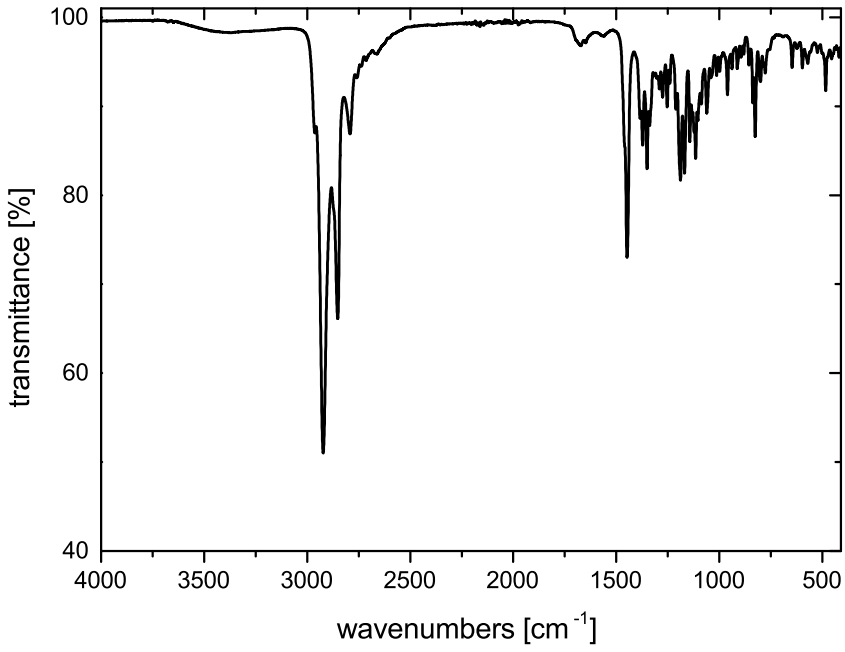

Figure 98: Ir of dodecahydro-n-ethylcarbazole

GC data

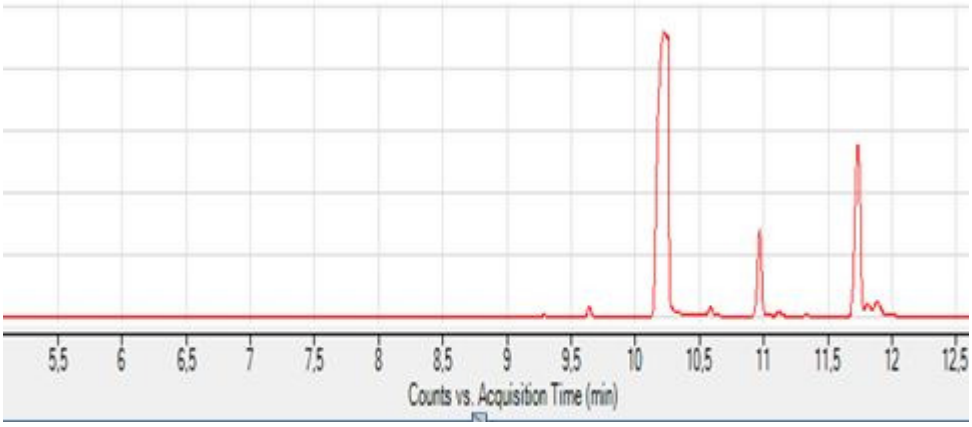

Figure 99: GC of H12-NEC

Chronoamperometric measurements (CAs)

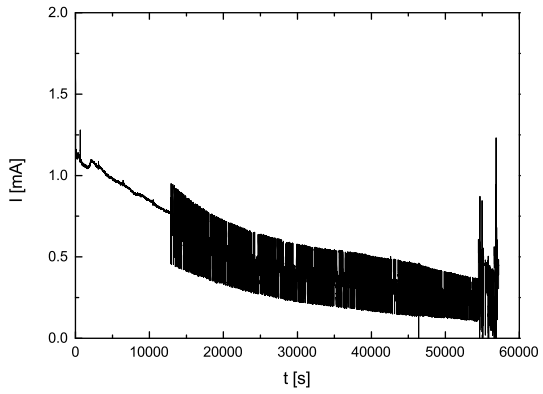

Figure 100: H4-NEC in CH_3CN/0.1 M $NaClO_4$ at 0.6 V. After 12000 sec. high resistance because of deposition of H4-NEC radical species on the catalyst surface.

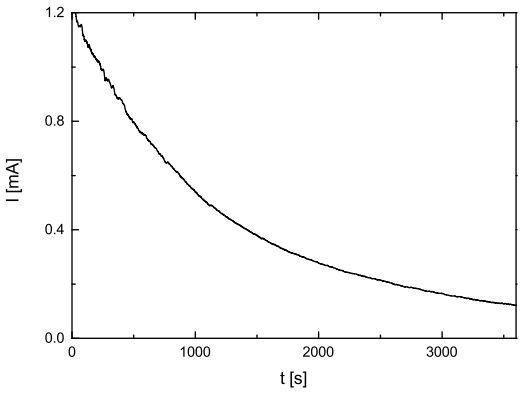

Figure 101: Indoline in CH_3CN/0.1 M $NaClO_4$ at 0.5 V

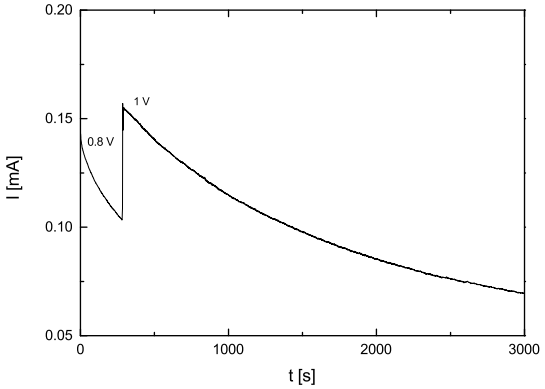

Figure 102: GuaH in CH_3CN/0.1 M $NaClO_4$ at two different potentials

Attachment

Erklärung

Hiermit erkläre ich, dass ich die Dissertation "Electrochemcial Hydrogen Storage in Organic Molecules" selbstständig verfasst und keine anderen als die angegebenen Hilfsmittel genutzt habe. Alle wörtlich oder inhaltlich übernommenen Stellen habe ich als solche gekennzeichnet.

Ich versichere außerdem, dass ich diese Dissertation nur in diesem und keinem anderen Promotionsverfahren eingereicht habe und dass diesem Promotionsverfahren keine endgültig gescheiterten Promotionsverfahren vorausgegangen sind.

Mülheim an der Ruhr, den 17.02.2017

Frederic Buttler

Danksagung (acknowledgement)

First of all thank you to Prof. Schlögl for the great possibility to work in his group at the CEC. The discussions about my work and the confidence in my abilities helped a lot to finish this it successfully. Furthermore i would like to thank Chinmoy Ranjan who was a great supervisor. He gave me the right guidance and was opened for new ideas.
Not to forget the Bavarian Hydrogen Center which supported the LOHC project in which i was involved. Thank you to Prof. Juri Grin who provided the IMCs and thank you to Prof. Wasserscheid who provided some of the needed chemicals in this work. Last but not least thank you to the whole staff of the Max Planck institute for chemical energy conversion and the colleagues in the group of Prof. Schlögl. We had a fun time, sometimes so fun that i forgot my work :).